The impact of dendritic calcium control on interneurons function within the hippocampal circuit

Dissertation

zur

Erlangung des Doktorgrades (Dr. rer. nat.)

der

Mathematisch-Naturwissenschaftlichen Fakultät

der

Rheinischen Friedrich-Wilhelms-Universität Bonn

vorgelegt von

Sabrina Delattre

Aus Sainte Foy La Grande, France

Bonn, September 2017

Angefertigt mit Genehmigung der Mathematisch-Naturwissenschaftlichen Fakultät der Rheinischen Friedrich-Wilhelms-Universität Bonn

1. Gutachter: Prof. Dr. Dirk Dietrich
2. Gutachter: Prof. Dr. Walter Witke

11.01.2018	2018
Tag der Promotion	Erscheinungsjahr

Summary

In the past few decades, dendritic integration has been extensively studied in hippocampal excitatory cells (for review see Stuart and Spruston 2015). However, much less effort has been put into understanding inhibitory neurons input integration since they are so diversified and are mostly aspiny (Klausberger and Somogyi 2008). In this thesis we sought to contribute to the understanding of input integration in interneurons by studying calcium signaling in three different morphologically defined interneuron subtypes.

As calcium is one of the most prominent second messengers in the brain, we postulated that it can contribute to the input integration and thus to the output response of interneurons, leading to a specific control of pyramidal cells output.

Calcium amplitude, duration and location trigger the direction of plasticity (Evans and Blackwell 2015). A high amplitude and fast calcium entry will most likely trigger LTP; while long lasting and low amplitude calcium, should trigger LTD (Evans and Blackwell 2015). As a mechanism controlling calcium diffusion and free calcium concentration, endogenous buffer is a key component for neurons to regulate intracellular calcium signal. Indeed, depending on the buffer identity and the buffering fraction, free calcium will be rapidly or slowly bound which could influence the direction of the plasticity given the same input within a cell type.

CCK positive basket cells, PV positive basket cells and PV negative dendritic targeting cells were chosen according to their specific pyramidal somatic/dendritic target and their distinct involvement in hippocampal oscillations.

To resolve the importance of calcium signaling regulation on those interneurons' function, we directed our study from calcium signaling biophysical determination to more physiological relevance within network activity.

Biophysical determination including calcium entry, endogenous buffering capacity and diffusion environment of calcium signaling in CCKBC, PVBC and D-T cells were found to be unique in each interneuron subtype. As a consequence, this sole mechanism of calcium signal regulation points to different dendritic input integration and may lead to different calcium dependent plasticity mechanisms for each interneuron subtype. Therefore, we investigated the

backpropagation of action potential induced calcium transient (bAP-CaT) in CCKBC, PVBC and D-T cells. We discovered a similar medial limit to bAP-CaT in CCKBC and PVBC; however D-T cells showed a stable distal bAP-CaT.
bAP-CaT is not modulated by mobile and fixed endogenous buffering capacity in PVBC and D-T cells, but the fixed buffering fraction of CCKBC does influence its bAP-CaT. This finding indeed shows the importance of calcium buffering in shaping calcium entry and so controlling the input integration in a cell-dependent manner.

Finally, upon network activity, interneurons are differently recruited (Klausberger and Somogyi 2008). We investigated CCKBC electrophysiology and calcium signaling during network activity via cholinergic activation. CCKBC experience a drastic change in intrinsic excitability, a small change in their resting calcium concentration and a larger amplitude calcium entry during cholinergic network activation. These changes may happen because of an increase in intrinsic excitability mediated by a reduction of SK current upon M1 and M3r activation as for OLM interneurons (Bell, Bell et al. 2015)
In conclusion, calcium signaling handling appears unique for the 3 interneurons subtypes studied, which might confirm their differential recruitment and output seen during hippocampal rhythmogenesis. This study is the first step toward understanding the importance of calcium signaling in synaptic and somatic input integration in interneurons.

Zusammenfassung

In den vergangenen Jahrzehnten wurde die Integration dendritischer Signale in exzitatorischen Zellen des Hippocampus intensiv untersucht (Stuart und Spruston 2015). Aufgrund der Diversität inhibitorischer Neurone und dem Fehlen synaptischer Spines wurde deren Signalverarbeitung mit weitaus weniger Aufwand erforscht (Klausberger und Somogyi 2008). Durch die genauere Betrachtung von Calciumsignalen in drei morphologisch unterscheidbaren Subtypen von Interneuronen soll diese Arbeit zum Verständnis ihrer Signalverarbeitung beitragen.

Da Calcium einen der wichtigsten sekundären Botenstoffe im Gehirn darstellt, nehmen wir an, dass er zur Integration synaptischer Eingänge von Interneuronen beiträgt und somit auch ihre Signalantwort beeinflusst, was letzendlich spezifisch die Aktivität von Pyramidalzellen steuert.

Die Größe, Dauer und Lokalisation der Calciumantwort bestimmen die Richtung der Plastizität (Evans und Blackwell 2015). Eine hohe Konzentration und ein schneller Einstrom von Calcium löst tendenziell LTP aus, wohingegen ein langanhaltender, geringer Einstrom LTD assoziiert ist (Evans und Blackwell 2015). Endogene Calciumpuffer sind eine Schlüsselkomponente zur Regulation intrazellulärer Calciumsignale, da sie die freie Calciumkonzentration und –diffusion kontrollieren. Abhängig von der Art des Puffers und seiner Konzentration werden freie Calciumionen schnell oder langsam gebunden, was ausgehend von einem gleichbleibenden Input bei gleichem Zelltyp die Plastizität in die eine oder andere Richtung lenken kann.

Für die vorliegende Arbeit wurden CCK positive Korbzellen (CCKBC), PV positive Korbzellen (PVBC) und PV negative Interneurone, die auf Dendriten projizieren (D-T Zellen), ausgewählt. Aufgrund der unterschiedlichen Lokalisation ihrer Synapsen an den Zielzellen, sind sie eindeutig zu identifizieren und nehmen jeweils andere Rollen in hippocampalen Oszillationen ein.

Die Bedeutung der Calciumsignalregulation auf die Funktion dieser Interneuronen aufzuzeigen, die bisher biophysikalischen geprägten Betrachtungen zur Calciumpufferkapazität in physiologischer Hinsicht zu untersuchen und dessen Auswirkung auf die Netzwerkaktivität zu bestimmen war das Ziel dieser Arbeit.

Biophysikalische Untersuchungen zum Calciumeinstrom, der endogenen Pufferkapazität und den jeweiligen Diffusionsbedingungen zeigten, dass jeder Subtyp der untersuchten

Interneurone ein charakteristisches Verhalten aufweist. Wir vermuten, dass die interneuronspezifische Calciumregulation zu einer variablen dendritischen Signalintegration führt. Dies wiederum legt eine jeweils unterschiedliche calciumabhängige Plastizität in den Interneuronen nahe.

Aus diesem Grund wurde in CCKBC, PVBC und D-T Zellen Zurücklaufende-durch-Aktionspotentiale-ausgelöste Calciumtransienten („backpropagation of action potential induced calcium transient"; bAP-CaT) untersucht. BAP-CaT konnten in CCKBC und PVBC nur bis zu einer Distanz von 120 µm ausgehend vom Soma detektiert werden, wohingegen in D-T Zellen das Signal bis zu einer Distanz von 250 µm erhalten blieb.

Wir konnten zeigen, dass BAP-CaT in PVBC und D-T Zellen nicht durch den mobilen Anteil des Calciumpuffers beeinflusst wird, wohingegen in CCKBC der stationäre Pufferanteil Auswirkungen auf bAP-CaT hat. Diese unterschiedliche Calciumpufferkapazität äußert sich in einer zelltypabhängigen Signalintegration.

Es ist bekannt, dass Interneurone unterschiedlich in die Netzwerkaktivität involviert sind (Klausberger and Somogyi 2008). Deswegen untersuchten wir die Elektrophysiologie und die Calciumsignalgebung in CCKBC während cholinergisch induzierter Netzwerkaktivität. Während cholinerger Netzwerkaktivität zeigen CCKBC einen Anstieg der intrinsischen Erregbarkeit, eine leichte Zunahme der Ruhecalciumkonzentration und einen höheren Calciumeinstrom.

Diesen Veränderungen liegt möglicherweise eine Erhöhung der instrinsischen Erregbarkeit zugrunde, die durch eine Verringerung von SK Strömen durch M1 und M3r Aktivierung verursacht wurde - wie bereits bekannt für OLM Interneurone (Bell, Bell et al. 2015). Zusammenfassend lässt sich sagen, dass der Umgang mit Calciumsignalen für den jeweils untersuchten Interneuronsubtyp charakteristisch ist. Dies würde ihre unterschiedliche Einbindung und Aktivität, die während der hippocampalen Rhythmogenese beobachtet wurden, erklären. Diese Arbeit stellt den ersten Schritt zum Verständnis der Calciumsignale während synaptischer und somatischer Signalintegration in Interneuronen dar.

Table of Contents

Summary **2**

Zusammenfassung **4**

Table of Contents **6**

Figure index **10**

Table index **12**

1 Introduction **13**

1.1 The hippocampus from structure to function 13

1.1.1 The hippocampal formation 13

1.1.2 Hippocampus intrinsic and extrinsic connectivities 15

1.1.2.1 Trisynaptic pathway and extrinsic connections 15

1.1.2.2 Rhythm generation 16

1.1.2.3 The inhibitory microcircuit 17

1.2 Morphology and function of hippocampal interneurons 18

1.2.1 Basket cells (BC) 20

1.2.1.1 PV basket cells (PVBC) 20

1.2.1.2 CCK basket cells (CCKBC) 22

1.2.2 Dendritic targeting cells (D-T cells) 24

1.3 Calcium: an important signaling molecule 26

1.3.1 Dendritic calcium entry in neurons 27

1.3.2 Endogenous buffering capacity and diffusion environment 29

1.3.2.1 Endogenous buffers: the right component to shape the spatiotemporal aspect of calcium signaling 29

1.3.2.2 Interaction between mobile and immobile buffer on calcium diffusion 33

1.3.3 Calcium extrusion mechanisms 35

1.3.4 Role of calcium in plasticity and neuron excitability 36

1.3.4.1 Calcium induced plasticity 37

1.3.4.2 Calcium activates calcium dependent channels required for intrinsic excitability 38
1.4 Modulation of calcium signaling by cholinergic drive 39
2 Aim of the study 41
3 Materials and methods 43
3.1 Slice preparation 43
3.2 Confocal microscope 44
3.2.1 Patch clamp recording and cell fluorescence visualization 44
3.2.2 Confocal calcium imaging setup 45
3.3 Calcium dye properties 47
3.4 Analysis of calcium transient signals 48
3.5 Theory of the single compartment model, and dendrite diffusion environment 49
3.6 Field potential recordings 53
3.7 Extracellular stimulation 54
3.8 Two photon (2P) microscopy 55
3.8.1 Principle of multiphoton microscopy 55
3.8.2 Calcium imaging and patch clamp recordings 56
3.8.3 Glutamate uncaging 56
3.8.4 Measure of D_{app} from the uncaging experiment 57
3.9 Fluorescence Life Time Imaging (FLIM) 58
3.9.1 Theory 58
3.9.2 FLIM experiment and imaging analysis 59
3.10 Immunostainings and biocytin revelation 60
3.10.1 Axon recovery 60
3.10.2 Calbindin and calretinin stainings 61
3.10.3 PV staining in PVCre-Ai14TDtomato line and Tg (Gad2-EGFP) DJ31Gsat line .. 62
3.10.4 CB1r staining in the Tg (Gad2-EGFP) DJ31Gsat mouse line 64

3.11 Virus injection in mice 65
3.11.1 Principle of the iGluSnFR probe 65
3.11.2 Procedure of virus injection in mice 65
3.11.3 Virus types 67
3.12 Analysis, standard error propagation and statistics 68
4 Results 69
4.1 Examining the selectivity of the 2 mouse lines used 69
4.2 Confirmation of CCKBC, PVBC and D-T cells morphology 71
4.2.1 Passive electrophysiological properties 71
4.2.2 Axonal location 73
4.3 Biophysical measurements of CCKBC, PVBC and D-T cells' calcium signaling ... 73
4.3.1 Confirmation of the added buffering approach prediction 73
4.3.2 Endogenous buffering capacity measurement 75
4.3.3 Calcium binding protein identity 78
4.3.4 Extrusion rate and rundown of the extrusion rate over time 81
4.3.5 Assessment of the calcium entry produced by 3 somatic AP 82
4.3.6 Dendritic calcium apparent diffusion coefficient and its action range 83
4.4 Resting calcium concentration of CCKBC, PVBC, and D-T cells 84
4.5 Dendritic synaptic activation leads to calcium transient 85
4.5.1 iGluSnFR injection 85
4.5.2 Synaptic stimulation induced calcium transient 87
4.6 bAP-CaT toward CCKBC, PVBC and D-T cells' dendritic tree: contribution of the endogenous buffer 89
4.6.1 Assessing the gradient of endogenous buffer in dendrites of CCKBC using glutamate uncaging technique 93
4.7 Calcium signaling properties during network activity 95
4.7.1 Induction of network activity in submerged slices 95
4.7.2 CCKBC behavior in an active network 97

4.7.2.1 Electrophysiology features 97
4.7.2.2 Calcium signaling features 101
4.8 Study of somato-dendritic calcium signaling of Purkinje cells 105
5 Discussion 108
5.1 Biophysical determination of CCKBC, PVBC and D-T cells' calcium signaling 108
5.2 bAP-CaT in interneurons and gradient of endogenous buffer in CCKBC 113
5.3 Synaptic input induced calcium in CCKBC 116
5.4 CCKBC behavior during network activity 116
6 Perspectives 119
References 120
Appendix 130
Virus injection in mouse: dosage and study endpoints 130
Abbreviations 132
Acknowledgement 134

Figure index

Figure 1 : Illustration of the hippocampal formation 13
Figure 2 : Drawing of a CA1 pyramidal cell along the diverse strata of CA1 region..... 14
Figure 3 : Schematic view of the trisynaptic pathway 15
Figure 4 : Representation of interneuron diversity in the CA1 hippocampal region 19
Figure 5 : CCK-expressing interneurons contribute to sparse coding by CA1 pyramidal cells during theta oscillations 24
Figure 6 : EF-hand domain motif..... 32
Figure 7 : mGluR1/M1 mAChR regulate spine Ca^{2+} transient via inhibition of SK channels. 38
Figure 8 : Single compartment model..... 49
Figure 9 : Schematic view of Purkinje cells connectivity..... 55
Figure 10 : 2P microscopy 56
Figure 11 : Theoretical distribution of a diffusing substance over time 58
Figure 12 : Principle of the TCSPC 59
Figure 13 : Illustration of the iGluSnFR properties 65
Figure 14 : Anesthetic injection and bregma location in mouse 66
Figure 15 : Coordinates determination for virus injection in the ventral hippocampus..... 67
Figure 16 : Quantification of the Tg(Gad2-EGFP)DJ31Gsat and PVCre-Ai14TDtomato mouse lines..... 70
Figure 17 : Double GFP, CB1r staining of the GADGFP mouse line 70
Figure 18 : Determination of the interneurons subpopulation via their axon location 72
Figure 19 : CCKBC, PVBC and D-T cells have distinct calcium transients induced by somatic stimulation..... 74
Figure 20 : Experimental verification of the single compartment model prediction in CCKBC, PVBC and D-T cells..... 75
Figure 21 : Prediction of the linear fit of the buffering capacity plot from Equation 4 and Equation 5 76
Figure 22 : Determination of the endogenous buffering capacity fraction of CCKBC, PVBC and D-T cells 77
Figure 23 : Wash out measure of PV in PVBC..... 79
Figure 24 : Staining of D-T cells against calbindin (Cb) 80
Figure 25 : Staining of D-T cells against calretinin (Cr)..... 80

Figure 26 : Extrusion run-down over time is similar between CCKBC and D-T cells..... 82
Figure 27 : Summary of the calcium entry regulation in CCKBC, PVBC, and D-T cells..... 84
Figure 28 : Similar calcium resting concentration in CCKBC, PVBC and D-T cells 85
Figure 29 : Example of iGluSnFR response induced by stimulating the Shaffer Collaterals .. 86
Figure 30 : Setting the minimal stimulation intensity in CCKBC 87
Figure 31 : Calcium signaling differs from synaptic stimulation to bAP in CCKBC..... 88
Figure 32 : bAP-CaT in CCKBC, PVBC and D-T cells 90
Figure 33 : Similar decrease in dendrite diameter with the distance (from soma) in CCKBC, PVBC and D-T cells..... 91
Figure 34 : Minimally disturbing mobile endogenous buffering fraction does not disturb the bAP-CaT of CCKBC, PVBC and D-T cells 92
Figure 35 : Out-competing endogenous buffering capacity uncover distal calcium entry in CCKBC 93
Figure 36 : uEPSP at CCKBC's dendrites induces calcium transient with similar extent in proximal and distal dendrites portion. 94
Figure 37 : Pharmacologically eliciting network activity in submerged chamber..... 96
Figure 38 : Electrically eliciting network activity in submerged chamber 97
Figure 39 : CCKBC's electrophysiological characteristics during network activity induced by Cch 98
Figure 40 : Spontaneous firing of CCKBC upon Cch application is not abolished by blocking the glutamatergic drive, or by MLA but is blocked by atropine 99
Figure 41 : Variation of ADP and AHP in CCKBC upon Cch application 100
Figure 42 : CCKBC possess SK current which is sensitive to Cch 101
Figure 43 : Cch induces an increase in $\Delta F/F$ and τ in CCKBC..... 102
Figure 44 : Cch induces an increase in baseline brightness in CCKBC soma 103
Figure 45 : CCKBC exhibit different dendritic calcium transients upon Cch application..... 104
Figure 46 : Climbing fiber stimulation induced calcium transient in the dendritic shaft of Purkinje cells 106

Table index

Table 1 : Mobile endogenous buffer's characteristics 33
Table 2 : Summary of calcium dyes properties 48
Table 3 : Triple staining biocytin, Cb, and Cr protocol 62
Table 4 : PV/GFP staining's protocol used for assessing the specificity of Tg(Gad2-EGFP)DJ31Gsat mouse line 63
Table 5 : PV staining's protocol used for assessing the specificity of the of the PVCre-Ai14TDtomato mouse line 64
Table 6 : Cb1r/GFP staining's protocol used for assessing the specificity of Tg(Gad2-EGFP)DJ31Gsat mouse line 65

1 Introduction

1.1 The hippocampus from structure to function

1.1.1 The hippocampal formation

The famous case of H.M., who endured a bilateral resection of his temporal lobes and suffered from anterograde amnesia, established the role of the hippocampal region in memory formation (Scoville and Milner 1957). Since then, a more precise picture of the hippocampus role has been settled: the dorsal hippocampus encodes spatial information, the ventral hippocampus processes non spatial, emotional information while the intermediate hippocampus has been suggested to integrate both spatial and non-spatial information and to translate learning into behavior (Forro, Valenti et al. 2015).

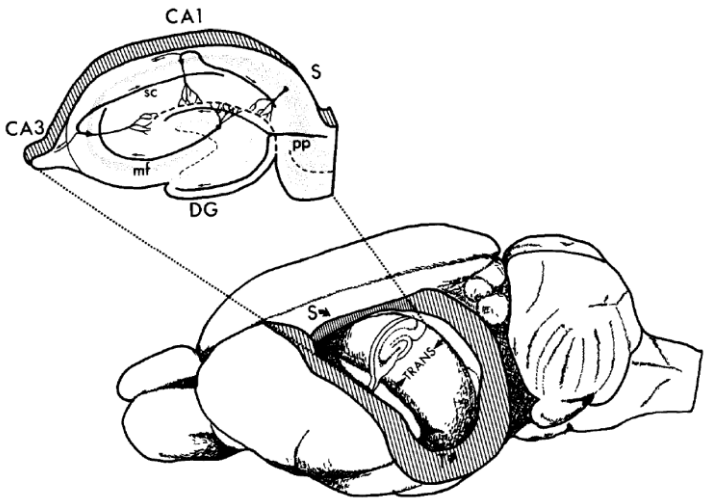

Figure 1 : Illustration of the hippocampal formation
"Removal of the cortical surface let appear the hippocampus. The hippocampus is an elongated C shape structure running along the septotemporal axis from the septal nuclei (S) rostrally to the temporal cortex (T) ventrocaudally. The transverse axis (TRANS) is perpendicular to the septotemporal axis. The slice (top left) is a summary representation of the major component and connection of the hippocampal formation. Abbreviations: DG: dentate gyrus, mf: mossy fibers, pp: perforant path, SC: Schaffer collaterals, S: subiculum". Adapted from (Amaral and Witter 1989)

The hippocampus is part of the hippocampal formation formed by: two interlocking "C" shaped structures, which are the dentate gyrus (first C) and Ammon's horn formed itself by

CA3, CA2 and CA1 (2nd C), the subiculum and finally by the entorhinal cortex (**Figure 1**). (Amaral and Witter 1989)

Strictly speaking, the singular shape of 2 inverted C given by the dentate gyrus and Ammon's horn and its resemblance with the sea horse has given the structure its name: hippocampus. This paired structure is located in the medial temporal lobe and belong to the limbic system.

The hippocampus is formed by a laminar organization shaped by diverse strata (**Figure 2**).

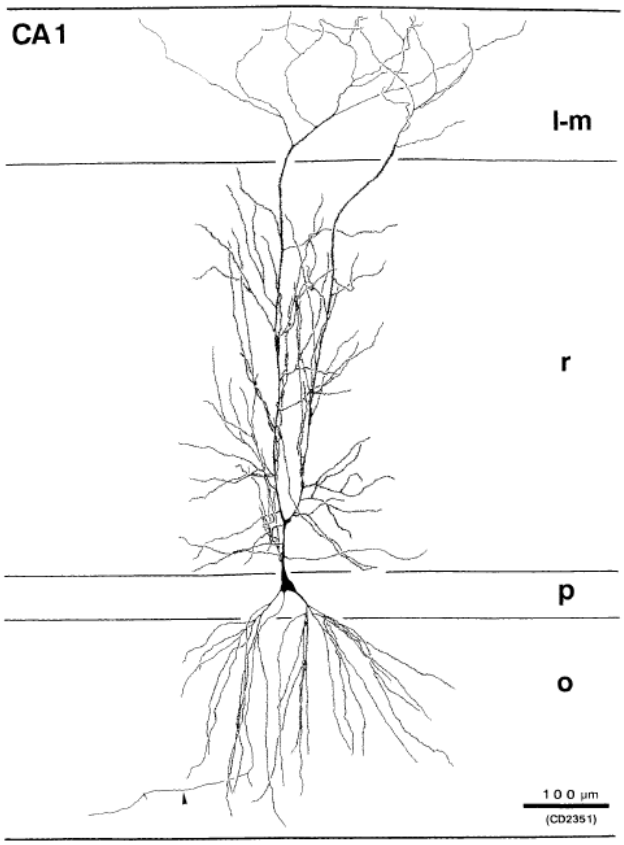

Figure 2 : Drawing of a CA1 pyramidal cell along the diverse strata of CA1 region
Pyramidal cell have their soma restricted in the pyramidal layer. Their dendrite arbor is found in all CA1 region strata (L-m: lacounosum moleculare, r: radiatum, p: pyaramidal, o: oriens), and their axon is located in the stratum oriens (Black arrow).
Adapted from (Ishizuka, Cowan et al. 1995)

The stratum pyramidal, as its name suggests, is formed of excitatory pyramidal cell bodies, tightly packed in CA1 but more loosely in CA2 and CA3. Few interneurons cells bodies are also located in this stratum. As seen in the **Figure 2,** a narrow stratum situated beneath the stratum pyramidal is called the stratum oriens. Basal dendrites of both excitatory cells and inhibitory neurons run through this layer. In addition to basal dendrites, pyramidal cells axons

as well as inhibitory cell somata are located in this stratum where mostly feedback (FB) inhibition occurs. In the stratum radiatum, found above the stratum pyramidal (**Figure 2**), many subtypes of inhibitory cell somata are established. The Schaffer collaterals are also located in this stratum, in which the CA3 and CA1 regions are synaptically connected in a feedforward manner (FF). The most superficial layer of the hippocampus is the stratum lacunosum-moleculare, in which the fibers from the entorhinal cortex and afferents from other regions finish.

1.1.2 Hippocampus intrinsic and extrinsic connectivities

1.1.2.1 Trisynaptic pathway and extrinsic connections

The superficial cells of the entorhinal cortex (EC) project their axons to the dentate gyrus (DG), among other brain regions. This so called "perforant path" is the major input pathway of the hippocampus. The granule cells of the DG, whose axons have large boutons called "mossy fibers", contact then the principle cells and interneurons of CA3. The CA3 region in turn projects to CA1 via the Schaffer collateral pathway. Finally CA1 contacts the subiculum region which closes the unidirectional hippocampal processing loop. (Amaral 1993; Andersen 2007).

This trisynaptic pathway (**Figure 3**) is however, only a portion of the functional circuitry of the hippocampal formation; for instance, the EC not only projects to the DG but also directly connects to the CA1 region (Witter, Griffioen et al. 1988).

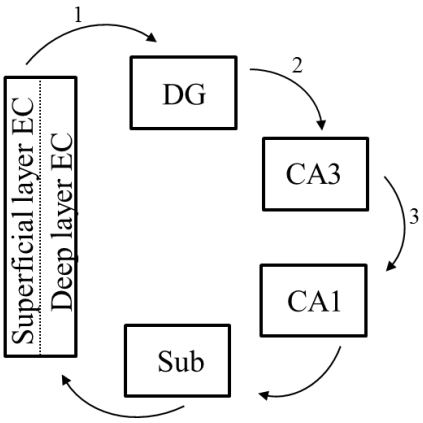

Figure 3 : Schematic view of the trisynaptic pathway
Numbers 1, 2, and 3 refer to the synapses of the trisynaptic pathway

Certainly, the hippocampus is not a separate region of the brain, and it is connected to other structures. As an extrinsic connection, the septal neurons located in the basal forebrain project cholinergic (excitatory) afferents to the hippocampus via three main routes: the fimbria, the

dorsal fornix and the supracallossal striae, and within the hippocampus the septum fibers connect to the DG and the CA1 region (Dutar, Bassant et al. 1995).

Another important afferent to the hippocampus is the median raphe that sends serotoninergic fibers toward the hippocampus. It was previously assumed that this projection was indirect, and was first projecting onto the septum (Assaf and Miller 1978; Vanderwolf 1989), but Freund et al in 1990 showed direct evidence of serotonin fibers located in the DG, the lacunosum molecular of the CA1 and CA3, as well as in the stratum radiatum and oriens of CA1 region (Freund, Gulyas et al. 1990). Finally, the hippocampus also receives and sends input to the neocortex and the amygdaloid complex (see review Andersen 2007).

1.1.2.2 Rhythm generation

The hippocampus is also known for its internal rhythmogenesis by the synchronization of neuronal activity in a certain frequency band. Three rhythms can be cited as the main oscillatory activities recorded in the hippocampus of human and rodent both *in vitro* and *in vivo* (for review see Colgin 2016): theta rhythm (4-14Hz), gamma rhythm (30-90Hz) and sharp wave ripples (SWR, 120-200Hz). These three oscillatory rhythms support different cognitive information processing (see review Axmacher, Mormann et al. 2006) and are differently generated.

Theta rhythm is a low frequency sinusoidal wave present during rapid eye movement (REM) sleep, locomotion and exploratory behavior. Theta rhythm had been recorded in CA1, DG and CA3, but also in other cortical areas such as the EC, the perirhinal cortex, the cingulate cortex and the amygdala. This indicates that the hippocampus is not the main generator of the theta oscillations. However, a disruption of theta oscillations occurred upon a lesion of the medial septum diagonal band of Broca (MS-DBB) (Buzsaki 2002). This finding demonstrated that MS-DBB, by its cholinergic afferents toward the hippocampus, is the main rhythm generator of the theta oscillation (see review Buzsaki 2002).

Gamma oscillation is a higher frequency but lower amplitude wave than the theta rhythm, and appears in many behavioral states. Two gamma current generators reside in the hippocampus. The first is generated in the DG via the EC, and disrupting it leads to an extinction of gamma oscillation in the DG but an increase in the CA1 hippocampal region. The second gamma generator is in CA3/CA1 region where it is internally generated and thus does not require extra hippocampal drive (Csicsvari, Jamieson et al. 2003).

SWR is a large amplitude and irregular local field potential (LFP) which occurs more frequently during slow wave sleep, drinking or grooming but never during running. The generation of the SWR seems to be intrinsic to the hippocampus, indeed, Buzsaki in 1986 demonstrated that damaging the fimbria, the fornix or blocking the cholinergic drive of the septum failed to abolish the SWR in the hippocampus. Therefore, the best candidate for the generation of this SWR is CA3, because of the tendency of CA3 pyramidal cells to have pacemaker effects (burst of APs) (Buzsaki 1986). The EC, by sending its output to DG and CA3 only biases the SWR by advancing or delaying SWR (Sullivan 2011).

These oscillatory activities have in common an excitatory/inhibitory balance. Thus the next subsection will further emphasize the role of inhibition onto principal cells in order to generate rhythmic activities, and particularly in the hippocampal CA3 and CA1 region.

1.1.2.3 The inhibitory microcircuit

GABAergic interneurons synchronize principal cell's activity (Cobb, Buhl et al. 1995). They thus, generate and maintain oscillatory activity (Buzsaki 2002; Buzsaki and Wang 2012) by setting time windows for the synaptic integration of the pyramidal cells (Buhl, Halasy et al. 1994; Pouille and Scanziani 2001). Consequently, it appears evident that inhibition, either somatic or dendritic, regulates efferent and afferent signaling in pyramidal cells: somatic inhibition was shown to suppress the discharge of sodium spikes whereas the dendritic inhibition suppressed the calcium dependent AP generation in CA3 pyramidal cells (Miles, Toth et al. 1996).

Pouille and Scanziani in 2004 revealed that stimulating the alveus at low frequency leads to a predominance of perisomatic inhibition but increasing the stimulating frequency shifts the inhibition to the dendritic sites of pyramidal cells (Pouille and Scanziani 2004), which also indicates a difference in interneurons recruitment depending on the stimulation frequency. This was verified by Klausberger's *in vivo* study where recordings of interneuron subtypes attested to their phase preference to theta frequencies and their differential recruitment during theta and SWR (Klausberger, Magill et al. 2003). Similar differential recruitment of interneurons was reported during gamma oscillation *in vitro*. Indeed, perisomatic inhibitors seem more involved in gamma oscillations than dendritic-targeting interneurons which showed less or sometimes no significant phase coupling with gamma oscillations (Hajos, Palhalmi et al. 2004). The role of perisomatic inhibitory cells was further emphasized as a generator of gamma oscillation mediated by the fast, recurrent excitation from pyramidal neurons axon in the CA3 region (Mann, Suckling et al. 2005).

By contrast, the dendritic-targeting interneurons involvement in the ascending gamma oscillation phase was described by Tukker's study (Tukker, Fuentealba et al. 2007). These two previously presented studies, however, characterized different subtypes of dendritic targeting interneurons which could explain the distinct conclusions drawn from their experiments.

Finally, Klausberger exposed the importance of dendritic targeting cells in the descending phase of the theta oscillation and thus in controlling the input/output conversion of pyramidal cells (Klausberger, Marton et al. 2004).

Thus, GABAergic neuron subclasses are able to regulate pyramidal cells for coherence oscillations within the hippocampal circuits. To do so, interneurons must have distinct intrinsic properties, and characteristic structures which relate to their functions. Consequently, the next sections highlight the interneuron's intrinsic characteristics which make them efficient in the generation and maintenance of oscillatory activities.

1.2 Morphology and function of hippocampal interneurons

Interneurons form short and local axonal connections to the surrounding cells where they release GABA or glycine as a neurotransmitter and so are in the majority inhibitory cells.

Interneurons represent 11% of CA1 and CA3 cells (Bezaire and Soltesz 2013) and are found in a tremendous diversity in the hippocampus. In the late 1980's, different studies attempted to classify interneurons according to their molecular contents such as calcium binding proteins or peptides (Somogyi, Hodgson et al. 1984; Sloviter and Nilaver 1987; Kosaka, Wu et al. 1988). Other studies have used interneurons morphological features to establish a classification (Schwartzkroin and Kunkel 1985; Ribak, Seress et al. 1993; Seress, Gulyas et al. 1993), others have classified them according to their firing pattern (Kawaguchi and Hama 1987; Kawaguchi, Katsumaru et al. 1987), or finally by their targeted domain of connectivity (Sik, Penttonen et al. 1995)

A summarized version of interneuron classification based on the morphology, molecular content, electrophysiological properties and targeted domain of connectivity, points to 21 different types (**Figure 4**) of interneurons in the CA1 hippocampal region (Klausberger and Somogyi 2008).

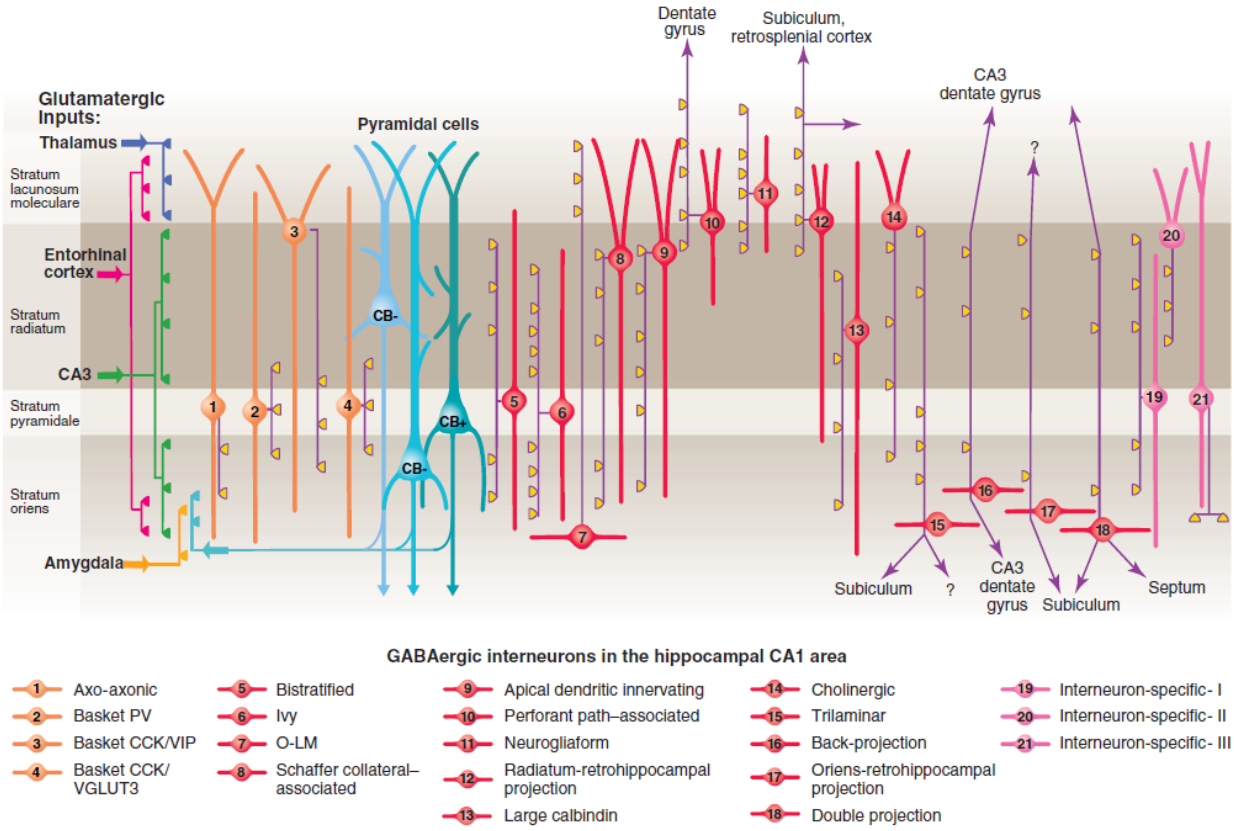

Figure 4 : Representation of interneuron diversity in the CA1 hippocampal region
Interneurons are found in huge diversity within the hippocampus. In our project we only focused on the number 2, 3 and 8/9 depicted in this figure. These 3 interneurons subtypes contact differently pyramidal cells (blue cells).
Modified from (Klausberger and Somogyi 2008).

The latest attempt to classify interneurons was made by Kepecs, postulating that the immense interneuronal diversity might not be so tremendous. In contrast, interneurons arise from cardinal classes (parvalbumin, somatostatin, nitric oxide, cholecystokinin, vaso-intestinal peptide, and reelin) based on genetic developmental ground states, and the fine specifications of interneuron subclasses occur through later interactions with their external environment and synaptic partners (Kepecs 2014).

Since such massive diversity exists among interneurons, our project focused on 3 different subtypes represented by the number 2, 3 and 8/9 interneurons in the Klausberger classification (**Figure 4**). These interneurons subtypes will thus be further detailed in the next subsections.

1.2.1 Basket cells (BC)

Perisomatic inhibitors of pyramidal cells also called basket cells (BC) are one of the biggest subclass of interneurons studied in the cortex and the hippocampus. Their first description goes back to Lorente de Nó in 1934 where he continued the work of Ramon y Cajal in studying the structure of the cerebral cortex (Nó 1934)

BC innervate both the soma and the proximal dendrite of pyramidal cells where they make basket-like synapses. Two subtypes of BC have been characterized according to their molecular content in the hippocampus and cortex: the cholecystokinin containing basket cells (Acsady, Arabadzisz et al. 1996; Acsady, Gorcs et al. 1996) and the parvalbumin expressing basket cells (Kawaguchi, Katsumaru et al. 1987). Although they both inhibit the pyramidal cell soma, and could be seen as one single unit of perisomatic inhibition, they vary quite importantly in their molecular contents, synaptic input, receptor expression, form of plasticity and their output signals.

1.2.1.1 PV basket cells (PVBC)

Parvalbumin (PV) interneurons represent 24% of the total interneuron population of the CA1 hippocampal region (Hu, Gan et al. 2014) and PVBC represent 60% of the PV positive interneurons (Baude, Bleasdale et al. 2007; Bezaire and Soltesz 2013).

Generated from the medial ganglionic eminence (Tricoire, Pelkey et al. 2011; Armstrong and Soltesz 2012), PVBC, although often seen as one population might be actually separated into two further subtypes. Donato et al revealed two classes of PVBC, early born PVBC (generated during the first half of neurogenesis) which exhibit high PV levels and experience plasticity during fear conditioning whereas, later born PVBC (generated during the second half of neurogenesis) which express lower PV levels, and show plasticity upon environmental enrichment and maze learning.

In addition, early and late born PVBC preferentially target distinct CA1 pyramidal cells; the early born target the deep layer of pyramidal cells and the late born the superficial layer (Lee, Marchionni et al. 2014; Donato, Chowdhury et al. 2015).

PVBC have been extensively studied because they provide direct inhibitory input onto somata of pyramidal cells and thus tightly control the number of active pyramidal cells and their firing frequency (Jonas, Bischofberger et al. 2004). PV^+ interneurons and particularly BC have a high speed of input integration, indeed from excitatory input to their output and thus GABA release, the time ranges from 1 to 2ms. Such high effectiveness comes from the fact

that PVBC are well suited for fast signaling from their dendritic input integration to their action potential generation (AP).

PVBC dendritic glutamate receptors are preferentially AMPAR, from which the current rises and decays rapidly compared to NMDAR current, in the dentate gyrus (Geiger, Lubke et al. 1997), and in the visual cortex (Goldberg, Yuste et al. 2003).

Considering the intrinsic and passive properties, PVBC have a low input resistance ($R_i \approx$ 120MΩ) (Glickfeld and Scanziani 2006; Norenberg, Hu et al. 2010) and so a fast membrane time constant ($\tau_m \approx$ 10ms), which ultimately shortens the duration of the EPSPs (4-10 ms). PVBC, as with the majority of the interneuron subtypes, have a mostly aspiny dendritic tree, indicating that the synapses are formed directly on their dendritic shafts. Their dendritic trees are quite spread across different strata (from statum oriens to stratum radiatum), indicating a potential to receive varied input from distinct afferent pathways (Gulyas, Megias et al. 1999). Indeed, in CA3 and CA1 regions, PVBC receive from 16,000 to 34,000 synapses: 6% inhibitory and 94% excitatory inputs (Gulyas, Megias et al. 1999). However, dendrites of PVBC function as a passive cable, much more so than for other interneurons (Emri, Antal et al. 2001). Indeed, back propagation of AP (bAP) decrements rapidly with distance (Aponte, Bischofberger et al. 2008; Hu, Martina et al. 2010) in PVBC found in the hippocampus and in the cortex (Goldberg, Tamas et al. 2003) and no dendritic spikes can be elicited, by either dendritic current injection, or synaptic stimulation (Hu, Martina et al. 2010). However Chiovini et al lately showed dendritic spike generation with a massive glutamate uncaging at the dendrite of PVBC (Chiovini, Turi et al. 2014). This feature might be explained by the low amount of voltage gated sodium channels in the dendritic arbor of PVBC (almost absent >100µm). However, a high density of voltage gated potassium channels, and particularly Kv3 type is expressed in their dendritic tree. It is interesting to point out, that those potassium channels work well with small diameter dendrites and the fast time course of AMPAR-induced EPSPs, because of their high activation threshold and their fast activation and deactivation kinetics. As a consequence of the high abundance of Kv3 channels, the time course of the EPSP is further accelerated, leading to a shortened period of temporal summation, which ultimately promotes AP firing with high speed, precision and temporal summation (Hu, Gan et al. 2014).

Although the dendritic trees of PVBC are poorly excitable, their axons represent a highly excitable compartment. The cumulative axonal length of PVBC is about 30 to 50 mm, and the number of terminals is 10,440 in CA1 pyramidal region (Bezaire and Soltesz 2013). Finally,

the release of neurotransmitter is also shaped for fast transmission. The AP propagates reliably with high velocity (≈ 1.5µm/s) and with rare failures (synchronous release) (Daw, Tricoire et al. 2009). Indeed, the presynaptic calcium channels of PVBC are exclusively P/Q type channels which are the fastest gating calcium channels. This high velocity is even more impressive given that the axons of PVBC are unmyelinated (Hu, Gan et al. 2014). To ensure such high velocity of transmission, the axon of PVBC is enriched with sodium channels that increase gradually with distance. This enrichment in sodium channels allows a rise in speed and frequency of AP generation and propagation, which compensates for the fact that the axon is small and highly branched (for review see Hu, Gan et al. 2014).

Another interesting feature of PVBC is their connectivity via gap junctions to other PVBC. (Fukuda and Kosaka 2000; Traub, Kopell et al. 2001; Fukuda and Kosaka 2003). This characteristic may also affect dendritic integration. Indeed, the spatial range of detection of pyramidal cells activity might be widened and relayed to different PVBC and thus forming a tight inhibitory network.

PVBC are primarily involved in FF inhibition, indeed because of their fast membrane time constant and the large EPSC received from the Shaffer Collaterals, they can quickly relay input. Additionally, since they have a short window of input integration, it is unlikely for them to be able to integrate input from FF and FB. Consequently, PVBC are suited for FF inhibition (Glickfeld and Scanziani 2006).

In vivo, PVBC fire during the descending phase of theta, but are also recruited during SWR (Klausberger, Magill et al. 2003; Klausberger, Marton et al. 2005; Klausberger and Somogyi 2008). Moreover, a specific intrinsic plasticity was established in PVBC by Campanac et al in 2013 leading to an increased in firing probability through a glutamate receptor-dependent down regulation of potassium channel activity. This increase in intrinsic excitability facilitates FF inhibition of pyramidal cells and lead the PVBC to fire in the gamma range, which was absent in the other class of interneurons studied (Campanac, Gasselin et al. 2013)

1.2.1.2 CCK basket cells (CCKBC)

CCK basket cells (CCKBC) originate from the caudal ganglionic eminence, and follow a tangential migration from the caudal ganglionic eminence to the hippocampus (Tricoire, Pelkey et al. 2011; Armstrong and Soltesz 2012).

Different studies have made sub-classifications of the CCKBC based on their molecular expression of vesicular glutamate transporter 3 (VGLUT3), which is not expressed in all

CCKBC (Somogyi, Baude et al. 2004) and/or vasointestinal peptide (VIP) (Acsady, Arabadzisz et al. 1996; Freund and Buzsaki 1996) which was not confirmed by the Somogyi's study (Somogyi, Baude et al. 2004).

In the hippocampus, CCKBC receive excitatory input from the Shaffer collaterals (45%), from CA1 pyramidal collaterals in stratum oriens (20%), as well as inhibitory input from the surrounding interneurons, much larger in dendritic segments than in their soma. Overall CCKBC receive 65% excitatory drive and 35% inhibitory inputs (Matyas, Freund et al. 2004). Additionally, they receive cholinergic inputs from the medial septum (Dutar, Bassant et al. 1995), and serotonergic afferents from the median raphe (Freund, Gulyas et al. 1990). By receiving these particular inputs, CCKBC have been considered to have a modulatory and a fine tuning role on the pyramidal cells in the hippocampus (Freund 2003). Furthermore, they are not suited to follow high frequency stimulation, unlike PVBC, and thus reinforce the fine tuning role they play on hippocampal pyramidal cells (Freund 2003).

At the passive properties level, CCKBC have a slow membrane time constant (25ms) and thus a large input resistance (280MΩ) (Cope, Maccaferri et al. 2002). These features allow them to attenuate EPSPs less, but also to have a longer window of input integration. Indeed, Glickfeld have demonstrated the role of this large window of integration for CCKBC to integrate both FF and FB inputs from CA3 and CA1 pyramidal cells (Glickfeld and Scanziani 2006), which reinforce the role of CCKBC as a precise modulator of pyramidal cell output.

Another important feature of CCKBC is their expression of presynaptic endocannabinoid receptors (Marsicano and Lutz 1999). Indeed, upon intense activity of pyramidal cells (Cch activation or glutamate activation) (Neu, Foldy et al. 2007) or theta rhythm firing, postsynaptic release of endocannabinoid ligands activate endocannabinoid receptors (CB1R) located on synapses of CCKBC. This leads to depolarization induced suppression of inhibition (DSI) of the pyramidal cells (Pitler and Alger 1992; Pitler and Alger 1994; Wilson, Kunos et al. 2001). DSI is believed to increase the signal to noise ratio of activated pyramidal cells which suppress their own inhibition through the endocannabinoid system. In contrast, other non-active pyramidal cells will preserve CCKBC's inhibitory inputs (**Figure 5**) (Klausberger, Marton et al. 2005).

In terms of neuronal output, CCKBC release GABA asynchronously (Daw, Tricoire et al. 2009), which is a consequence of the loose coupling of N type calcium channels to the calcium sensor at CCKBC axonal terminals (Freund and Katona 2007).

Finally, CCKBC contribution to network oscillation is sparse. As highlighted previously (**1.1.2.2**), three types of oscillations are generated in the hippocampus. However, CCKBC participate only during theta rhythm, minimally during gamma oscillation and not at all during the ripple oscillations (Klausberger, Marton et al. 2005; Klausberger and Somogyi 2008).

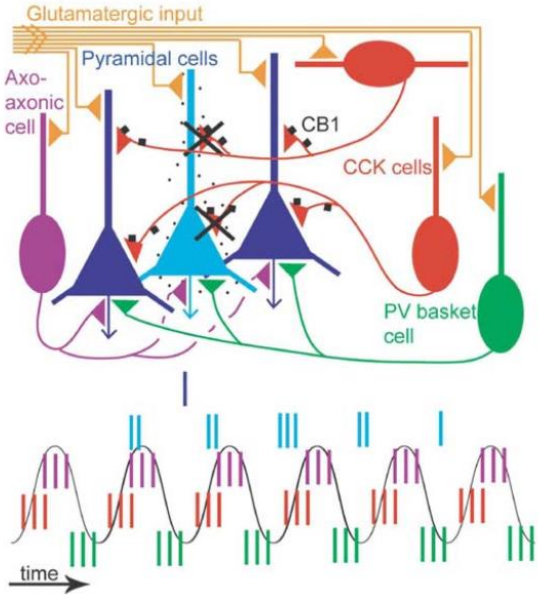

Figure 5 : CCK-expressing interneurons contribute to sparse coding by CA1 pyramidal cells during theta oscillations

"Pyramidal cells receive GABAergic input from PV-expressing basket cells (green) and several types of CCK-expressing cell (red).The PV basket cells fire, on average, before the pyramidal cells fire. The CCK-expressing interneurons fire, on average, at the ascending theta phase, at the same time when pyramidal cells start to fire. Thus, the glutamatergic excitation of pyramidal cells (yellow) must overcome the peak of inhibition by CCK-expressing cells for the cell to start firing. Only CCK-expressing cells have CB1 receptors on their presynaptic boutons (black squares), and when activated, these suppress GABA release.
CCK-expressing interneurons will fire and continue to release GABA to the majority of pyramidal cells, which are silent, keeping a high threshold for activation. In contrast, the other pyramidal cells continue to fire with high frequency as a result of decreased inhibition and increasing excitation. Thus, the specific spike timing of CCK- expressing interneurons during theta oscillations and the expression of cannabinoid receptors on their terminals contribute to increasing the difference in firing between activated and non-activated pyramidal cells". From (Klausberger, Marton et al. 2005).

1.2.2 Dendritic targeting cells (D-T cells)

In contrast to BC, the dendritic targeting cells make synapses onto the dendritic tree of the hippocampal pyramidal cells in both the stratum oriens and the stratum radiatum. In the sparse literature on this cell type, it has also been referred to as Schaffer collateral associated cells (SC-AC) (Evstratova, Chamberland et al. 2011; Camire and Topolnik 2012), apical

dendritic innervating cells (Klausberger, Marton et al. 2005), or bistratified cells (Klausberger, Marton et al. 2004; Tukker, Fuentealba et al. 2007). This chapter will thus review the few studies about dendritic innervating interneurons with the assumption that it reflects one major subpopulation of dendritic inhibitors and referred to as D-T cells in this thesis.

D-T cells are immunopositive for CCK and a part of the population is also immunopositive for Cb (Cope, Maccaferri et al. 2002), thus, they must be generated from the caudal ganglionic eminence (Kepecs and Fishell 2014). However, a PV^+ D-T cell population was also reported and consequently are born from the medial ganglionic eminence (Klausberger, Marton et al. 2004; Klausberger and Somogyi 2008), and are found solely in stratum pyramidal and oriens.

D-T cells have a high input resistance (Ri≈ 480MΩ) (Cope, Maccaferri et al. 2002), have an accommodating firing pattern and possess an I_h current (Evstratova, Chamberland et al. 2011). Additionally, their membrane time course is similar to the CCKBC (τ≈26ms) (Cope, Maccaferri et al. 2002). Consequently, they may have the same large window of input integration as CCKBC. Indeed, D-T cells receive multiple convergent inputs and can contribute to both, FF and FB inhibition (Bartos, Alle et al. 2011).

Regrettably, only the involvement of PV^+ D-T cells has been elucidated during hippocampal oscillations: they fire during the descending phase of theta (Klausberger, Marton et al. 2004), and are the strongest interneuron subclasses recruited during gamma oscillation and thus might be responsible for the membrane oscillation of pyramidal dendrites by promoting gamma-modulated GABA input and synchronize dendritic branches of CA1 pyramidal cells (Tukker, Fuentealba et al. 2007). Additionally, they are very active during SWR (Tukker, Fuentealba et al. 2007).

The behavior of PV^- D-T cells during hippocampal oscillations is less known, but have been touched on in a review by Klausberger (Klausberger 2009). PV^- D-T cells are weakly coupled during gamma oscillations, and fire earlier during the gamma cycles which set a threshold for pyramidal cells. In addition, they fire in the ascending phase of theta oscillation, and could play a role in sparse place coding of pyramidal cells in the CA1 region since these D-T cells also express CB1R as CCKBC.

CCKBC, PVBC and D-T cells are distinct in morphology, inputs and molecular content. Thus, their electrical dendritic input integration also appears different. Another important aspect of differentiation resides in the dendritic calcium signaling integration, which triggers short-term and long-term changes relative to the electrical input integration. However, as it was shown by Tran-Van-Minh, sublinear summation of voltage in cerebellar stellate cells dendrites is concomitant with linear or supralinear calcium transient summation in response to synchronous activation of synaptic input located on the same dendritic branch (Tran-Van-Minh, Abrahamsson et al. 2016). Consequently, not only the electrical input integration of a neuron would affect its output but also its calcium signaling mechanisms.

1.3 Calcium: an important signaling molecule

Calcium is an important second messenger involved in numerous mechanisms in the brain, and can have opposing effects such as cell apoptosis (Mattson and Chan 2003), or synaptic plasticity leading to strengthening of various synapses (Cummings, Mulkey et al. 1996).

In the past decades, intracellular calcium has been recognized to be crucial for plasticity, and there is cumulative evidence that excitatory and inhibitory neurons can have multiple dendritic calcium signaling mechanisms (Kullmann and Lamsa 2011). This efficacy of dendritic calcium mechanism is spatially regulated (Goldberg, Tamas et al. 2003; Goldberg and Yuste 2005) on different time scales, and as it is reviewed by Evans, different calcium amplitude, duration and location, promote distinct downstream calcium signaling cascades leading to either long term potentiation (LTP) or long term depression (LTD) (Evans and Blackwell 2015). Consequently, to exert a control on calcium signaling, cells must chelate, thus compartmentalize, and extrude calcium (Clapham 2007).

The life cycle of calcium within a cell begins from the opening of calcium channels either with ligand binding or membrane depolarization. Free calcium enters the cell cytoplasm which produces an increase in calcium concentration that constitutes a calcium signal (Berridge, Lipp et al. 2000). Additionally, intracellular calcium mobilizing signals, generated by stimuli through various cell receptors (coupled to protein G), can be part of calcium life cycle (for review see Berridge, Lipp et al. 2000).

Once entered, free calcium interacts and binds with different sensor molecules within the cell compartments. This free and bound calcium refers to the total calcium, but only in its free state, can calcium acts on other proteins inducing conformational change leading to

subsequent calcium signaling cascades. Eventually, calcium ends up being extruded via extrusion machinery (Berridge, Lipp et al. 2000).

Accordingly, temporal and spatial restriction of a cell's calcium signaling is mediated by calcium entries, endogenous and exogenous buffers, extrusion mechanisms, and dendrite geometries (Augustine, Santamaria et al. 2003), and are the mechanisms further detailed in the following sections.

1.3.1 Dendritic calcium entry in neurons

Calcium can arise from three main sources: glutamate receptors (NMDA and AMPA), voltage gated calcium channels (VGCC) and release from the internal stores.

Calcium can be released by the endoplasmic reticulum or by mitochondria with the so called calcium induced calcium release mechanism. However, since the calcium induced calcium release has a slow time scale (range of second), this mechanism won't be emphasized in this thesis (see review Laude and Simpson 2009)

Most of the literature has investigated dendritic calcium signaling in excitatory cells; however as this project focuses on interneurons, particular attention will be on inhibitory neurons with the benefit of studies from excitatory cells where information is lacking for interneurons.

1.3.1.1.1 Glutamatergic and ionotropic receptors

NMDAR and non NMDAR are found in the dendritic shaft of different neuron subclasses (Higley and Sabatini 2008), and additionally, AMPAR permeable to calcium have been characterized in interneurons. Unfortunately, few studies have fully investigated the presence and distribution of AMPAR and NMDAR in interneurons. In pyramidal cells, only NMDAR have been shown to mediate calcium entry upon synaptic stimulation (Sabatini, Oertner et al. 2002), and Koh's study in 1995 showed a similar NMDA component in BC of the DG (Koh, Geiger et al. 1995). However, in addition to NMDAR, BC from the DG contain AMPAR that are permeable to calcium, which are not present in pyramidal cells (Geiger, Melcher et al. 1995). This finding was also reported by Goldberg's study where he investigated three cortical interneuron subtypes and found that AMPAR and, to a small extent NMDAR, contribute to dendritic calcium entry in PVBC. The contribution of AMPAR to calcium entry in the two other interneuron subtypes (calretinin-positive irregular spiking cells and adaptive cells) studied was less or non-existent, suggesting that each interneuron subtype might have different calcium entry sources (Goldberg, Yuste et al. 2003). Studying the CA1 fast- spiking BC, Camiré and Topolnik in 2014 also showed the requirement of calcium

permeable AMPAR (60-80%) for dendritic calcium entry and a small portion from NMDAR (Camire and Topolnik 2014). Thus PVBC, although studied in different hippocampal regions, seem to rely on the same major calcium entry source: calcium permeable AMPAR.
Finally, uncaging glutamate onto the dendritic tree of stratum radiatum interneurons established a high density of glutamate receptors in distal dendrites, with less present in proximal dendrites (Pettit and Augustine 2000).

In addition to inducing calcium entry, AMPAR activation, calcium permeable or not, depolarizes the dendrite membrane, thereby activating NMDAR, but also VGCC which are another calcium entry source.

1.3.1.1.2 Voltage gated calcium channels

Voltage gated calcium channels activate upon membrane depolarization and mediate calcium entry in cellular compartments. Their structure and regulation are too varied to be detailed in this thesis (for review see Catterall 2000). Instead, VGCC distribution in interneurons will be the major point developed here.
VGCC distributions have been studied first in cultured cortical interneurons. L- and R-type calcium channels, which are high-threshold activation channels, were located in the somato-dendritic region and were absent in the presynaptic terminals. In contrast N-type calcium channels, another high voltage threshold channel, are solely located in presynaptic terminals of cortical interneurons. Finally the A isoform of P/Q-type calcium channels, also a high voltage activated channel, is expressed in the somato-dendritic region but the B isoform is only located in the terminals (Timmermann, Westenbroek et al. 2002).
The VGCC distribution in interneurons was extended by Vinet in 2006, where they coimmuno-labeled subpopulations of interneurons with L-, N-, T- and P/Q-types channel antibodies. Interestingly, P/Q-type and T-type calcium channels are expressed in all interneuron subtypes, while L-type calcium channels are more expressed in PV negative interneurons, and N-types are expressed in all interneurons except Calbindin positive ones (Vinet and Sik 2006).
More specifically, calcium entry in CCKBC, PVBC and D-T cells has been studied upon synaptic input. CCKBC and D-T cells' calcium entry is in the majority (70%) from L-type calcium channels. However, 30% is mediated by T-type channels in D-T cells but only 20% in CCKBC. Finally, it seems that P/Q-type channels play a role in synaptic calcium entry in CCKBC but not in D-T cells (Evstratova, Chamberland et al. 2011).

Camiré's study reported a low proportion of L-type channels for calcium entry in CA1 PVBC, which is mainly mediated by calcium permeable AMPAR (Camire and Topolnik 2014).
Interneurons rely on different VGCC for dendritic calcium entry, however the actual distribution of VGCC subtypes through their dendritic tree have not been investigated so far though this information will give hints as to the likelihood of calcium signaling integration in the dendrite arbor of interneurons.

1.3.2 Endogenous buffering capacity and diffusion environment

1.3.2.1 Endogenous buffers: the right component to shape the spatiotemporal aspect of calcium signaling

The buffering capacity (kappa, κ) of a cell is defined as the ratio of calcium bound for each free calcium ion. Thus the buffering capacity is the consequence of calcium binding to protein partners. Considering a model of free calcium diffusion (without buffer), Nowycky emphasized that free calcium diffusion is only limited by the calcium influx rate and its diffusion properties. At equilibrium between influx and extrusion, free calcium concentrations would reach too high concentration, causing calcium precipitation and crystal formation within the cell which ultimately should lead it to apoptosis (Nowycky and Pinter 1993). Therefore endogenous buffer is required for regulating calcium amplitude and diffusion, thereby decreasing its free concentration.

Strictly speaking, calcium buffer does not act as a true chemical buffer. Indeed at rest, a neuron has a free calcium concentration of 20 to 150 nM, however most calcium binding protein's K_d is almost one order of magnitude larger: from 200 nM to 1.5 µM (see table from Schwaller 2010), Thus, when a neuron is at rest, most of the calcium binding proteins are in a free state (unbound to calcium) and ready to bind calcium whenever calcium increases.

Distinct factors influence the efficacy of an endogenous buffer to modulate the spatiotemporal aspect of calcium signaling. The first parameter is the forward rate constant (k_{on}) which determines how fast the calcium buffer is going to bind calcium. The second parameter is the buffer's intracellular concentration. The third one is its affinity for calcium determined by the kinetics of calcium binding and release (k_{off}), and the last one is the buffer's intracellular mobility (Schwaller 2010). In addition, the free calcium concentration of a cell at rest is considered to be 20-150nM, and influences the availability of calcium binding sites by determining the occupancy of any given buffer.

By varying k_{on} in a model system, Nowycky demonstrated its importance as a dominating factor in determining calcium entry peak amplitude. However, at equilibrium the affinity of calcium buffer for calcium is the main determinant of free calcium concentration (Nowycky and Pinter 1993).

Buffering capacity measurements were first established in chromaffin cells by Neher and Augustine in 1992, and were further expanded by Zhou and Neher in 1993 (Neher and Augustine 1992; Zhou and Neher 1993). This model, however only included slow endogenous buffer. The rapid buffer assumption was then added to the model a year later (Wagner and Keizer 1994).

Two methods of endogenous buffer determination have been established; the first one is based on the loading time constant of calcium dye within the cytoplasm of a single cell, whereas the second one uses the added exogenous buffer approach, thus involving different cells for the determination of the buffering capacity ((Neher and Augustine 1992; Helmchen and Tank 2011)

Since then, many researchers have attempted to assess the cells' buffering capacity which varies among neurons. For instance pyramidal cells of the CA1 region have an endogenous buffering capacity of approximately 60-200 (Helmchen, Imoto et al. 1996; Lee, Rosenmund et al. 2000; Liao and Lien 2009), while interneurons display a larger buffering fraction 30-350 (Lee, Rosenmund et al. 2000; Kaiser, Zilberter et al. 2001; Aponte, Bischofberger et al. 2008; Liao and Lien 2009; Evstratova, Chamberland et al. 2011; Matthews, Schoch et al. 2013) and to a greater extent Purkinje cells have about 2000 (Fierro and Llano 1996).

By their different intracellular mobility, calcium binding proteins can be divided in two subcategories: mobile and immobile yielding two subclasses of endogenous buffers, which are present in different proportion within neurons.

The previously mentioned buffering capacity of neuronal subpopulations were measured at different loading times of the cells and thus, in general, did not account for the possible washout of mobile calcium binding proteins (Muller, Kukley et al. 2005; Matthews, Schoch et al. 2013). Therefore, the buffering capacity measurement might be underestimated, especially in neurons expressing mobile calcium binding proteins. It is worth noting that a difference in proportion of mobile or immobile endogenous buffers implies distinct modulation of calcium diffusion, since the mobile buffer accelerates the diffusion while the immobile buffer retards the diffusion (Sala and Hernandez-Cruz 1990; Nowycky and Pinter 1993; Zhou and Neher 1993; Goldberg, Tamas et al. 2003; Matthews, Schoch et al. 2013; Delvendahl, Jablonski et

al. 2015). Thus, mobile and fixed buffers permit the cell to differently manipulate calcium diffusion which ultimately will allow it to exert different calcium signaling integration.

1.3.2.1.1 Immobile buffer

The physical definition of an immobile buffer is that its coefficient of diffusion is 0 $\mu m^2/s$ (Matthews and Dietrich 2015). Practically, this immobile fraction does not wash out over long period of recordings.

Not much is known about the identity of the immobile buffer found in neurons, or its features like k_{on}, k_{off}, and affinity. Neher's studies have demonstrated in chromaffin cells that only a fixed buffer was present, and estimated it to have low calcium affinity because this fixed buffer was not saturated with a range of 1-3µM calcium (Neher and Augustine 1992; Zhou and Neher 1993). Considering that k_{on} is the predominant factor to compete with other buffers (Nowycky and Pinter 1993), fixed endogenous buffer must be fast enough to compete with typical exogenous buffer: BAPTA, EGTA or calcium dyes used in experiments to assess the endogenous buffering capacity (Markram, Roth et al. 1998). k_{on} of the immobile endogenous buffer has been measured in chromaffin cells and is indeed fast: $1.07X10^8$ M^{-1} (Xu, Naraghi et al. 1997) and was estimated at $1.3X10^9$ M^{-1}/s in Lumpkin study to match their findings of fixed buffer in hair cells (Lumpkin and Hudspeth 1998). Finally, because of the relationship between affinity, and the kinetics of calcium binding and release, the k_{off} of the fixed buffer must be very fast to yield its low affinity, and was estimated at $283s^{-1}$ (Lumpkin and Hudspeth 1998).

Few indications are available in the literature of the identity of the immobile endogenous buffer measured in cells. Neher and Augustine stated the hypothesis that annexin 2 might be a good candidate (Neher and Augustine 1992). Indeed, annexin 2 is a protein that binds to membrane phospholipids and has a low affinity for calcium. It is found in many neurons types, both excitatory and inhibitory. Similarly, Tillotson's study reported stronger calcium buffering near the membrane in comparison to the middle of aplysia neurons (Tillotson and Gorman 1980; Tillotson and Gorman 1983) and thus might confirm that proteins and phospholipids anchored to the plasma membrane are good candidates for the fixed buffer. In addition, calcium dependent channels like potassium channels may also account for a fixed endogenous buffer since they have a low affinity for calcium (5-10µM) (Fakler and Adelman 2008). As another buffer, nucleic acid has been suggested to buffer calcium with a very low affinity (Baylor and Hollingworth 1998). Consequently, all of these mixed components may

be part of the fixed buffer pool measured in cells, and so, fixed buffer may be a heterogeneous population; however no study has so far deeply investigated this matter.

1.3.2.1.2 Mobile buffer

By contrast, mobile buffers have been well studied, and considered to have a coefficient of diffusion > 0 µm²/s. The mobile buffers belong to the large EF family protein which contains both pure calcium buffers and calcium sensors. Only the term mobile buffer is applied to a small subset of calcium binding protein from the EF family (**Figure 6**) including parvalbumins (PV; alpha and beta isoforms), calbindin-D9k (Cb-D9k), calbindin-D28k (CbD28k), and calretinin (CR) (Schwaller 2010). Mobile buffer are different from calcium sensors, which upon calcium binding will undergo a conformational change. Nevertheless, some calcium buffers may also act as "calcium sensors", such as calretinin (Schwaller 2010).

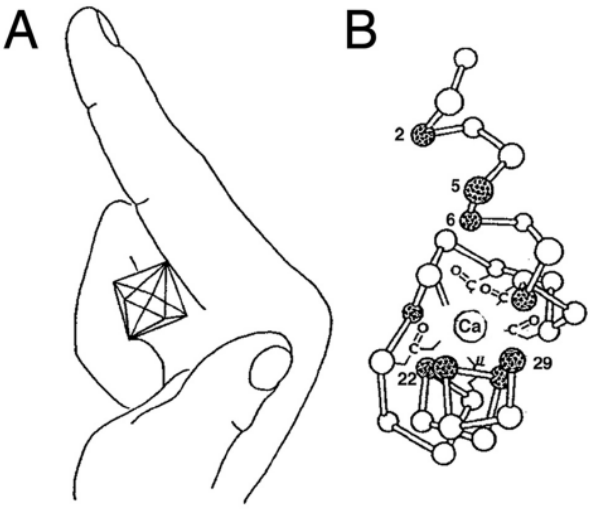

Figure 6 : EF-hand domain motif
(A) "The three-dimensional structure of the EF-hand motif can be visualized by the right hand: the index finger represents the E-helix (residues 1–10), the bent middle finger stands for the 12 amino acids of the canonical $Ca2^{+}$-binding loop (10–21), and the thumb signifies the F-helix (19–29). The seven oxygen ligands coordinating the $Ca2^{+}$ ion are located at the seven corners of a pentagonal bipyramid
(B) X-ray structure from the EF-domain of carp parvalbumin"
from (Schwaller 2009)

PV possesses three types of EF hands (**Figure 6**) but only two are functional and bind calcium. The two EF domains have particular affinities for magnesium and calcium, with a higher affinity for calcium than magnesium. Under basal conditions, PV binding sites are occupied by magnesium. Thus the on-rate of calcium will be determined by the off-rate of magnesium, meaning that in the absence of magnesium the on-rate of calcium should be faster. However in the cell, the magnesium concentration is about 0.5-1mM, thus PV's k_{on} for calcium will be slow, two orders of magnitude slower than fixed buffer, PV is therefore considered a slow calcium buffer (Schwaller 2009; Schwaller 2010).

Calretinin (Cr) contains five calcium biding sites, and one of which has a low affinity (EF5) (Schwaller, Durussel et al. 1997). The four other binding sites work in an allosteric manner,

meaning than upon increase in intracellular calcium concentration, Cr's k_{on} will increase. Thus two states can be distinguished: a tense state (T) were the intracellular calcium is not elevated, when Cr has a slow binding and a low affinity; and a relaxed (R) state with fast binding and an increased affinity (Schwaller 2009). Another characteristic of Cr is a decrease in its mobility when bound to calcium, and thus may be considered as an immobile buffer once bound to calcium (Arendt, Schwaller et al. 2013).

Calbindin D28k (Cb) has four binding domains for calcium which also have an affinity for magnesium, and can be separated in high (H) and medium (M) affinities sites. An increase in cooperativity occurs upon calcium binding leading to a fast k_{on} for calcium, and so Cb is considered as a fast mobile buffer.

Although Cb is assumed to be mobile, its interaction with other membrane proteins can immobilize it, as it was shown in dendrites and spines, but not in axon of Purkinje neurons (Schmidt, Schwaller et al. 2005).

	Parvalbumin (PV)	**Calbindin-D28k (Cb)**	**Calretinin (Cr)**
Kon Ca2+ (µM-1/s)	3-10	Hsite: 12 Msite: 82	2 T site:1.8 2 R site: 310 Site EF5: 7.3
Koff Ca2+ (s-1)	0.9-1.3	Hsite: 2-3 Msite: 34-42	T state:50 R state: 20 Site EF5: 260
Affinity (µM)	0.7-0.15	Hsite: 0.18-0.24 Msite: 0.41-0.51	T state:28 R state: 0.68 Site EF5: 1.4
Mobility (µm2/s)	12-43	20	2.2
Concentration (µM)	0.8-70.6	20-47	60-80

Table 1 : Mobile endogenous buffer's characteristics
Values taken from (Muller, Kukley et al. 2005; Schmidt, Schwaller et al. 2005; Schwaller 2009; Arendt, Schwaller et al. 2013)

1.3.2.2 Interaction between mobile and immobile buffer on calcium diffusion

As for the resting calcium concentration, the concentration of fixed and mobile buffers influences the calcium peak amplitude, free calcium availability and calcium diffusion. Similarly, adding more fast buffer reduces the peak of calcium entry and also increases the redistribution phase of calcium (Sala and Hernandez-Cruz 1990).

As was pointed out previously, the forward rate (k_{on}) is the factor that mostly determines the calcium's buffer partners upon calcium entry. Thus as fixed buffer has the fastest $k_{on,}$ it is most likely the first to bind calcium upon calcium entry. As it was modeled by different groups, fixed buffer retards the diffusion of calcium and leaves a substantial plateau of free calcium after calcium entry termination, when it is the only buffer present (Nowycky and Pinter 1993; Markram, Roth et al. 1998; Matthews, Schoch et al. 2013; Matthews and Dietrich 2015). This plateau of calcium could serve as a facilitation paradigm when a following calcium entry occurs and/or may serve as a second calcium source when calcium would be released from its bound partner (Sala and Hernandez-Cruz 1990; Nowycky and Pinter 1993).

When a mobile buffer is added to the system, calcium diffusion is facilitated and will depend on the mobility and amount of the mobile buffers (Goldberg, Yuste et al. 2003; Goldberg and Yuste 2005). Thus the mobility of the buffer determines the time course of calcium redistribution (Sala and Hernandez-Cruz 1990).

As mentioned in **Table 1** mobile buffers like PV with a slow k_{on} compared to fixed buffer are not fast enough to catch fast calcium influxes (Markram 1998). This mobile buffer should not have a great influence on the calcium entry peak amplitude but instead increase the diffusion of calcium away from the entry source. However an interesting fact for PV is its occupancy by magnesium (see section **1.3.2.1.2**). Thus PV, at the cell resting calcium concentration, is mostly bound to magnesium (80-90%) and only 10% is in a free state (Eggermann and Jonas 2012). Consequently this 10% of free PV binds calcium, but is quickly saturated. In the meantime, a subsequent amount of magnesium bound to PV is released and thus the pool of unbound PV is continuously renewed giving the potential for PV to have an anti-facilitating effect on neurotransmission within a nanodomain (Eggermann and Jonas 2012). As a consequence, PV will only accelerate the decay of the calcium transient during the first 300ms and only slightly affect the rapid kinetics of calcium transients in Purkinje cells (Schmidt, Stiefel et al. 2003).

The k_{on} of Cb is one magnitude higher than PV (**Table 1**), indicating the possibility for Cb to influence the calcium peak amplitude. As a confirmation of this assumption, Purkinje cells lacking Cb were shown to have an increase in their calcium peak amplitude induced by climbing fiber stimulation in comparison to the wild type cells, indicating that Cb acts as a fast, high affinity calcium buffer (Airaksinen, Eilers et al. 1997; Schmidt, Stiefel et al. 2003).

Cb is mobile in dendrites but has been shown to be immobile in spines and dendrites and so might also account for fixed buffer in some cases (Schmidt, Schwaller et al. 2005), similar to Cr which undergoes a reduction of its mobility when bound to calcium (Arendt, Schwaller et al. 2013).

As mitochondria are mobile and take up calcium, it might be considered that they serve as a mobile buffer, however as it is well demonstrated in Matthews review, the kinetics of mobile endogenous buffer highlighted so far are much faster that mitochondria's calcium on-rate (Matthews and Dietrich 2015).

As a consequence of their protective role in limiting cellular calcium overload, PV, Cb and Cr deficiency have been associated with epilepsy and Alzheimer disease in both animal models and humans (Heizmann and Braun 1992; Schwaller, Tetko et al. 2004; Schwaller 2009).Furthermore, neuron's fixed buffer has been observed dysregulated in concomitance with calcium entry with aging (Khachaturian 1994; Oh, Oliveira et al. 2013).

A last determinant of calcium diffusion is the geometry of cellular compartments. For instance, Schmidt evaluated the diffusion of PV depending on the cell compartment, and demonstrated that in dendrites the diffusion is slower (12µm^2/s) than in the soma or axons (43µm^2/s) (Schmidt, Brown et al. 2003; Schmidt, Arendt et al. 2007). This difference was assumed to be due to dendrite tortuosity or cytoplasmic differences within cell's compartments. In addition, decreasing the radius of the dendrite increases the amplitude of calcium, but since the extrusion is also scaled with the surface-to-volume ratio, this excess of calcium should not diffuse to adjacent sites. Another compartment of interest is spines, which serve as a natural spatial restriction for calcium signal (Sabatini, Maravall et al. 2001). As interneurons are mostly aspiny, such simple physical restriction of calcium signal is not possible. As a consequence, interneurons may have to rely on other mechanisms to spatially restrict calcium.

1.3.3 Calcium extrusion mechanisms

The life cycle of intracellular calcium terminates by clearing the free calcium from the cytoplasm. Two extrusion mechanisms allow a cell to clear calcium from its cytoplasm: the plasma membrane ATPase (PMCA) and the sodium/calcium exchanger (NCX).

PMCA works in 1:1 calcium to ATP stoichiometry. PMCA is regulated by calcium concentration and is in an inhibited and low affinity state when calcium concentration is in 50-100nM range. Additionally, PMCA works in cooperation with calmodulin, a sensor for

calcium, which has four calcium binding site with an affinity of 2-50nM (Strehler and Treiman 2004). The effect of calmodulin is to, upon binding, increase the PMCA affinity for calcium to 0.1-1µM (20µM without calmodulin) (Carafoli 1992; Caride, Filoteo et al. 2001; Strehler and Treiman 2004). Therefore PMCA are believed to have a "housekeeping" function within a cell (Brini and Carafoli 2011) with a dependence on the intracellular calcium concentration (Sedova and Blatter 1999; Caride, Filoteo et al. 2001; Wanaverbecq, Marsh et al. 2003).

The NCX uses the electrochemical gradient of sodium and calcium (3:1). NCX have much higher clearance rate (10 fold more than PMCA) but a lower affinity (1-10µM) for calcium in comparison to the PMCA and so are the first source of calcium clearance upon large calcium entry (Blaustein and Lederer 1999; Brini and Carafoli 2011).

As a last uptake system, the endoplasmic reticulum and the NCX of mitochondria play a role as well in calcium clearance from the cytoplasm by sequestrating it, leading the intracellular calcium concentration to return to its basal level (Brini, Bano et al. 2000; Carafoli, Santella et al. 2001). Additionally, 30% of the calcium clearance is orchestrated by the SERCA pumps in spines of the pyramidal cells, but almost no calcium buffer is present in spine and so might facilitate the uptake by the endoplasmic reticulum (Sabatini, Oertner et al. 2002).

1.3.4 Role of calcium in plasticity and neuron excitability

It is believe that learning and neuronal circuits formation critically depend on long-term modifications (Sjostrom, Rancz et al. 2008). These long term modifications take several forms of plasticity, either a long-term potentiation (LTP) or depression (LTD) or short-term transformation of synaptic activity. Synaptic plasticity was first shown to occur in excitatory cells (Bliss and Lomo 1973) but interneurons also express some forms of plasticity (Losonczy, Zhang et al. 2002). Dendrites of cells appear to be one of the major constituent to sustain plasticity by receiving, computing and integrating inputs. Consequently, dendrites will undergo possible changes.

Another form of plasticity, non-synaptic, involves modifications of ion channels and so alterations of the intrinsic excitability of a neuron. As a consequence distinct integration of inputs can occur, thereby increasing or decreasing input propagation, spike generation and synaptic integration (Sjostrom, Rancz et al. 2008).

As a powerful second messenger, calcium is involved in both synaptic plasticity and non-synaptic plasticity, which is the topic of the two next sections.

1.3.4.1 Calcium induced plasticity

Postsynaptic calcium influx through calcium permeable AMPAR upon high frequency stimulation results in LTD in stratum radiatum interneurons, but constantly produces LTP in principal cells due to their NMDAR (Bartos, Alle et al. 2011). The same high frequency stimulation which induces LTP in PVBC, has no effect on plasticity in CCKBC and produces LTD in PV^+ D-T cells (Nissen, Szabo et al. 2010) which clearly emphasizes the cell type specific machinery for plasticity induction.

Interestingly, a short term plasticity has been associated with a potentiation of L-type calcium channels through glutamatergic receptor activation (Topolnik, Chamberland et al. 2009) and thus should be specific to a certain interneuron subpopulation, since CCKBC, PVBC and D-T cells have different VGCC. Additionally, the differential distribution of VGCC was reported in DG PVBC to induce plasticity only in basal dendrites and not apical dendrites, which correlated with a poor propagation of bAP and the absence of VGCC in basal dendrites (Hu, Martina et al. 2010; Bartos, Alle et al. 2011).

Thus dendritic Ca^{2+} signaling evoked by the bAP plays a role in the induction of several forms of synaptic plasticity in interneurons (Perez, Morin et al. 2001; Lei and McBain 2002; Lapointe, Morin et al. 2004; Lamsa, Irvine et al. 2007; Lamsa, Heeroma et al. 2007). In addition, bAP-induced calcium transients (bAP-CaT) lead to dendritic calcium accumulation and have been reported to cause depression of IPSPs in pyramidal cells, which was prevented by loading the post-synaptic pyramidal cell with calcium chelator (Zilberter 2000). Consequently, bAP-CaT may be shaped by endogenous buffering capacity, which, as was previously mentioned (**1.3.2.1**), happens to be larger in interneurons than in pyramidal cells (Lee, Rosenmund et al. 2000; Kaiser, Zilberter et al. 2001; Goldberg, Tamas et al. 2003; Aponte, Bischofberger et al. 2008) and so might explained the high bAP-CaT in pyramidal cells (Stuart, Spruston et al. 1997) in contrast to interneurons (Kaiser, Zilberter et al. 2001; Aponte, Bischofberger et al. 2008; Evstratova, Chamberland et al. 2011; Camire and Topolnik 2014).

A bAP is additionally required for spike timing dependent plasticity (STDP), which involves a coincidence detection of synaptic input and somatic action potentials (Caporale and Dan 2008). This form of plasticity is dependent on calcium signaling integration from two distinct sources (Tigaret, Olivo et al. 2016), and so is a good example of how a neuron's specific calcium machinery (calcium entry source(s), endogenous buffer, and extrusion mechanism) sets the conditions for plasticity.

1.3.4.2 Calcium activates calcium dependent channels required for intrinsic excitability

In neurons, an AP is followed by an after hyperpolarization (AHP) component, important for regulating neuronal excitability through modulation of AP frequency (Dumenieu, Fourcaud-Trocme et al. 2015)

This AHP is mediated by calcium dependent potassium channels; Small conductance potassium (SK) and Big conductance (BK) channels. The SK channels cause (part) of the medium AHP, and the BK channels induce (most) of the fast AHP (Sah and Faber 2002).

Those channels require a rise in intracellular calcium and, in the case of BK channels an additional membrane voltage depolarization (Sah and Faber 2002). By chelating the intracellular calcium, Faber demonstrated the close proximity of SK channels with their calcium source (200nm) (Faber, Delaney et al. 2005), which may connect the endogenous buffer to the organization of a tight spatial extent of free calcium.

SK channels' calcium sources are distinct depending on cell types: L-type VGCC in hippocampal pyramidal neurons (Tonini, Ferraro et al. 2013) or NMDAR in amygdala pyramidal cells (Faber, Delaney et al. 2005) but the internal store is not considered as a calcium source for these channels (Herrera and Nelson 2002).

Through their activation by calcium, SK channels exhibit the ability to regulate postsynaptic calcium influx in neurons by a negative feedback loop causing the inhibition of NMDAR (Bloodgood and Sabatini 2007) and thus reducing the calcium influx. Consequently, when SK channels are inactivated by metabotropic glutamatergic receptor activation or muscarinic receptor activation (**Figure 7**), the AHP component is converted into an afterdepolarization (ADP) component, which ultimately leads to an increase in intrinsic excitability and a possible subsequent LTP (Park, Remy et al. 2010; Park and Spruston 2012; Tigaret, Olivo et al. 2016).

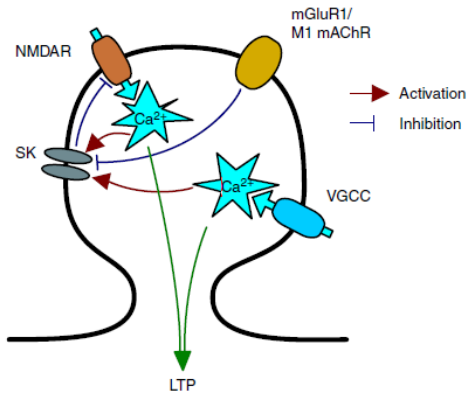

Figure 7 : mGluR1/M1 mAChR regulate spine Ca^{2+} transient via inhibition of SK channels

"mGluR1 or M1 muscarinic receptors inhibit SK channels, which removes a negative feedback regulation of NMDARs within dendritic spines thereby enhancing Ca^{2+} influx. Facilitated Ca^{2+} influx through NMDARs and Ca^{2+} influx through VSCCs are both required for the induction of LTP by STDP". From (Tigaret, Olivo et al. 2016)

1.4 Modulation of calcium signaling by cholinergic drive

As mentioned in **1.1.2.2**, theta oscillation is generated in the hippocampus by a cholinergic drive sent from the medial septum-diagonal band of Broca to the hippocampus (Cobb and Davies 2005; Alger, Nagode et al. 2014).

As shown in **Figure 7**, a close interaction between muscarinic receptor activation and changes in neuronal intrinsic excitability through calcium signaling has been suggested (Nagode, Tang et al. 2011; Park and Spruston 2012; Tigaret, Olivo et al. 2016).

Distinct muscarinic receptors (M1 to M5) coupled to G proteins are present within several interneurons. For instance, CCKBC express M1 and M3 receptors in the soma and proximal dendrites, while PVBC express mostly M2 receptors (Armstrong and Soltesz 2012). M1 and M3 receptors are coupled to a Gq protein which leads to an activation of the IP3 signaling pathway, whereas M2 receptor is coupled to a Gi protein which inhibits the cAMP pathway (Cea-del Rio, Lawrence et al. 2011; Nagode, Tang et al. 2011; Cea-del Rio, McBain et al. 2012). Upon cholinergic drive activation, CCKBC undergo a change in intrinsic excitability specifically via M3 receptor activation (Cea-del Rio, Lawrence et al. 2011). Additionally, M1 and M3 receptor activation are required for the conversion of an AHP into an ADP (Cea-del Rio, McBain et al. 2012). Since PVBC only express M2 receptor, they are not suited to undergo any intrinsic excitability change upon cholinergic activation (Bell, Bell et al. 2015) which again reflects the distinct role these perisomatic inhibitors exhibit in controlling excitatory neurons.

The mechanism underlying the increase in intrinsic excitability by M1 and M3 receptor activations was resolved in a specific interneuron called Oriens Lacounosum Molecular cells (OLM) (Lawrence, Grinspan et al. 2006; Lawrence, Statland et al. 2006) and pyramidal cells (Tigaret, Olivo et al. 2016) through modulation of the ADP/AHP (Lawrence, Statland et al. 2006; Park and Spruston 2012).

In OLM interneurons, activation of M1 and M3 receptors leads to spontaneous firing (Lawrence, Grinspan et al. 2006). This firing is due to an inhibition of SK current via a G protein activation as well as from NMDAR activation (Lawrence, Statland et al. 2006). This SK pathway mediated change in excitability is not a mechanism implicated in CA1 pyramidal cells' output facilitation (Chen, Benninger et al. 2014).

Extracellular calcium, and VGCC activation, but also another calcium permeable cation channels (probably due to intracellular store) leads to increases in calcium entry upon muscarinic stimulation (Akerman, Shariatmadari et al. 2004). However, more calcium entry

through VGCC does not contribute to the appearance of an ADP in stratum radiatum interneurons upon muscarinic receptor activation, but from extracellular sodium and inhibition of potassium channels (McQuiston and Madison 1999; McQuiston and Madison 1999).

Lastly, nicotinic receptor (α7 subunit) is permeable to calcium and was shown, upon activation, to increase bAP-CaT in stratum interneurons which facilitates the induction of LTP in interneurons (Rozsa, Katona et al. 2008).

Accordingly, it now clearly appears that intracellular calcium is an essential actor of the cholinergic regulation on neuron excitability, which leads to a fine tuning of neurons within hippocampal rhythmogenesis.

2 Aim of the study

Calcium triggers a variety of processes within neurons such as input integration, neuronal excitability and plasticity. To achieve these various functional impacts, it is critical for a neuron to tightly regulate its calcium signal, and so neurons must develop a calcium toolkit to spatially and temporally restrain calcium signal.

Within a cell dendrite, calcium signal is shaped by the calcium sources, the properties and distribution of calcium buffers and by extrusion mechanisms. These parameters, although very important to understand neuron's calcium signaling have not been studied in details in interneurons, despite their major role in generating and maintaining network activity. It is thus still unknown whether interneurons display different calcium handling parameters, and if so whether calcium signaling computation can highlight interneurons diverse roles in hippocampal circuits.

The main objective of this thesis work was to improve the understanding of calcium signal handling on interneurons function within the hippocampal CA1 region. To this purpose, the following aims were addressed:

1) The first goal was to elucidate the elementary mechanisms underlying calcium signaling regulation in interneurons. Three types of interneurons were selected due to their varied morphological features and molecular content: the perisomatic inhibitors of pyramidal cells; both CCK containing and PV expressing basket cells, and a dendritic targeting interneuron. The biophysical parameters determined were the endogenous buffering capacity, the calcium entry, the extrusion and the calcium's diffusion environment.
2) Calcium regulation may lead to a difference in synaptic and somatic input integration. Consequently, as a second aim, we investigated the backpropagation of action potential induced calcium transient (bAP-CaT) in CCKBC, PVBC and D-T cells and considered the effect of endogenous buffers on interneurons bAP-CaT.
3) As a third goal, we wanted to gain insight onto the functional role of calcium signaling within interneurons upon hippocampus network activity. The ultimate objective was to resolve the importance of calcium handling within interneurons for efficient interneurons output responses within the CA1 hippocampal network.

Calcium signaling rule determination would be the first step of understanding how interneurons manage to temporally coordinate and influence the function of the entire hippocampal network.

3 Materials and methods

3.1 Slice preparation

All animal experiments were performed in accordance with the national and institutional guidelines for animal welfare.

Adult male and female mice, postnatal day (P) 28-45, were anesthetized with isoflurane using a gas chamber. Once the mouse was unreactive to foot pinch and air puff on the whiskers, it was quickly decapitated using a guillotine. The brain was rapidly removed from the skull and submerged in cold (4°C) oxygenated (95% oxygen, 5% CO2) artificial cerebrospinal fluid (ACSF) with the following composition (in mM): 87 NaCl, 2.5 KCl, 1.25 NaH2PO4, 7 MgCl2, 0.5 CaCl2, 25 NaHCo3, 25 glucose, and 75 sucrose, pH 7.3(Sigma-Aldrich, Germany).

The cerebellum and the frontal cortex were removed, and the two hemispheres were separated from each other. A last cut was done along the dorsal edge of the cortex and glued on this side to the vibratome plate. Horizontal slices, 300 µm thick, were made from the ventral hippocampus (Microm HM650V, ThermoFisher Scientific). Slices were then incubated at 35°C for 30 minutes, using the previously mentioned ACSF solution. Finally slices were transferred and held at room temperature in an oxygenated (95% oxygen, 5% CO2) solution containing (in mM): 124 NaCl, 3 KCl, 1.25 NaH2PO4, 2 MgCl2, 2 CaCl2, 26 NAHCO3, and 10 Glucose, pH 7.3 (Sigma-Aldrich, Germany). This solution was used for the subsequent electrophysiology recording and imaging experiments.

In a side project, experiments on PCP2RIM4γ wild type (WT) and knock out (KO) mice, 4-6 weeks were performed. To achieve the specific KO of RIM4γ only in Purkinje cells, a floxed *RIM4* mouse, in which the *RIM4* gene is surrounded by two loxP sites, is bred with a PCP2Cre mouse (Jackson Laboratory). Upon Cre recombination the targeted gene, here *RIM4* is not transcript. Thus, solely Purkinje cells will not express RIM4γ, but all other cells in the brain do.

The same procedure was used to anesthetize and sacrificed those mice. In contrast to hippocampal slices preparation, the skull was detached at bregma and pulled apart laterally to avoid any damage on the cerebellum. The brain and cerebellum were then carefully removed from the skull cavity and submerged in cold modified ACSF. Next, the cerebellum was

separated from the brain and glued in a piece of agar for a better slicing procedure. Finally, a cut on the lateral hemisphere was performed, and this subsequent cut part was glued onto the vibratome plate to carry out cerebellar parasagittal slices. Only vermis slices were selected and were 250µm thick. As for hippocampal slices, vermis slices were transferred into a 35°C modified ringer beaker for 30 minutes and held at room temperature with normal oxygenated ACSF for the rest of the experiment.

3.2 Confocal microscope

3.2.1 Patch clamp recording and cell fluorescence visualization

Glass capillaries (0.86x1.50x80mm, science product GmbH, Germany) were pulled on horizontal puller (Sutter, USA) or vertical puller (Narashigi, Japan) to obtain recording pipettes with a resistance ranging from 4 to 6 MΩ. Those pipettes were filled for recordings with the following internal solution (in mM): 130 K-gluconate, 0.5 MgCl2, 5 KCl, 4 NaCl, 4 Na2ATP, and 10 HEPES, osmolarity 290, pH 7.3 adjusted with KOH. 0.5% biocytin, 100µM Tetramethyrhodamine (TMR-biocytin; Invitrogen, ThermoFisher scientific, Germany), and calcium dyes (OGB6F, Fluo4 or OGB1 (4mM stock solution), Invitrogen, ThermoFisher scientific, Germany), to the desired concentration, were added daily to the internal solution. Biocytin was used to determine the interneurons morphology post recording.

A slice was positioned in the submerged chamber of a LSM5 Pascal microscope (Axioskop; Carl Zeiss, Germany) and constantly perfused with oxygenated ACSF for recording and imaging. Fluorescent interneurons were visualized under a 63X 1.0 numerical aperture (NA) objective using a fluorescence lamp band passed filtered at either 450-490 nm for selectively looking at the GFP signal or 530-585 nm to excite the TDtomato signal. GFP positive interneurons were mostly found in stratum radiatum while tomato positive interneurons were located in stratum pyramidal and oriens. Targeted neurons were patched using an NPI current-clamp amplifier (ELC-01X, NPI Electronics GmbH, Germany) and WinWCP (Strathclyde Electrophysiology Software, University of Strathclyde Glasgow) as the acquisition software. Cells electrical signals were amplified at 0.005 V/nA using the NPI current-clamp amplifier (ELC-01X) and post-amplifier (DPA-2FX, NPI Electronic GmbH, Germany), sampled at 2 kHz and low passed filtered at 10 kHz. Few cells were also recorded using a voltage clamp amplifier (NPI Electronics GmbH, Germany).

The liquid junction potential was corrected by setting the amplifier offset to -10mV before the seal formation. A slight positive pressure was applied to the patch pipette; then the targeted

cells were carefully approached. As soon as a dimple on the membrane surface was visible, the positive pressure was released leading to a seal formation between the pipette and the cell membrane (1-10GΩ) in less than a minute.

The pipette capacitance was compensated using the capacity compensation on the amplifier. The cell membrane was carefully disrupted by applying a gentle suction resulting in a whole cell clamp configuration. The bridge balance was compensated in the first minute of the recording, and both bridge balance and pipette capacitance were controlled for stability regularly throughout the experiment.

All of the interneurons recorded were filled with biocytin throughout the experiment (about 45 minutes). Following the end of the experiment, the tissue was fixed and processed for morphological identification, using the axon location.

3.2.2 Confocal calcium imaging setup

Calcium images were captured with Zen 2009 scanning software (Carl Zeiss microscopy, Germany). Prior to imaging recordings, the pinhole, an adjustable iris, was set to 3.5µm (2.3 airy units). The function of the pinhole is to reject the out of focus photons from the sample and thus increase the resolution of the focal plane. Additionally, the photomultiplier tube (PMT) was adjusted for each new cell recorded. The PMT is a sensitive detector that collects photons from the sample. The PMT gain is set directly from the Zen 2009 software for both red and green channels. The higher the gain setting is, the better amplified the signal will be, but also results in an increase in the noise level of the image. The PMT offset, which defines the level of black (background), is also adjusted from the Zen imaging software. To avoid any addition of noise or too low black level, the lookup table of the Zen software was used: the red pixel indicating a too high PMT gain, and blue pixels designating a too low background.

The acquisition of the line scans is represented by different parameters. The first one is the scanning speed defined by the pixel dwell time. The pixel dwell time is the time in which the laser beam stays focused on a single pixel and therefore exciting the sample at that point. It terms of acquisition, the longer the pixel dwell time, the more photons are collected per pixel, and the slower the scan speed will be. Additionally, more bleaching and phototoxic effects are likely to occur for slow pixel dwell time. Thus the pixel dwell time was kept short for the line scan acquisition.

The second parameter is the pixel resolution, which is defined by the resolution and the pixel size (512*512, 1024*1024).Throughout the line scan acquisition the pixel resolution was kept at 512*512, giving us enough resolution without damaging the cell recorded.

Finally, the number of cycles (repetitions) and the line time interval (pause between repetitions) have to be considered for the time scan calculation. Indeed the total line scan is the scan time in addition to the cycle delay. For instance : A line scan with a pixel dwell time of 1.6µs, a pixel resolution of 512, 500 cycles and a line interval of 5ms would give a total scan time of 4.12s ((512*pixel dwell) + interval)* n° of cycles).

The excitation wavelength used for exciting the calcium dyes and TMR was 488 nm (HeNe laser), calcium dyes were collected with a band passed filter at 505-530nm and TMR fluorescence was collected with a long pass filter of 560nm.

Calcium transients were evoked by somatic current injection (0.5ms, 2-2.5 nA) inducing cell action potentials responses or Schaffer collateral stimulation (1ms, 0.1-1mA). Lines scans were set in order to record the change in calcium dye fluorescence when an action potential back propagates into dendrites, or in the case of synaptic stimulation, when the calcium source enters a dendritic portion. Line scans were drawn perpendicularly to the proximal dendrite (on average 13 ± 0.5 µm away from the soma) for the buffering capacity measurement. In the case of the evaluation of bAP-CaT in interneurons, line scans were drawn throughout the dendritic arbor.

Line scans were 500 cycles long with a time interval of 5ms and a pixel dwell of 1.6 to 3.6µs for an elicited calcium transient recording. In the case of spontaneous calcium transient recordings during Cch induced network activity, the line scans were increased to 1000 lines with a time interval of 6ms. Lastly, to avoid any phototoxicity risks, line scans were only repeated after a minimum interval of 30s.

In another set of experiments, calcium transients in Purkinje cells were visualized using OGB1 at 1mM concentration. Their calcium transient was slow enough to detect it via frame images. Thus frame images of the dendritic shaft were recorded with a frame rate of 20Hz (49-64ms per frame) during climbing fiber stimulation. Once the T-series frame was acquired, they were analyzed post recordings with Image J using the ROI tool manager and Igor Pro 7. Whole frames were background subtracted and normalized to the prestimulus image.

3.3 Calcium dye properties

In this thesis all calcium dye used were BAPTA based. BAPTA is a pH insensitive analog of EGTA, and has calcium selectivity in the presence of Mg^{2+} in a mM range concentration.

As it was introduced in **1.3.2.1,** calcium dye, which can be considered as exogenous buffer, have similar parameters like endogenous buffers: k_{on}, k_{off}, affinity and mobility.

BAPTA is a very efficient chelator, indeed its on (k_{on}) and off (k_{off}) rates for calcium are 50-400 times faster than EGTA.

The buffering reaction: where B represents a buffer molecule (here the calcium dye) is given by:

$$[Ca^{2+}] + [B] \underset{k_{off}}{\overset{k_{on}}{\rightleftharpoons}} [BCa^{2+}]$$

The affinity of calcium dyes can be assessed from their k_{on} and k_{off}

Dissociation constant:

$$K_d = \frac{k_{off}}{k_{on}}$$

Thus, the dissociation constant reflects the inverse of the dye affinity. This affinity can be varied by modifying the binding site of BAPTA and so give birth to a wider range of calcium dyes affinities (**Table 2).**

Another important property of calcium dye is its signal to noise ratio, which is represented by the dynamic range of the dye. The **Table 2** below gives the dynamic ranges of calcium dyes used for the subsequent experiment of this thesis. The dynamic range is calculated as the ratio of the fluorescence at 0 calcium (f_{min}) and at saturating calcium concentration (f_{max})

Equation 1

$$Rf = \frac{f_{max}}{f_{min}}$$

If the dynamic range is small, the variation of fluorescence intensity will be hardly appreciable, thus calcium dyes needs to be chosen according to the expected calcium concentration.

	Dye color	K_d (µM)	Dynamic range	Buffering capacity (example of 100µM dye with 100nM $[Ca^{2+}]_r$)
OGB6F	Green	3.1	14-fold	30.3
OGB1	Green	0.170	14-fold	225.9
Fluo4	Green	0.345	100-fold	174.2
Xrhod5F	Red	1.6	50-fold	55.4

Table 2 : Summary of calcium dyes properties

Additionally, based on their K_d, calcium dyes have a distinct buffering capacity. This exogenous buffering capacity is taken into account when using calcium dye in an experiment. As an example, we can see the variation of the buffering capacity of the 4 different dyes used in this thesis. Although 100µM is used of each dye and the resting calcium concentration of a cell is assumed to be 100nM, their buffering capacity varies strongly. The buffering capacity is calculated from the **Equation 2**

Equation 2

$$\kappa = \frac{\partial[\text{Buffer} - \text{Ca}^{2+}]}{\partial\,[\text{Ca}^{2+}]_{\text{rest}}} = \frac{[\text{Buffer}]_{\text{total}}\,\text{K}_\text{d}}{([\text{Ca}^{2+}]_{\text{rest}} + \text{K}_\text{d})^2}$$

And in the case of calcium dyes equation 2 can be rearranged as:

Equation 3

$$\kappa \approx \frac{[B]}{Kd}$$

Finally, according to their K_d, calcium dyes might undergo saturation in conditions of highly elevated calcium. For instance OGB1, with its high affinity, might be more fully bound to calcium depending of the $[Ca2^+]_r$ of a cell and thus be more subject to saturation than a low affinity dye like OGB6F. However, a low affinity dye won't detect small changes in calcium concentration.

Consequently, particular care has to be taken when selecting the calcium dye and concentration as a tool for calcium imaging and calcium signal recordings.

3.4 Analysis of calcium transient signals

As explained in the previous subheading, calcium dyes experience a change in fluorescence upon calcium binding. This subsequent variation of fluorescence is the base of

the analysis of calcium transient signals induced by either somatic or synaptic stimulation. Calcium transient signals were measured as the variation of fluorescence over the baseline fluorescence ($F-F_0/F_0$). The baseline fluorescence is dependent on the $[Ca^{2+}]_r$ and the [dye], so expressing the resulting change in fluorescence via a ratio with the baseline fluorescence allows us to measure the calcium transient signal independent of the [dye], optical path length, excitation intensity and chelator efficiency. Thus comparison is possible among cells. However, the ratio is still dependent on the $[Ca^{2+}]_r$ and the saturation of the dye.

Indeed, in the case of calcium dye saturation, although calcium continues to flow in, no change of fluorescence will be reported, thus leading to an underestimation of the calcium transient's peak amplitude. (Maravall, Mainen et al. 2000)

Another parameter measured from the calcium transient trace is the decay time constant (τ). Calcium transient amplitude decays over time due to extrusion and removal of calcium from the intracellular space, and this decrease in amplitude follows an exponential decay. Thus by fitting an exponential curve into the time course of the transient, τ is determined.

3.5 Theory of the single compartment model, and dendrite diffusion environment

We used the added buffering approach (Neher and Augustine 1992) in the single compartment model to determine the endogenous buffering capacity of our interneurons of interest (**Figure 8**).

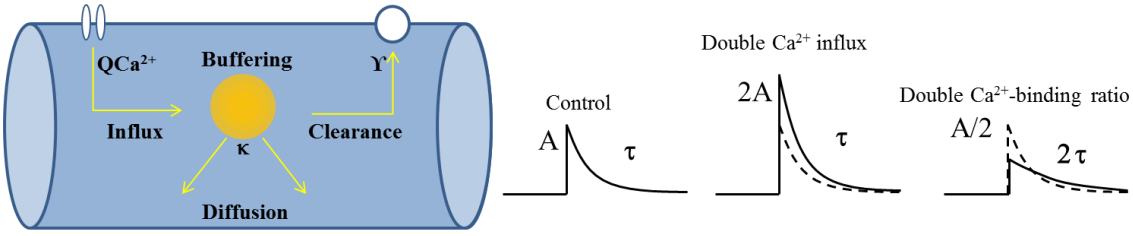

Figure 8 : Single compartment model

Left: The single compartment model considers the dendrite as a closed cylindrical compartment. Calcium, once entered into the dendrite, will be buffered by either endogenous buffers or exogenous ones (calcium dyes), meanwhile the remaining unbuffered calcium will either diffuse or will be extruded via calcium pumps. Moreover, calcium bound to buffer can also diffuse in its bound state.

Right: Theoretical representation of the calcium transient shape when the source of calcium or the calcium binding ratio is doubled. Note, that increasing the calcium influx will only influence the amplitude of calcium signal, while increasing buffer influences both amplitude and decay time constant of the calcium transient.

Abbreviations: A:amplitude, τ: decay time constant, κ: buffering fraction , γ clearance rate

Modified from (Helmchen and Tank 2011)

The buffering capacity of the each interneuron subtype is extrapolated from the kinetic changes of the τ signal produced by adding known and varied amount of calcium dye (either OGB6F, Fluo4 or OGB1).

In the theory of buffered calcium diffusion, we used two assumptions about calcium reaction and diffusion. First of all, we assumed that calcium binding with all buffers was linear. The linearity of calcium binding in the system with respect to free calcium is likely to be correct because free calcium in response to 3 APs (protocol we used) is probably less than 500nM. Additionally, the buffering capacity determination of the CCKBC and the D-T cells used OGB6F which is a low affinity dye (see **Table 2**).

However, Fluo4 was used in the case of PVBC buffering capacity determination. Fluo4 has a much larger affinity than OGB6F, but the fluorescence response was linear with the increment of 1, 3 and 5 action potential protocols (**Figure 20**) which make us confident that no saturation of Fluo4 occurred in the experiments where we determined buffering capacity with 3APs. Second of all, we assumed that the buffers and calcium are in equilibrium at the start of the transient decay.

The calcium binding ratio of a buffer at resting calcium concentration is given by (Neher and Augustine 1992, Wagner and Keizer 1994): **Equation 2**. Different dye concentrations, contributing known amounts of exogenous buffering capacity were used to measure the τ of Ca^{2+} transients from 3 APs. By plotting the known buffering capacity given by the dye versus the decay time constant (τ), the endogenous buffering capacity (κ_{endo}) can be extrapolated. This linear relationship is described by:

Equation 4

$$\tau = \frac{1}{\gamma}\left(1 + k_{dye} + k_{endo}\right)$$

where γ is the extrusion rate of the cell.

This relationship was used to extrapolate the endogenous buffering capacity of the 3 interneurons of interest. ΔF/F measures could also be used to determine the endogenous buffering capacity,

Equation 5

$$\frac{1}{\Delta[Ca^{2+}]_{free}} = \frac{1}{\Delta[Ca^{2+}]_{total}}\, k_{dye} + \frac{1 + k_{endo}}{\Delta[Ca^{2+}]_{total}}$$

but as it is explained in the subheadings **3.3** and **3.4**, ΔF/F is dependent on the $[Ca^{2+}]_r$ of the cell and is more sensitive to underestimation due to saturation. Consequently, we only used τ to assess the endogenous buffering capacity of CCKBC, PVBC and D-T cells.

The theory of buffered calcium diffusion was used for extending the findings on the buffering capacity to the general diffusion environment of the dendrite. Once the buffering capacity had been determined, another parameter can be considered: the apparent diffusion of calcium (D_{app}) which describes how rapidly both free and buffer-bound calcium ions (assumed to be in equilibrium) diffuse in dendrites.

D_{app} in a mixed endogenous buffer is given by:

Equation 6

$$D_{app} = D_{Ca^{2+}} \frac{\left(1 + \frac{D_m}{D_{Ca^{2+}}} k_m\right)}{(1 + k_m + k_f)}$$

Where D_{Ca}^{2+} is the diffusion coefficient of free calcium in the cytosol D_{Ca}^{2+}= 223 $\mu m^2/s$ (Allbritton, Meyer et al. 1992), D_m is the diffusion coefficient of mobile buffer, and κ_m and κ_f are the calcium binding ratio of mobile and fixed buffers respectively.

But in the case of no mobile endogenous buffer, **Equation 6** can be simplified as:

Equation 7

$$D_{app} = D_{Ca^{2+}} \frac{1}{(1 + k_f)}$$

Because fixed and mobile endogenous buffers are in the denominator of these equations, the experimentally determined values predict that fixed buffers as well as the mobile buffer in CCKBC, PVBC and D-T cells will slow diffusion of calcium.

The D_{app} value informs us about how fast calcium will diffuse in both free and bound state, but to understand the action range of calcium, the extrusion rate needs to be taken into consideration. Thus, the 1D displacement (λ) of calcium entering a dendrite is given by

Equation 8

$$\lambda = \frac{2}{\sqrt{\pi}} \sqrt{D_{app} \tau}$$

But to ensure that all calcium entry had time to be fully extruded 2 times τ was used in the equation, thus the calcium 1D displacement together with the D_{app} measurement give us the calcium action range:

Equation 9

$$\lambda = \frac{2}{\sqrt{\pi}}\sqrt{D_{app}2\tau}$$

In order to quantify the concentration of calcium following an entry event, a relationship between fluorescence and $[Ca^{2+}]$ has to be assessed. Thus the classical equation from Grynkievicz 1985 (Grynkiewicz, Poenie et al. 1985) was used to calculate the $[Ca^{2+}]$ entry induced by 3 bAPs:

Equation 10

$$[Ca^{2+}]i = K_D \frac{(f - f_{min})}{(f_{max} - f)}$$

Where K_d is the dissociation constant of the dye, f_{max} and f_{min} are the maximal and minimal fluorescence of the dye and f represents the change of fluorescence over the baseline (ΔF/F).

The primary challenge to precisely quantifying $[Ca^{2+}]_i$ with conventional microscopic techniques is the inability to really measure fmin and fmax in a cell. We either have to rely on those measures in a cuvette (where the Mg, pH, are different), or we have to hope that we get a true min and max with some kind of extreme procedure like strong BAPTA addition to the intracellular solution or strong depolarizations (killing the cell and allowing extracellular calcium free entry to the cytosol).

Additionally depending on the dynamic range of the calcium dye used, ΔF/F will be influenced. Thus to overcome this obstacle and calculate the actual $[Ca^{2+}]_i$ entry upon APs protocol, the dye dynamic range have been calculated using 100µM calcium dye (OGB6F, or Fluo4) and a calcium calibration kit (Sigma-Aldrich, Germany). fmin was determined at 0 calcium concentration and fmax at a calcium concentration saturating the calcium dyes (39µM).

For Fluo4, the Kd is 335nM and the dynamic range obtained is Rf= 16.6 (fmin=150, fmax=2500). Fluo4 was used only in PVBC were the resting calcium concentration was found to be 140nM. Thus the f in resting stage from **Equation 10** is:

$$140\text{nM} = 335\text{nM} \times \frac{(\text{f} - 150)}{(2500 - \text{f})}$$

$$\text{f} = 828.35$$

For OGB6F, the Kd is 3100nM and the dynamic range obtained is Rf= 1.85 (fmin=1400, fmax=2600). OGB6F was used in the recording of CCKBC and D-T cells where the resting calcium concentration was found to be 106 and 111nM respectively. Thus the f in resting stage from **Equation 10** is:

$$106\text{nM} = 3100\text{nM} \times \frac{(\text{f} - 1400)}{(2400 - \text{f})}$$

$$\text{f} = 1433.07 \text{ for CCKBC}$$

$$\text{f} = 1434.58 \text{ for D-T cells}$$

f_{3AP} is calculated via

Equation 11

$$f_{3AP} = f(1 + \frac{\Delta F}{F})$$

Where ΔF/F is the y intercept of the ΔF/F versus kappa dye.

Finally the $[Ca^{2+}]_{3AP}$ is calculated from the **Equation 10** from which the $[Ca^{2+}]_r$ is subtracted.

3.6 Field potential recordings

Field potential recordings were done in slices where network activity in the hippocampus was induced. In this kind of experiment, particularly healthy slices were needed. To optimize slice health, slices were placed on a filter paper and stored in an interface chamber instead of being submerged in a beaker containing RT ringer as was done in the case of patch clamp experiments. A 30 min step at 35°C with sucrose-ringer was done as for the experiment involving patch clamp recording, they then were held at RT and continuously perfused (flow rate of 1.6 mL/min) with RT ringer. Throughout the day, particular attention was given to the slice: slices that were too submerged degraded their potency to induce network activity; in contrast slices not submerged enough dried out and were thus discarded. Moreover, in order to let the slices fully recover from the slicing procedure, they remained in the interface chamber for at least an hour prior to recording.

In some experiments, recordings were done at 31°C (see **Figure 37**), in that case, a modified ringer with the following composition (in mM): 125NaCl; 3KCl; 1.25 NaH2PO4; 2MgCl2; 2CaCl2; 20.3 NaHCO3; 12 Glucose, was used.

The recording chamber of the LSM microscope is coupled to a heated bath system that allowed us to record at 31°C. Additionally, the ringer itself was continuously oxygenated and heated to 35°C in a separate bath heater to ensure that the temperature in the recording chamber reached a stable 31°C.

In the submerged chamber of the LSM microscope, the flow rate of oxygenated ringer needed to be higher than in normal patching conditions and was set to 4.5 mL/min to better elicit network activity (see **4.7.1**). To record the local field potential, a recording pipette (2-5MΩ) filled with the modified ringer was placed in the CA1 pyramidal layer. The local field potential recordings were amplified 2000 times (EXT-02-F/2, NPI electronic, Bauhofring, Germany, and BF 48 DGX, NPI Electronic GmbH, Germany), sampled at 2kHz, low pass filtered at 3kHz and high pass filtered at 300Hz. Recordings were acquired with WCP software as for the patch clamp recordings.

3.7 Extracellular stimulation

In order to elicit minimal synaptic responses of interneurons from axonal Schaffer collateral stimulation, a stimulator was used with the confocal microscope (AM system, model 2100, Carlsborg, USA). A stimulating pipette with a resistance from 5 to 10MΩ, was placed in the stratum radiatum and elicited EPSPs were recorded from the patched interneuron. The stimulus strength and the stimulating pipette position were altered until an approximately unitary or minimal EPSP was evoked (around 1mV).

Extracellular stimulation was also used to induce hippocampal network activity for the investigation of interneuron calcium signaling in a network activity context. For this purpose, the stimulating pipette (2-4MΩ) was placed in the Schaffer Collaterals and pulses of 45-60µA intensity were used. No spontaneous activity could be recorded from the field pipette; we thus changed our protocol with an incremental intensity ranging from 45 to 60µA (increment of 2-5µA, interpulse interval of 45s), see **4.7.1**.

In a subset of experiment, Purkinje cells were recorded in current clamp mode as for other interneurons. In addition, a stimulating electrode (2-4MΩ) was positioned next to the soma of the patched Purkinje cell in order to elicit a complex spike, which is mediated by climbing fiber's neurotransmitter release onto the dendritic shaft of Purkinje cells (**Figure 9**). The

stimulus pulse was 100µs duration and the intensity varied from 7-15V to obtain complex spike (**Figure 9** left trace).

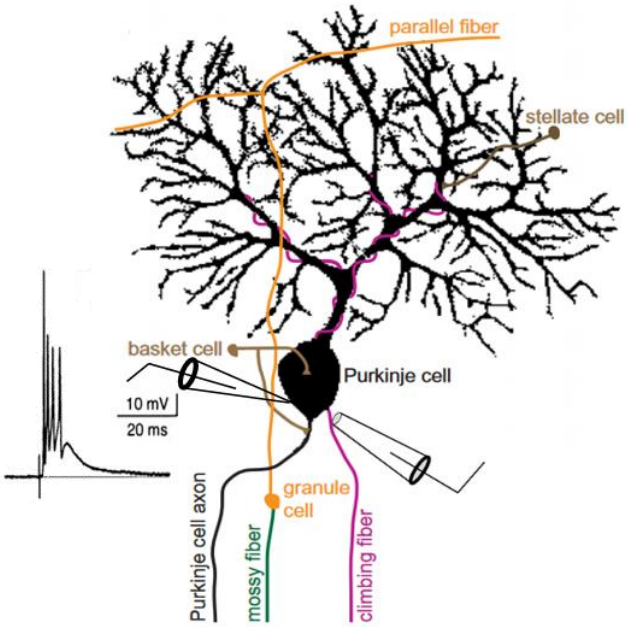

Figure 9 : Schematic view of Purkinje cells connectivity
A Purkinje cell is patched in whole cell configuration. Another electrode is placed next to the Purkinje cell soma in order to stimulate climbing fiber (purple) and elicit a complex spike (left trace)
Modified from (Airaksinen, Eilers et al. 1997; Bosman and Konnerth 2009)

3.8 Two photon (2P) microscopy

3.8.1 Principle of multiphoton microscopy

In contrast to the confocal microscopy, 2P microscopy uses nonlinear excitation involving absorption of multiple photons, and not 1 photon, for contrast generation. The principle of the 2P microscopy resides in the cooperation of two low-energy photons (from the same laser) to induce a higher energy transition in a fluorescent molecule (**Figure 10A**) (Svoboda and Yasuda 2006).

Near infrared light is used, with a wavelength in a range of 700-1000nm, which penetrates deeper into scattering tissue but also is generally less phototoxic. Consequently, the excitation volume of the sample is small, as a result the out of focus emission is non-existent and less photo-bleaching of the sample occurs (**Figure 10B**) (Helmchen and Denk 2005). This principle is important when long recording of neurons has to be done to preserve the health of the tissue and cells recorded longer.

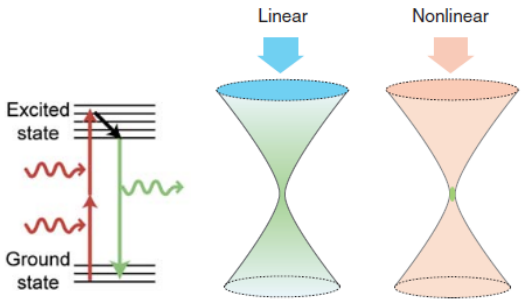

Figure 10 : 2P microscopy
A) Simplified Jablonski diagram of the 2P microscopy process. Two high energy photons are simultaneously absorbed to move electrons to the excited state. Fluorescent photons are emitted when the electron returns to the ground state.
B) "Spatial confinement of signal generation with nonlinear excitation. Visible ('blue-ish') light is used for excitation in single-photon microscopy, whereas near-infrared ('red-ish') light is used in 2P microscopy. In single-photon microscopy an entire cone of fluorescence light (green) is generated, whereas nonlinear signal production is localized to the vicinity of the focal spot".
Modified from (Helmchen and Denk 2005; Svoboda and Yasuda 2006)

3.8.2 Calcium imaging and patch clamp recordings

2P calcium imaging experiments including uncaging of glutamate were performed with a Prairie Technologies Ultima Multiphoton Microscopy System (Bruker, USA) equipped with two 80MHz femtosecond pulsed Ti:Sapphire lasers (Chameleon Vision II, Coherent) for simultaneous imaging and uncaging.

The imaging laser's wavelength was set at 820 nm, and the Fluo4 (100µM) and TMR (100µM) fluorescence were collected with two PMTs via 490–560/575/585–630 nm and 500–550/560/570–655 nm filter cubes. The imaging laser intensity was set to approximately ~ 4-5mW at the surface of the slice. GFP^+ cells were patched under a 60X objective (NA 1.0; Nikon). Cells electrical signals were amplified to 20mV/pA with an HEKA EPC10 amplifier (Harvard Bioscience Inc, HEKA Elektronik Dr. Schulze GmbH, Germany), sampled at 20 kHz and low-pass filtered at 10kHz.

As a quick check of calcium transient detection, the patched cell was stimulated somatically with 3APs and a line scan was drawn perpendicularly to the proximal dendrite. The line scan was set to 300 lines at 8-10ms with a pixel dwell time of 2.8µs.

For the detection of calcium transients induced by glutamate uncaging, the line scans were 4-6ms and were longitudinally drawn in a 10µm portion of dendrite.

3.8.3 Glutamate uncaging

Prairie Technologies Ultima Multiphoton Microscopy System (Bruker) is equipped with two tunable Ti:sapphire lasers and two scan heads, which allowed us to uncage glutamate and image calcium simultaneously. When a bAP-CaT was detected in the cells and

the cells had a stable membrane potential as well as a good access resistance (< 30MΩ), the perfusion of the chamber was stopped and MNI glutamate 5mM (stock 30mM, Tocris Bioscience, UK) and tetrodotoxin 2µM (TTX 1mM stock solution, Biotrend, Zurich) were directly added to the recording chamber. TTX and MNI glutamate were allowed to diffuse 10 minutes preceding the experiment. The cell was subsequently recorded for a maximum of 40 minutes in anoxic conditions.

The uncaging laser was tuned to 720nm and the laser intensity was between 20 to 30mW at the surface of the slice. The uncaging protocol was defined in PrairieView software (Bruker) and uncaging experiments were triggered by the PatchMaster software to synchronize imaging and electrophysiological data acquisition.

To reliably induce calcium transients via uncaging MNI-glutamate, a single point was drawn at the edge of the randomly selected portion of the dendrite shaft. The uncaging pulse was 0.6ms. In some cases, three points separated by 100nm and with an interval between points of 0.6ms were drawn.

In order to increase the signal-to-noise ratio, three line scans were taken and averaged to analyze the calcium apparent diffusion coefficient within the dendrite.

3.8.4 Measure of D_{app} from the uncaging experiment

Three line scan images were averaged together, and a line profile along the spatial dimension of the image of the dendrite was taken. The average image was then normalized to a smooth pre-uncaging baseline profile to eliminate any variation of fluorescence along the longitudinal scan of the dendrite.

Horizontal profiles, showing the calcium transient along the spatial axis were then taken every 20-30ms starting from the uncaging pulse. Those subsequent horizontal line profiles were each then fitted, via the global fitting command in Igor Pro 7 (Wavemetrics, USA), with the following equation for diffusion in one dimension (Crank's book):

Equation 12

$$C = \frac{M}{2(\pi D t)^{1/2}} exp^{(\frac{-x^2}{4Dt})}$$

Where M is the amount substance a t (time) =0, and D is the diffusion.

In theory a typical linear diffusion distribution should look like **Figure 11** where at t close to 0 the substance is very localized. With time increasing, the amplitude of the substance will

decrease and spread widen. This increase in width is directly related to the apparent diffusion coefficient of the substance, and is assessed by resolving **Equation 12**.

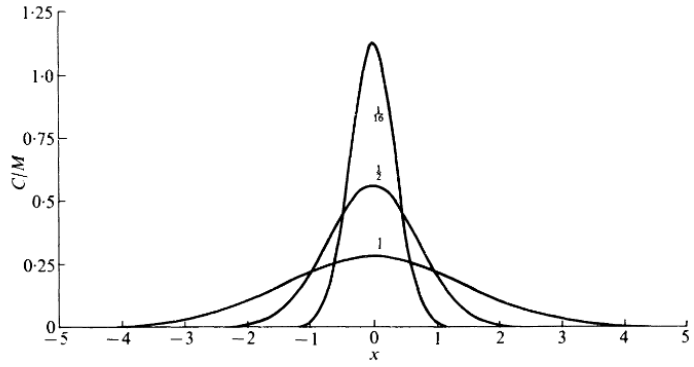

Figure 11 : Theoretical distribution of a diffusing substance over time
A t=0, a localized source of substance is detectable. Note the decrease in the substance amplitude and the increase in diffusion with time.

3.9 Fluorescence Life Time Imaging (FLIM)

3.9.1 Theory

The FLIM technique relies on the fluorescence lifetime of fluorescent molecules. The lifetime is defined as the time needed for a population of fluorescent molecules to become excited and to return to their ground state, meanwhile emitting fluorescent photons. The life-time of different molecules varies, and in the case of some calcium dyes, exhibits a strong shift depending on the bound or unbound state of the molecule at the time of excitation.

The method used for measuring time-resolved fluorescence is the time domain method of pulse fluorometry. More concretely, the sample is excited by a laser with an 80MHz pulse repetition rate (Ti:sapphire lasers) and the emitted photons are filtered (550/100, 632/60), amplified, and detected (HPM100-40 hybrid detector) by a time-correlated single photon counting PMT (TCSPC) (Becker 2012). Once acquired, the photon count distribution is fitted with a single exponential or double exponential.

The pulse light's width is made as short as possible; shorter that the decay time of the fluorescence probe. Additionally, the probe concentration is low in order to detect a distribution of photon probabilities (**Figure 12**). Indeed if every laser excitation pulse sequence would give rise to a fluorescence signal this time correlated single photon counting (TCSPC) technique would not be usable. Therefore, the signal detected by the detector has to be sparse to obtain a distribution of photon probability. Finally, the instrument response has to be taken into account, because a slow instrument response won't resolve the ns time scale of

event decay times (Becker 2012). In our case, the instrument response was 120ps, short enough to not disturb the detection of the calcium dye's decay time.

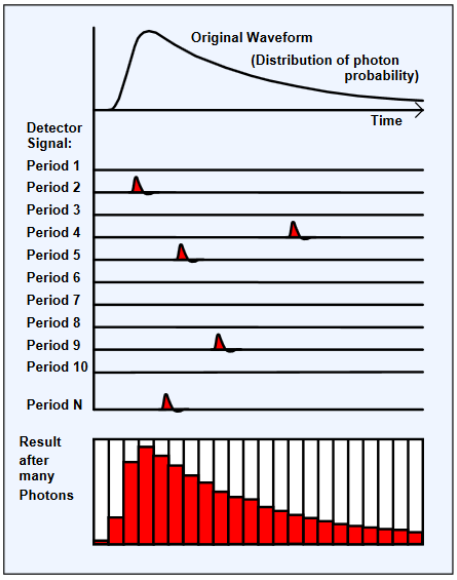

Figure 12 : Principle of the TCSPC
When a photon is detected, its arrival time is measured. After many signal periods a large number of photons have been detected, and the distribution of the photons over the time in the signal period builds up. The result represents the 'waveform' of the optical pulse. From (Becker 2012)

3.9.2 FLIM experiment and imaging analysis

The probe we used to measure resting calcium concentration ($[Ca^{2+}]_r$) in interneurons was OGB1. OGB1 has a fast decay time when unbound to calcium, but has a slower one when bound to calcium.

To extract the calcium concentration from FLIM images, a cell was patched in whole cell patch clamp mode and filled with 20µM OGB1 for approximately 10 minutes prior to image acquisition. The patch pipette was withdrawn, and the cell was allowed to recover from the dye loading. FLIM frame images were collected by the SPC software from Becker & Hickl, taking care that the excitation power was low enough to avoid overflow of the very sensitive TCSPC detectors. The digital zoom was between 8 and 10, such that the soma and proximal dendrite filled a majority of the field of view.

The photon arrival time histograms from each pixel were summed across a Region Of Interest (ROI) drawn around the soma, and fitted with a biexponential. The slow and fast decay time constants were constrained in the fitting procedure to reduce the complexity and variability of the fits across cells. Thus, the fast and slow decay time constants had to be determined prior to the analysis of CCKBC, PVBC and D-T cells resting calcium concentration.

Fast and slow decay time constant were determined by Dr. Matthews in a series of experiment including granule cells (excitatory cells of the DG) and CA1 pyramidal cells. Cells were stimulated (3s) with different frequency trains (10, 33 and 50Hz) which resulted in different

and stable intracellular calcium concentrations. The subsequent life-time decay curves from each stimulation intensity was fitted using a global fitting procedure, which yielded fast and slow decay time constants of $3.778X10^{-10}$ s and $2.978X10^{-9}$ s.

The relative amplitudes (α_S and α_F below) contributing to the fast and slow components of the life-time decay curve were then converted to calcium concentrations according to the equation from Wilms & Schmidt (Wilms, Schmidt et al. 2006):

Equation 13

$$[Ca^{2+}]_r = K_{d(eff)} \frac{\alpha_S - \alpha_{Smin}}{\alpha_F - \alpha_{Fmax}}$$

The coefficient $K_{d(eff)}$ represents the affinity constant of OGB1 accounting for the 2P efficiency of the free and calcium bound dye, and α_{Smin} and α_{Fmax} are the calibrated life-time decay time amplitude of OGB1.

These $K_{d(eff)}$, α_{Smin} and α_{Fmax} factors were determined with a series of experiments using OGB1 (10µM) in known concentrations of calcium (0 nM to 39 µM) obtained using a calcium calibration solution kit (Sigma-Aldrich). The experimentally determined $K_{d(eff)}$ was 145.5nM, α_{Smin} was 0.965, and α_{Fmax} was 0.898.

In the actual analysis of CCKBC, PVBC and D-T cells intracellular calcium concentration, the fitted life-time decay curve were constrained to the previously determined slow and fast decay time constant, which yielded a fit 5-20% error in comparison to a fitted life-time decay curve in a free run. Additionally, in some experiments glutamatergic blockers (50µM APV and 20µM CNQX) were washed into the bath and 10µM CCh was also applied after the initial resting calcium images were acquired. All images were analyzed in Igor Pro using custom written routines.

3.10 Immunostainings and biocytin revelation

3.10.1 Axon recovery

To confirm the cell identity, the morphology and the axon location were used. Throughout the recording, neuronal compartments (dendrites and axon) were filled with 0.5% biocytin. When the recording was over, the patch pipette was carefully pulled off and the slice containing the neuron recorded was fixed for 24 hours using paraformaldehyde (PFA 8%). Slices were then rinsed 3 times in Tris Buffer Saline (TBS), and held in 10% TritonX-100 solution for 5 hours in order to permeabilize the cells. Finally, to reveal the biocytin,

Streptavidin complexed with RRX (SAVRRX, 1:350, Jackson ImmunoResearch Laboratories Inc) was added and held overnight at 4°C. The following day, slices were rinsed in TBS and mounted between slide and coverslip, and conserved at 4°C. Neurons morphology was inspected on a wide-field Nikon with 25X and 40X coverslip corrected objective for a detailed view of the axon.

To illustrate the axonal location and the morphology of CCKBC, PVBC and D-T cells, some of the best examples were reconstructed. To do so, Z-stacks were taken in the confocal microscope using an excitation from the ArKr laser (543) low pass filter 560, slow pixel dwell time and a Z step of 1µm, for good resolution. Because the field of view of the confocal microscope can be too small to acquire the complete dendritic tree and axon collaterals, the 2P Nikon system with a programmable stage was used in a few cases.

Once the Z-stack was acquired, it was imported in ImageJ (Rasband, W.S., ImageJ, U. S. National Institutes of Health, Bethesda, Maryland, USA, https://imagej.nih.gov/ij/, 1997-2016.) where the Neuron J plugin (version 1.4.3) was used to retrace dendrites and axons of CCKBC, PVBC and D-T cells.

3.10.2 Calbindin and calretinin stainings

Some D-T cells and CCKBC were labelled for the expression of both calretinin (Cr) and calbindin (Cb). Prior to the immunostaining, 300µm slices were ressectionned to 50µm (VT 1000S Leica Biosystems, Nussloch GmbH, Germany) in order to get a good penetration of the antibodies and a better view of any overlapping signal. Slices were incubated in 2% bovine serum albumin (BSA) for 2 hours and subsequently with Cb antibody (mouse, 1:250, Swant, Bellinzona, Switzerland) or with Cb antibody (rabbit, 1:2500, Swant, Bellinzona, Switzerland) in some cases, together with RRX SAV, and 0.2% Triton X-100 for 24 hours at 4°C. The secondary antibody (Alexa405 anti-mouse, 1:350, ThermoFisher Scientific, USA) was applied for 24 hours at 4°C.

An antigen retrieval step was needed to label the calretinin protein. This step consisted of incubating slices in trisodium citrate (10 mM, pH 8.5, Sigma Aldrich) at 80°C in Eppendorf tubes and placed in an incubator (Thriller, Peqlab, Germany) for 30 minutes at 300 rotations per min. The primary Cr antibody (rabbit, 1:1000, Swant, Bellinzona, Switzerland) was applied together with 0.2% Triton X-100 for 24 hours at room temperature on a rocking platform. The secondary antibody (Alexa 488 anti-rabbit, 1:250, Thermofisher, USA) was applied for 24 hours at 4°C. Cell morphology and colabeling for the targeted proteins was

imaged using a confocal microscope (Leica) equipped with 3 imaging channels. (**Figure 24, Figure 25**).

	Product	Volume µL	Time
Day 1			
blocking	with BSA and triton	1mL	2 hours at RT
	Flush with TBS		3 * 10 min
	Triton 10 X RRX SAV Anti cb (m) swant 1:250 TBS	10 3 2 485	Overnight
Day 2			
	Flush with TBS		3 * 10 min
	ALexaF 488 anti-mouse TBS with BSA and triton	3 497	3h at 35°C
	Flush with TBS		3 * 10 min
	Trisodium citrate (preheated at 80°C)	1 mL	30min at 300 rpm Cool down at room temperature
	Flush with TBS		3 * 10 min
blocking	with BSA and triton	1mL	2hours at RT
	Triton 10 X Anti cr (rb) 1:1000 TBS	10 0.5 489.5	Overnight at RT on a rocking platform
Day 3			
	Flush with TBS		3 * 10 min
	dyelight 405 anti Rb Triton 10 X TBS	3 10 487	Overnight

Table 3 : Triple staining biocytin, Cb, and Cr protocol

3.10.3 PV staining in PVCre-Ai14TDtomato line and Tg (Gad2-EGFP) DJ31Gsat line

In order to verify the specificity of the two mouse line used in this thesis, a staining against PV and GFP was completed in the Tg(Gad2-EGFP)DJ31Gsat mouse tissue.

After having been fixed for 24h with 8% PFA, slices were rinsed with TBS and ressectioned at 50µm. 50µm slices were incubated overnight with anti-PV (rabbit, 1:500, Swant PV27, Bellinzona, Switzerland) and anti-GFP (chicken, 1:100, Molecular Probes A10262, ThermoFisher scientific) and 0.2% Triton-10X. The following day slices were rinsed and a biocytin amplification step was used to amplify the weak GFP signal. This step consisted of

incubating overnight the slices with anti-chicken biotin (Donkey, 1:200, Jackson ImmunoResearch), in addition, the secondary antibody against rabbit and complex to RRX was used (1:150, Jackson ImmunoResearch) together with 0.2% Triton-10X. The next day, slices were rinsed 3 times with TBS and incubated with streptavidin complexed with dyelight 488 (1:350, Jackson ImmunoResearch) and 0.2% Triton-10X. Finally, slices were rinsed and mounted between slide and coverslip and imaged using the LSM confocal microscope.
The following table illustrates the protocol used in the Tg(Gad2-EGFP)DJ31Gsat line:

	Product	Volume µL	Time
Day 1			
	Flush with TBS		3 * 10 min
	Triton 10 X	10	Overnight
	Rb anti-PV	1	
	Ck anti GFP	5	
	TBS	485	
Day 2			
	Flush with TBS		3 * 10 min
	RRX anti rb (1:150)	3	Overnight
	Dk anti-ck biotin	2.5	
	Triton 10 X	10	
	TBS	484.5	
Day 3			
	Flush with TBS		3 * 10 min
	SAV dyelite 488	3	Overnight
	Triton 10 X	10	
	TBS	487	

Table 4 : PV/GFP staining's protocol used for assessing the specificity of Tg(Gad2-EGFP)DJ31Gsat mouse line

The same protocol of PV staining was used for the assessment of the specificity of the TDtomato signal in PV positive interneurons. However, the native TDtomato signal did not need further amplification. Thus the staining protocol was reduced to only two steps as written in the **Table 5**. The slices were also fixed 24 hours with 8% PFA, rinsed with TBS the following day and ressectioned at 50µm. Slices from PVCre-Ai14TDtomato were then incubated with PV antibody together with 0.2% Triton-10X, and held overnight at 4°C. The next day, they were rinsed 3 times with TBS, and incubated with the secondary antibody anti-rabbit complexed with RRX, they were held overnight at 4°C. On day 3, they were rinsed 3

times with TBS and mounted between slide and coverslip and imaged using the LSM confocal microscope.

	Product	Volume µL	Time
Day 1			
	Flush with TBS		3 * 10 min
	Triton 10 X	10	Overnight
	Rb anti-PV	1	
	Ck anti GFP	5	
	TBS	485	
Day 2			
	Flush with TBS		3 * 10 min
	RRX anti rb (1:150)	3	Overnight
	Triton 10 X	10	
	TBS	484.5	

Table 5 : PV staining's protocol used for assessing the specificity of the of the PVCre-Ai14TDtomato mouse line

3.10.4 CB1r staining in the Tg(Gad2-EGFP)DJ31Gsat mouse line

Another staining against CB1r was applied to further investigate the GADGFP mouse line, and detailed in the following **Table 6**.

As for the other staining, slices were fixed 24 hours with 8% PFA, rinsed afterward and ressectioned to 50µm. The next step consisted of incubating them with 0.2% Triton-10X, primary antibody against CB1r (rabbit, 1:1000, Frontier) and a primary antibody against GFP, at4°C overnight. Then, slices were rinsed 3 times with TBS and incubated with the secondary antibody against rabbit coupled to RRX, and anti-chicken complexed to biotin overnight at 4°C. Next, slices were rinsed with TBS and held overnight at 4°C with SAV complexed with dyelite 488 and 0.2% Triton-10X. The following day, slices were rinsed, mounted and imaged using the LSM confocal microscope.

	Product	Volume µL	Time
Day 1			
	Flush with TBS		3 * 10 min
	Triton 10 X	10	Overnight
	Rb anti Canna (1:1000)	1	
	Ck anti GFP	5	
	TBS	484	
Day 2			

	Flush with TBS		3 * 10 min
	Anti Rb RRX	3	Overnight
	Dk Anti-ck biotin	2.5	
	Triton 10 X	10	
	TBS	484.5	
Day 3			
	Flush with TBS		3 * 10 min
	SAV dyelite 488	3	overnight
	Triton 10 X	10	
	TBS	487	

Table 6 : Cb1r/GFP staining's protocol used for assessing the specificity of Tg(Gad2-EGFP)DJ31Gsat mouse line

3.11 Virus injection in mice

3.11.1 Principle of the iGluSnFR probe

Marvin *et al* (Marvin, Borghuis et al. 2013) introduced a glutamate sensor ("iGluSnFR") constructed from E. coli (**Figure 13**). The iGluSnFR is a bright green and photo-stable sensor (up to 4 weeks after infection) with a 4.5-fold increase of ΔF/F when bound to glutamate. They showed that it is fairly sensitive (K_d= 4.9 ± 1.3 µM) and fast to glutamate binding that correlates with simultaneous electrophysiology.

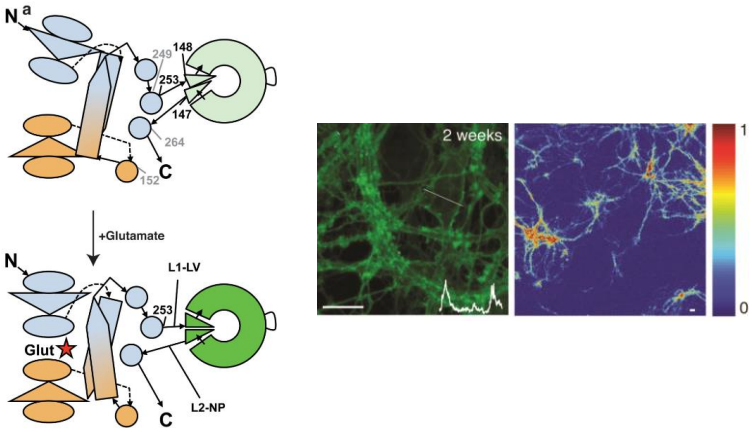

Figure 13 : Illustration of the iGluSnFR properties
Left "Schematic representation of GltI-cpGFP insertion. Both domains (blue and orange) contribute to the binding site for glutamate. Binding of glutamate (star) induces a conformational change.
Right: "iGluSnFR localizes to the membrane of neurons."
Adapted from (Marvin, Borghuis et al. 2013)

3.11.2 Procedure of virus injection in mice

Male mice were injected at (or after) P30. Depending on the body weight, the amount of anesthetic was varied (for further detail, see **Appendix**). The mouse body weight was the

most important criterion to decide on the surgery. Indeed, a mouse with a body weight less than 20g, although it was in the right age range, was not injected. This precaution was to avoid any risks that the mouse would not survive the surgery

The mice were anesthetized via an intraperitoneal injection (IP), as seen from the scheme in **Figure 14 left.**

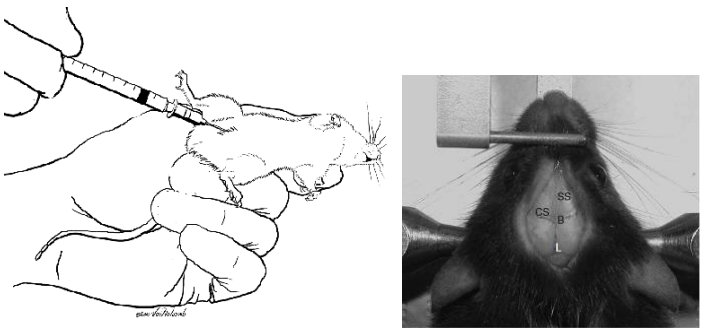

Figure 14 : Anesthetic injection and bregma location in mouse

Left: Scheme of the IP injection in mouse.
From:
https://www.brl.uic.edu/node/37

Right: The mouse is placed in a stereotaxic frame. Once the skin and the plexus were removed, the skull with representative landmarks is visible.
B, bregma; L, lambda; CS, coronal suture; SS, sagittal suture.
From: (Rynkowski, Kim et al. 2008)

After 5 to 10 minutes, the mouse was completely unreactive to foot pinches and received an antibiotic and a pain killer injection, to limit any bacterial infections and to help the mouse recover after the surgery. The mouse was then carefully shaved between the ears. Next, the mouse was installed in the stereotaxic frame. The teeth were placed on the bite bar, and then the ear bars were carefully placed inside the ears. These ear bars were tightened enough to securely hold the mouse's skull. Particular attention was given to the flatness of the skull in the rosto-caudal and lateral planes. Prior to the surgery, eye cream was placed the mouse's eyes to preserve ocular moisture.

The exposed skin was decontaminated with iodine. An incision of 1.5cm long was made between the ears toward the eyes. Once the skin was opened, the plexus, a well innervated membrane, was cautiously removed **(Figure 14 right)**. The coordinate of the virus injection were calculated from the bregma point to target the hippocampus and were 3mm bregma and 3mm interaural (**Figure 15A**).

The injection positions were marked and a hole was drilled into the skull. The needle containing the virus was then positioned to touch the skull, from there lowered a further 3mm. The volume of virus injected was 1µL per hemisphere with a rate of 200nL/minutes. Once the injection was finished, a waiting time of 5 minutes was given to allow the virus to spread, and then the syringe was cautiously withdrawn.

Finally, when the two hemispheres were injected, the mouse was released from the stereotaxic frame and the wound was closed with sutures.

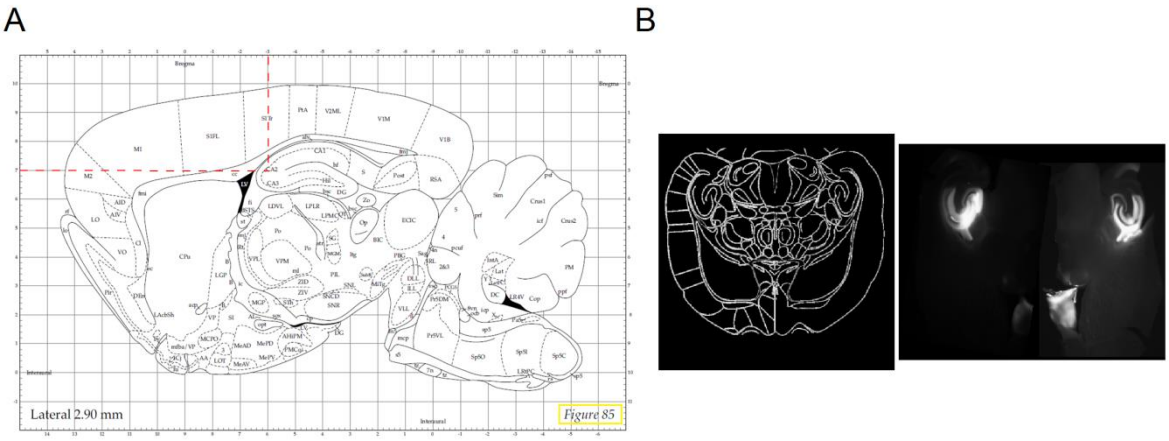

Figure 15 : Coordinates determination for virus injection in the ventral hippocampus
A) According to the Paxinos and Franklin brain atlas, coordinates were chosen to inject virus in the ventral hippocampus. (Paxinos and Watson 1998)
B) A GFP virus was first injected in order to confirm the coordinates. After 2 weeks of infection the mouse was sacrificed and the brain was sliced horizontally. As seen by the illustration, the coordinate were correct to infect CA1 layer of the ventral hippocampus.

Post-surgery, mice were injected twice a day with pain killer (Buprenovet) and antibiotics (Gabrilen) for 4 days. Their health status was also recorded from no symptoms (category 0) to moribund (category D) (for further detail, see **Appendix**)
Mice were allowed to rest for 2-3 weeks to let the virus fully infect the targeted cells prior to the experiment.

3.11.3 Virus types

To confirm the stereotaxic coordinates, 6 wild type mice were first injected with an AAV-U6-*EGFP* with the original titer (10^{12}). This virus infects all neurons, and thus was an optimal marker to verify the coordinates used to target the ventral hippocampus (**Figure 15B**). For the interneuron experiment the AAV1-hSyn.FLEX.iGluSnFR.WPRE.SV40 virus (Penn VectorCore) was used to elicit iGluSnFR sensor in neurons (syn) and specifically in the PV^+ interneurons. Indeed, this virus transfects cells that express the Cre promoter, and this Cre promoter is upstream of the *PV* gene. Consequently the virus injections were made on PV Cre homozygous mice. This virus was used at its original titer ($4.24X10^{12}$) in 4 mice and at ½ of the original titer in 2 mice.

Different titers were used because the mice injected with the full titer had almost no living PV^+ interneurons transfected after 2 weeks of viral infection. Thus we thought to dilute the virus, however, the results were still not convincing since no great improvement in health of the transfected interneurons was visible.

The ultimate goal of the experiment was to simultaneously record iGlUSnFR signal (green) and calcium signal using X-Rho5F (red) within a PVBC induced by Shaffer-Collaterals stimulation.

3.12 Analysis, standard error propagation and statistics

Data manipulation of images and electrophysiological traces were carried out in Igor Pro, using built in and custom written procedures. All statistics were computed with the built in Igor Pro statistics package.

To compare CCKBC, PVBC and D-T cells a 1-way ANOVA followed by a post-hoc Tukey test was used. In the case of before and after Cch (carbachol) application, a paired t test was used with a confidence index of 0.05.

All the values are expressed as means plus or minus the standard error of the mean (SEM). Calculating the uncertainty for values extrapolated from the kappa plots (Result section **4.3.2**) used the following equation:

Equation 14

$$SEM = \frac{S_{x/y}}{b} \times \sqrt{\frac{1}{N} + \frac{\bar{y}^2}{b^2 \times \sum(x - \bar{x}^2)}}$$

Where b is the slope value, and N is the sample numbers and $S_{x/y}$ is calculated from:

Equation 15

$$S_{x/y} = \sqrt{\frac{\sum y_{residual}}{N - 2}}$$

All other values calculated used the error propagation rules for SEM determination.

4 Results

4.1 Examining the selectivity of the 2 mouse lines used

Two mouse lines were used in this thesis in order to discriminate interneurons subtypes among the interneuron diversity. The first one was the Tg(Gad2-EGFP)DJ31Gsat, which has a bacterial artificial chromosome (BAC) genomic modification. This genomic modification consists of multiple copies of BAC containing an *EGFP* reporter gene inserted upstream of the *GAD2* gene. The *GAD2* gene encodes for the GAD65 proteins which is a decarboxylase and is required for the synthesis of γ-Aminobutyric acid (GABA) from glutamic acid specifically in interneurons. However, Lopez-Bendito et *al* and Wierenga et *al* demonstrated an *EGFP* specific expression in interneurons originating from the caudal ganglionic eminence (Lopez-Bendito, Sturgess et al. 2004; Wierenga, Mullner et al. 2010) in this line and thus as mentioned in **1.2.1.2** targeting a specific class of interneurons.

The second mouse line used was the PVCre-Ai14TDtomato. To obtain this line, a PVCre knocking mouse, which expresses Cre recombinase in PV expressing neurons, was bred with an Ai14 Cre reporter mouse. The Ai14 mouse harbors a lox-stop cassette inserted in the Rosa locus (Gt(ROSA)26Sor) that is expressed ubiquitously in neurons. However to exhibit TDtomato signal Cre recombination is needed. Consequently, by breeding this reporter line with the PVCre knock-in mouse, the TDtomato signal will be expressed in neurons containing the *PV* gene and where the recombination occurs.

Using the Tg(Gad2-EGFP)DJ31Gsat referred to GADGFP mouse in this thesis, we verified that indeed only PV negative($^-$) neurons were GFP positive($^+$) (Lopez-Bendito, Sturgess et al. 2004)). We therefore stained our GADGFP mouse tissue against PV and GFP. As seen in the panel B of **Figure 16**, we indeed have two distinct populations of PV^+ neurons and GFP^+ cells. We quantified the PV and GFP staining in 10 different animals, and found 0.87 ± 0.2% of overlap between PV and GFP neurons. In other words, this quantification indicates that 99.1% of GFP^+ neurons do not express PV, and that we can be confident to select a subpopulation of PV^- interneurons.

As another confirmation of the selection of PV- neurons in the GADGFP line, we stained GFP and CB1r, which is known to be expressed only in CCK^+ cells and not in PV^+ cells (see **1.2.1**).

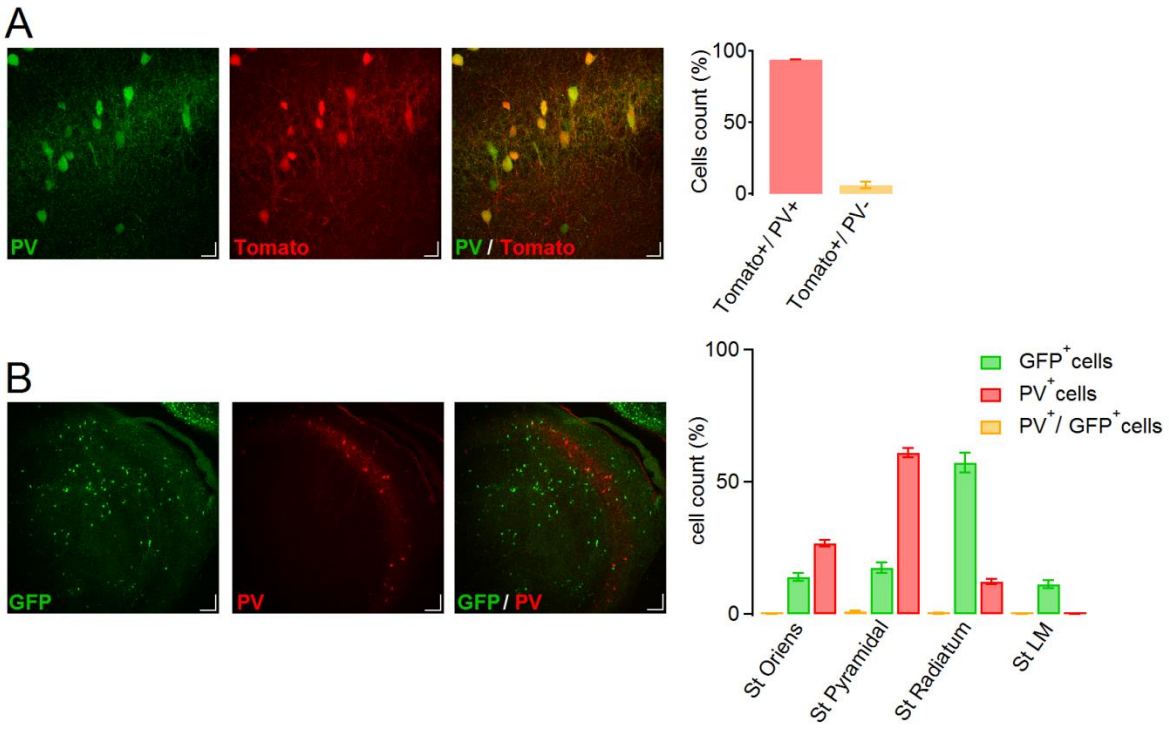

Figure 16 : Quantification of the Tg(Gad2-EGFP)DJ31Gsat and PVCre-Ai14TDtomato mouse lines

A) PVCre-Ai14TDtomato tissue was stained against PV. Note the 98 % overlap between the native tomato signal with PV

B) Staining of the GADGFP line against PV. Note the non-overlapping (<1%) GFP^+ population with PV in every hippocampal CA1 strata

CB1r is expressed only in axon terminals, and we eventually wanted to select the BC subtypes from this GADGFP mouse line. Thus by quantifying GFP^+ puncta in stratum pyramidal we saw 70% overlapping with CB1r puncta (n=2 animals, 5 CA1 region images). This staining gave us another indication of the selectivity for PV^- BC which are $CB1r^+$ using the GADGFP mouse line.

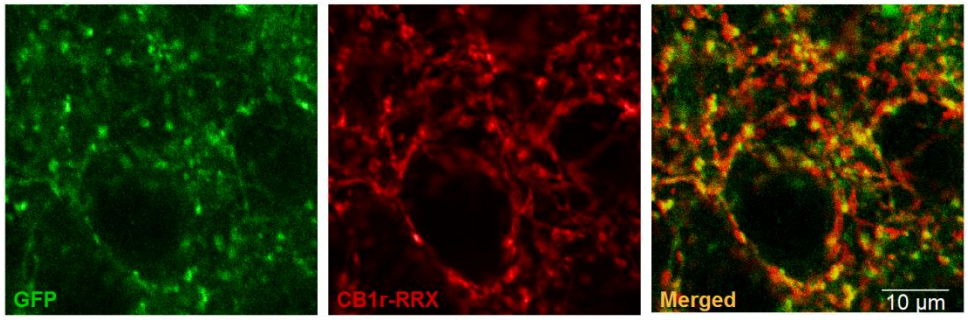

Figure 17 : Double GFP, CB1r staining of the GADGFP mouse line

Picture of the CA1 pyramidal layer with a higher magnification on the basket like synapse formed by the BC surrounding the pyramidal cell's soma. Note the important colocalization (70%) of GFP^+ and $CB1r^+$ terminals.

We also verified the correct recombination of the PVCre-Ai14TDtomato by staining brain slices of 7 different animals against PV. We then quantified PV^+ neurons that also expressed the native TDtomato signal (**Figure 16A**). The quantification indicates a very strong overlap between $TDtomato^+$ and PV^+ populations: 94 ± 2%. This means that 6 ± 2% of TDtomato positive cells were PV negative indicating an estimated 6% chance of falsely identifying targeted cells as PV^+ neurons when using this mouse line in the following experiments. However, those 6% of $TDtomato^+$ cells which are PV^- are located in the bottom part of the stratum oriens which is not the usual location used to patch $TDtomato^+$ cells in experiments (see **3.2.1**).

Finally, a subpopulation of PV^+ cells (16 ± 4%) was not $TDtomato^+$ indicating that in this subpopulation, the Cre recombination did not occur.

4.2 Confirmation of CCKBC, PVBC and D-T cells morphology

4.2.1 Passive electrophysiological properties

In order to discriminate the 3 interneurons subtypes studied in this thesis, in addition to the specific mouse line, we used their axonal location and their passive electrophysiological properties. The GADGFP line was used to record CCKBC and D-T cells with a further dichotomy using their axon location to firmly conclude their subtype.

CCKBC and D-T cells have a fusiform soma localized in the stratum radiatum and they could not be differentiated by their soma form or location. Only their axonal location gave us the subtype of either CCKBC or D-T cells: CCKBC having their axon in the pyramidal layer, while D-T cells display their axon in both stratum radiatum and oriens (**Figure 18**).

To further discriminate CCKBC from the D-T cells we recorded their passive electrophysiological properties. The resting membrane potential was not significantly different V_m= -61.4 ± 0.5 mV (n=97) and V_m=-60.3 ± 0.8 mV (n=50) for CCKBC and D-T cells respectively (1-way ANOVA, P-value > 0.05). However, their input resistance was found to be significantly different, D-T cells having a higher input resistance compared to CCKBC: R_{in}= 282.4 ± 6.9 MΩ and R_{in} =327.5 ± 14.5 MΩ (1-way ANOVA, P-value < 0.05).

Additionally, 1s long hyperpolarizing and depolarizing current injection steps (-200pA to 350pA, 50pA steps) were induced to assess the firing frequency and the hyperpolarization-induced sag component of the cells. The average firing frequencies of CCKBC and D-T cells (350pA step) were observed to be different: 37.7 ± 1.1 Hz and 24.9 ± 1.3 Hz (1-way ANOVA, P-value < 0.01). The sag measured as the peak hyperpolarization relative to the

steady state, was also found to be significantly different and of large amplitude: CCKBC: 12.7 ± 0.6 mV and D-T cells: 17.7 ± 1.1 mV (1-way ANOVA, P-value < 0.01) (**Figure 18**). These passive electrophysiological features from CCKBC and D-T cells are similar to the ones reported by Cope et al (Cope, Maccaferri et al. 2002).

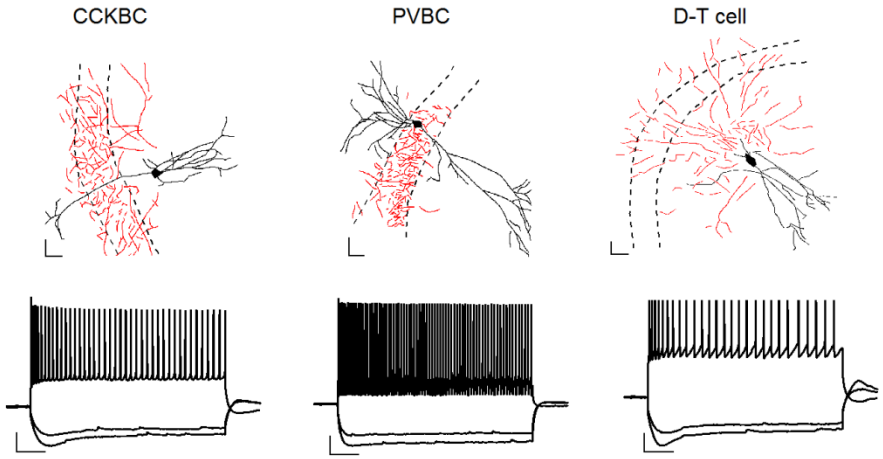

Figure 18 : Determination of the interneurons subpopulation via their axon location
The 3 interneurons targeted are distinguishable by their characteristic morphology but also by their electrophysiology features (firing frequency and sag). Dendrites of neurons are represented in black whereas their axon is depicted in red. The dashed line represents the stratum pyramidal.
Scale: interneurons morphology: 50µm. Depolarizing step : 150ms, 20mV

The PVBC were targeted via the PVCre-Ai14TDtomato line, but their electrophysiology properties were also assessed in addition to the mouse line selection. PVBC's somata were located in the stratum pyramidal and in stratum oriens. However, only somata that were found in stratum pyramidal were targeted in all the experiments involving PVBC in this thesis.
PVBC have generally only 1 to 2 dendrites in the stratum radiatum. Indeed 10 out of 16 cells have only 1 dendrite in stratum radiatum; however, this dendrite tends to branch quite extensively in the medial distance from the soma, approximately 40-60µm, as seen in the reconstruction **Figure 18**. More dendrites are found in the stratum oriens where they also divide in further secondary and tertiary branches. PVBC (n=76) have a more hyperpolarized resting membrane potential compared to CCKBC or D-T cells: V_m= -64.4 ± 0.6 mV (1-way ANOVA, P-value < 0.01) and have a higher APs frequency compared to both CCKBC and D-T cells: 73.3± 2.7 Hz (1-way ANOVA, P-value < 0.01). This AP frequency is consistent with the fact that PVBC are also known as fast spiking basket cells (see **1.2.1.1**). Additionally,

their input resistance is lower than both CCKBC and D-T cells: R_{in}= 162.1 ± 6.3 MΩ (1-way ANOVA, P-value < 0.05). These electrophysiological parameters are similar to those in the literature (Aponte, Bischofberger et al. 2008; Evstratova, Chamberland et al. 2011; Campanac, Gasselin et al. 2013; Camire and Topolnik 2014)

Finally, PVBC do not have an appreciable sag component compared to CCKBC and D-T cells: 3.10± 0.4 mV (1-way ANOVA, P-value < 0.01).

4.2.2 Axonal location

Slices containing the patched cells were fixed post recording and the biocytin filled neuron was revealed using the streptavidin complex (see **3.10.1**). From the GADGFP line, CCKBC and D-T cells were well differentiated by their axon position. Indeed, CCKBC have their axon in the pyramidal layer, although some CCKBC have collaterals in stratum radiatum and oriens, the majority of the axon was located in the stratum pyramidal (**Figure 18**). In contrast, D-T cells have their axon in stratum oriens and radiatum. The axon found in stratum pyramidal only crossed this stratum to reach either oriens or radiatum strata.

Finally, PVBC's axon location is similar to CCKBC. PVBC's axons are restricted to stratum pyramidal were we even can distinguished some "basket" surrounding some of the pyramidal somas (**Figure 18**). This last observation is similarly valid for CCKBC (see high magnification of basket like synapses in CA1 pyramidal layer **Figure 17**).

As a criterion of selection, interneurons displaying 80% of their axon in the pyramidal layer were considered as BC either CCK or PV depending on the mouse line, and interneurons with axon location on both stratum radiatum and oriens were identified as D-T cells (**Figure 18**). Cells that showed other axonal morphologies or in which the axon was not recovered were excluded from the present thesis.

4.3 Biophysical measurements of CCKBC, PVBC and D-T cells' calcium signaling

4.3.1 Confirmation of the added buffering approach prediction

To determine how interneuron subtypes modulate their calcium signaling, we have firstly studied the biophysical measures that influence calcium ion availability. The parameters that spatially and temporally restrict calcium are the following: endogenous buffering capacity, the extrusion mechanisms, the calcium entry and the dendritic geometry.

By qualitatively measuring the calcium transient shape induced by somatic stimulation among CCKBC, PVBC and D-T cells (**Figure 19**), we noticed distinct amplitudes (ΔF/F) and decay time constants (τ) that represent the calcium entry, the endogenous buffering capacity and the extrusion rate component of each cell type respectively. This difference implies a unique calcium signaling handling in dendrites of those interneurons, either from distinct calcium entry, extrusion pumps and/or buffering capacity.

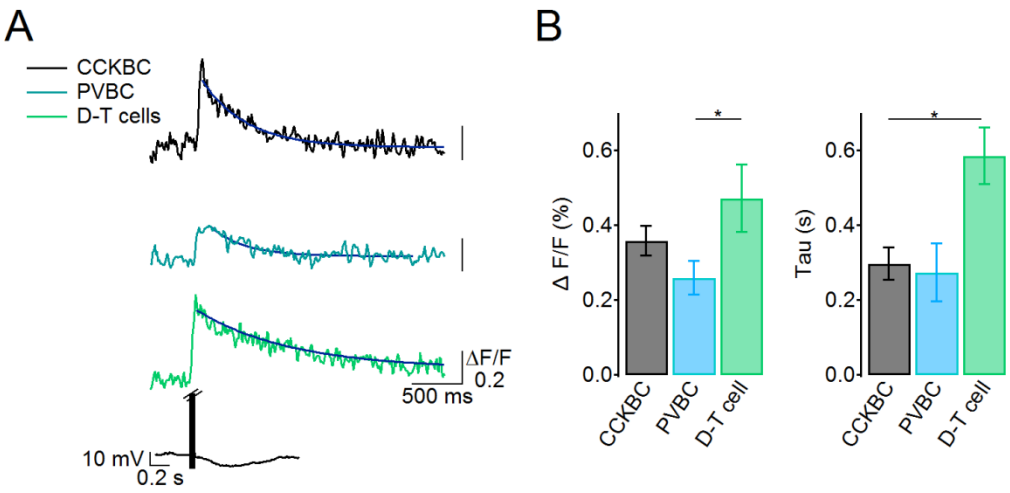

Figure 19 : CCKBC, PVBC and D-T cells have distinct calcium transients induced by somatic stimulation

A) Calcium transient traces obtained from somatic depolarization induced 3 AP in CCKBC (black), PVBC (blue) and D-T cells (green). (Bolus of 500µM OGB1 for 5 minutes).

B) Quantification of calcium transient's amplitude (ΔF/F) and decay time constant (τ) in the 3 interneuron subtypes studied (CCKBC (n=10), PVBC (n=6) and D-T cells (n=7)). Note the small calcium entry in PVBC compared to D-T cells (ΔF/F= 0.36 ± 0.04, ΔF/F= 0.26 ± 0.05, ΔF/F= 0.37 ± 0.09 for CCKBC, PVBC and D-T cells respectively, 1-way ANOVA, P-value<0,05), and the slower τ in D-T cells compared to both CCKBC and PVBC (τ=298 ± 43ms, τ=275 ± 77ms, τ=587 ± 75ms for CCKBC, PVBC and D-T cells respectively, 1-way ANOVA, P-value<0,05)

Consequently we carried on our experiment by determining the endogenous buffering capacity of CCKBC, PVBC and D-T cells. As explained in **3.5**, our method was the added buffering approach. **Figure 20A** shows an example of how elevating calcium dye concentration leads to a change in the shape of the calcium transient. Indeed, adding more calcium dye (exogenous buffer) in our pipette solution slows down the decay time constant and decreases the calcium amplitude of CCKBC' calcium transient (**Figure 20A** and **Figure 8**).

Additionally, this single compartment model predicts an increase of ΔF/F with an increase of calcium entry but no change in the τ. We thus verified this feature in our interneurons of interest and demonstrated a linear increase of ΔF/F with increasing number of somatically induced APs without any consistent variations in the τ (**Figure 20B**).

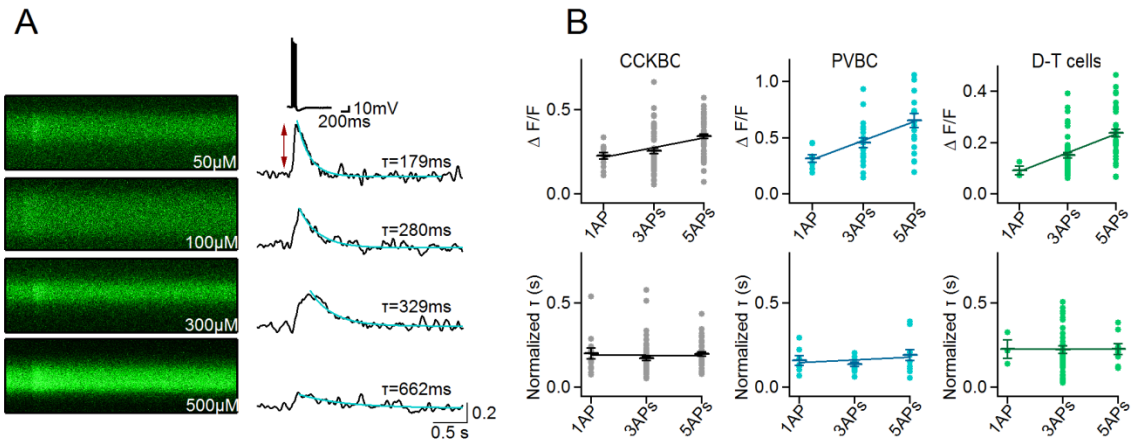

Figure 20 : Experimental verification of the single compartment model prediction in CCKBC, PVBC and D-T cells

A) Example trace of how the addition of exogenous buffer (OGB6F) leads to a decrease in ΔF/F (red arrow: ΔF/F= 0.5; ΔF/F= 0.4; ΔF/F= 0.3; ΔF/F= 0.15 for 50µM, 100µM, 300µM and 500µM respectively) and slowing of τ (blue fit)

B) Top, increase in ΔF/F with increasing the number of somatic APs. Bottom, no alteration of τ (normalized to the dendrite diameter) is seen when varying the number of APs

Consequently, as the single compartment model predictions were verified experimentally, we can use this approach to measure the endogenous buffering capacity of CCKBC, PVBC, and D-T cells.

4.3.2 Endogenous buffering capacity measurement

From the calcium transient trace, we can measure the change in fluorescence with the ΔF/F and τ.

Plotting either the inverse of the ΔF/F (**Equation 4**) or τ (**Equation 5**) versus the added buffering capacity from the dye reveals the linear relationship seen in the **Figure 21**. In addition to measuring the endogenous buffering capacity of cells, it also allowed us to segregate and quantify the mobile and immobile endogenous buffering fraction in a cell early

and late in a single experiment (x-axis intercept), the amplitude or decay of the calcium transient in the absence of dye (y-axis intercept), and the extrusion rate (slope) (**Figure 21**).

Thus, a cell was patched in whole cell patch clamp mode and was somatically stimulated inducing 3 action potentials (APs). The subsequent calcium transient induced by this back propagating action potential (bAP-CaT) was recorded at a proximal site of the dendrite (on average 13 ± 0.5 µm away from the soma).

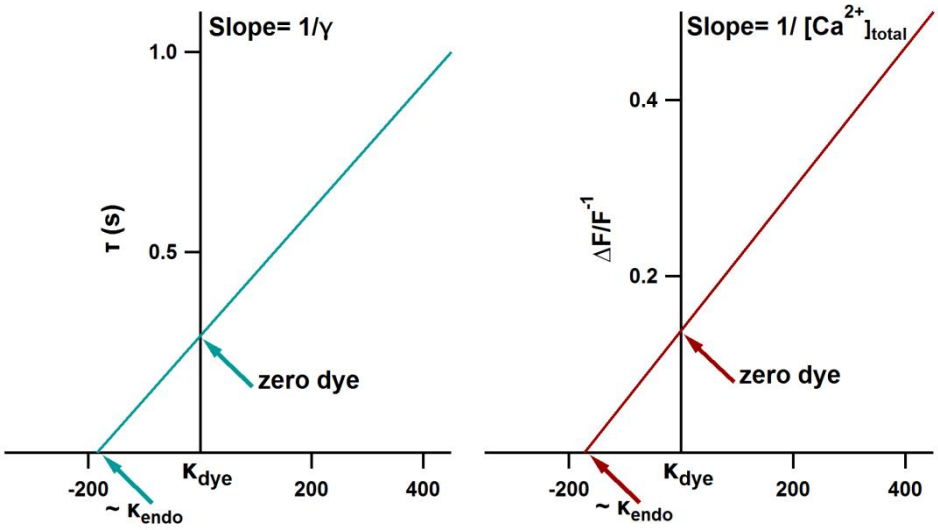

Figure 21 : Prediction of the linear fit of the buffering capacity plot from Equation 4 and Equation 5
The right (positive) portion of the x axis indicates the exogenous kappa introduced by the dye, while the left (negative) portion allows us to extrapolate the endogenous buffering capacity of the cell.
Left: τ vs kappa dye. The slope gives us the extrusion rate.
Right: Inverse of ΔF/F vs kappa dye. The slope yields the calcium entry concentration upon stimulation

As seen from the **Figure 21** extrapolating the x-intercept values from both buffering capacity plots give us an approximation of the whole endogenous buffering fraction.

The total buffering capacity of the two basket cells was nearly similar: 142 ±46 and 194 ±38 for the PVBC and CCKBC respectively (**Figure 22B**). Surprisingly, the D-T cells possess a larger buffering capacity of 332 ±122 (**Figure 22B**). Indeed, interneurons reported in the literature contain a total buffering fraction ranging from 30 to 350 ((Lee, Rosenmund et al. 2000; Lee, Schwaller et al. 2000; Goldberg, Tamas et al. 2003; Aponte, Bischofberger et al. 2008).

Two sets of bAP-CaT measures in the proximal dendrite of our 3 interneuron subpopulations were taken; the first one was done rapidly after opening the cell membrane (5-10 minutes) and the second after 20-25 minutes (**Figure 22**). Indeed, calcium binding proteins can be washed out during long patch clamp recording as seen by the PV wash out in PVBC (**Figure 23**) as well as Calbindin (Cb) wash out in granule cells from Muller's and Matthews' studies (Muller, Kukley et al. 2005; Matthews, Schoch et al. 2013).

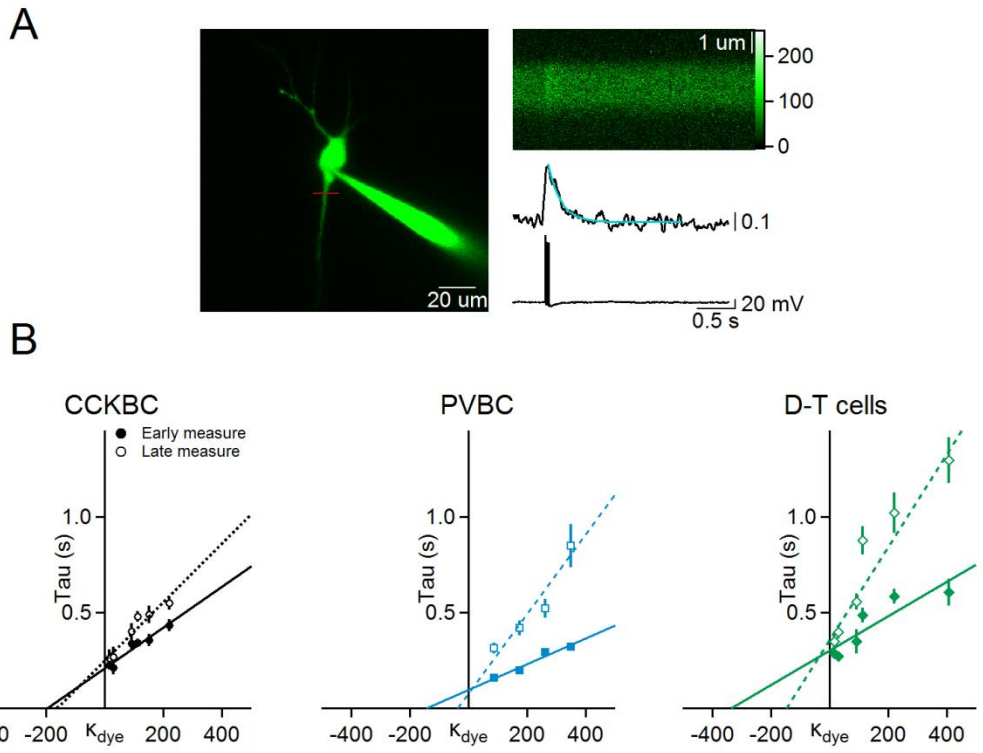

Figure 22 : Determination of the endogenous buffering capacity fraction of CCKBC, PVBC and D-T cells

A) bAP-CaT was elicited in the proximal dendrite of a patched neuron. Left example of a line scan (taken in proximal dendrite: red line) and its corresponding line profile of bAP-CaT in response to 3 somatic APs.

B) Buffering capacity plot of CCKBC, PVBC and D-T cells. Filled line: Early measure (5-10 minutes) and dashed line represent the late measure (20-25 minutes after break in)

Therefore, the first measure of bAP-CaT reflects a minimally-disturbed total endogenous buffering capacity, and the 2nd measure gave us an approximation of only the fixed endogenous buffering capacity of CCKBC, PVBC and D-T cells. The difference of the early and late endogenous buffering capacity measures revealed the mobile endogenous buffering fraction.

We noticed little wash out of endogenous buffer over the recording period in the CCKBC (κ_{early}= 194 ± 38, κ_{late}= 152 ±36) suggesting that CCKBC do not possess appreciable amounts of diffusible calcium binding proteins. As expected by the presence of PV, PVBC contain, in addition to a fixed endogenous buffer fraction, a mobile endogenous buffering capacity fraction which is: κ_{mob}= 105 ± 66, suggesting a high concentration of PV of 236.5µM, (K_d= 10nM) (Eggermann and Jonas 2012). Finally, we found a mobile fraction in the D-T cells of 170 ±133, suggesting that nearly half of the total buffering capacity of these interneurons is contributed by a diffusible calcium buffer (**Figure 22**). We therefore conclude that PVBC and D-T cells possess in addition to their fixed buffer, PVBC κ_{fixed}=38 ± 48, D-T cell κ_{fixed}=162 ± 55, a large mobile endogenous buffering fraction.

4.3.3 Calcium binding protein identity

We have seen that in addition to their fixed endogenous buffering capacity, PVBC and D-T cells contain a mobile buffering fraction, most likely from a mobile calcium binding protein (see **1.3.2.1**). To confirm the wash out of mobile protein in the second time point measurement of the kappa plot (**Figure 22**), we investigated the wash out of PV in PVBC. To do so, TDtomato$^+$ neurons were patched and loaded with biocytin for various durations (2 to 25 minutes). Once the patch pipette was withdrawn, the slice was held at room temperature in a beaker to let it be completely filled with biocytin for post hoc recovery of the axon, and immunostaining for PV content.

It is important to note that the PV staining intensity showed a fast decrease over time indicating a rapid (less than 2 minutes in the soma) wash out of the PV protein in PVBC (**Figure 23**). ROI of PV$^+$ cells and of the patched PVBC were drawn in order to measure the mean intensity value. A ratio (ROI intensity patched PVBC/ MeanROI intensity PV$^+$ cells) was then made between PV$^+$ cells and the patched PVBC. However a high variation of the ratio was observable among time point measures and will be further reviewed in the discussion section.

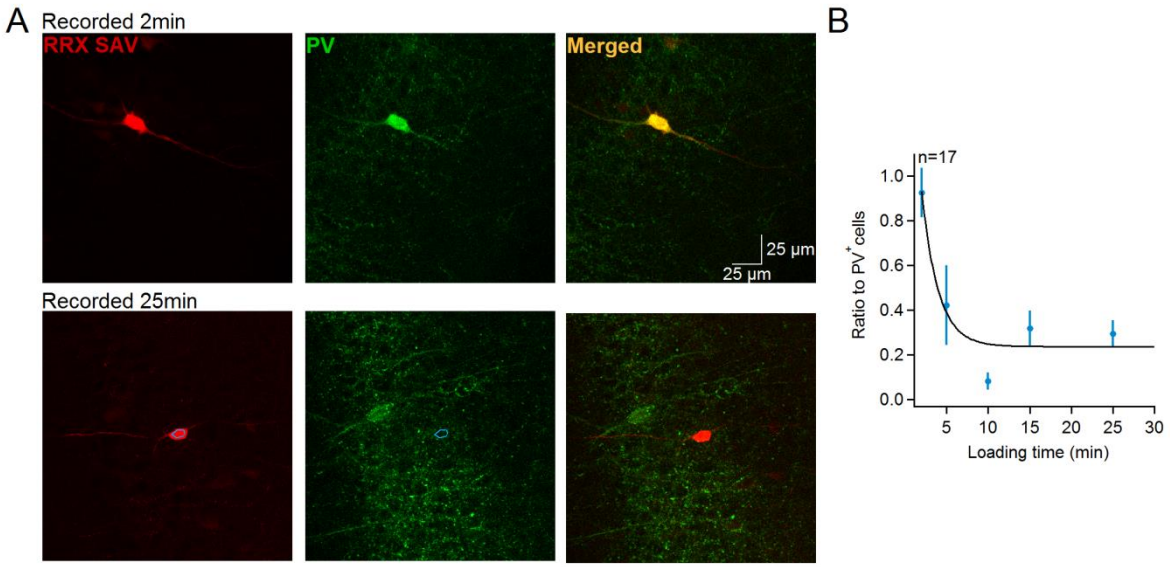

Figure 23：Wash out measure of PV in PVBC

A) Region of interest (ROI) was drawn on the soma of PVBC revealed by RRX SAV and stained against PV. Top panel cells were held in whole cell mode for 2 minutes, bottom panel were held for 25 minutes.

B) Quantification of the ROI intensities over the recording period relative to unrecorded PV^+ cells in the same slice. The solid line is the fitted time course of washout. The τ for this washout was: 1.96 minutes (Single exponential fit).

We then investigated the mobile calcium binding protein responsible for the mobile endogenous buffering capacity seen in the D-T cells. As is pointed out in the introduction, the D-T cells have been rarely studied. However, Cope et al have found 2 Schaffer Collateral associated cells (SC-AC) out of 7 that were positive for calbindin (Cb) (Cope, Maccaferri et al. 2002), and quantification of the GADGFP mouse line in the cortex done by Lopez-Bendito et al showed 43% of GFP^+ cells overlapping with Cb (Lopez-Bendito, Sturgess et al. 2004). Therefore, we examined the immuno-positivity of our D-T cells for Cb by patching them only for a short period of time, fixing them and staining them (see **3.10.2**). However, only 8 out of 15 D-T cells were positive for Cb (**Figure 24**). Additionally, because these D-T cells are not easily distinguishable from CCKBC before the axonal reconstruction, 17 CCKBC were also stained against Cb, but as expected by the data showing minimal mobile buffer in this population, only 2 were found to be Cb^+.

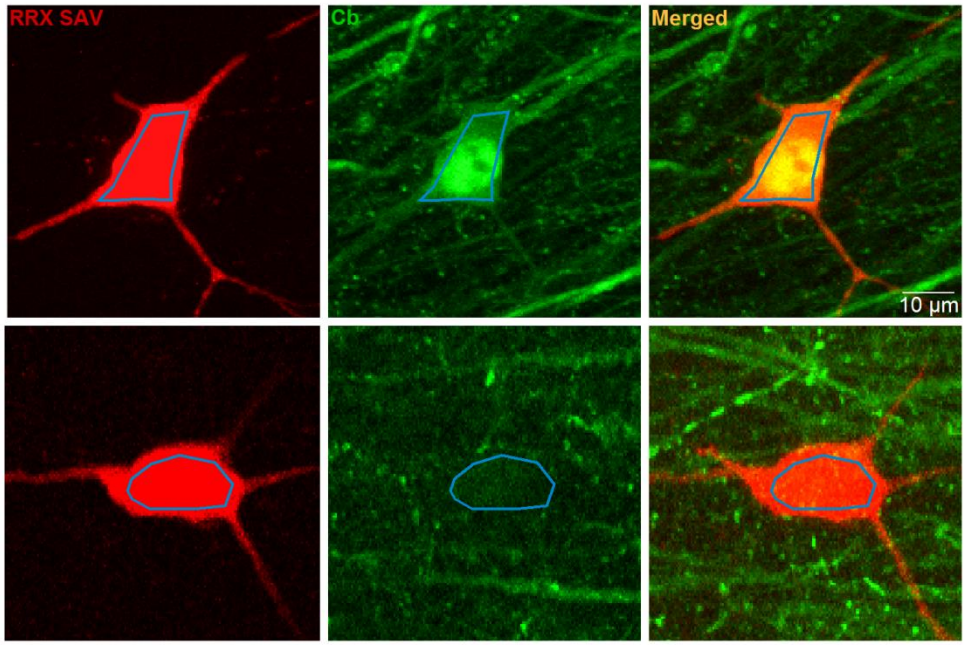

Figure 24 : Staining of D-T cells against calbindin (Cb)
Example of a D-T cell positive for Cb (top) and a D-T cell immuno-negative for Cb (bottom).

We also examined the immunopositivity of D-T cells for calretinin (Cr). We suspected that the reconstruction of Cr positive aspiny neurons found in CA1 stratum radiatum in Gulyás' study (Gulyas, Hajos et al. 1996) might correspond to the morphology of our D-T interneurons. However, all D-T cells (n=4) as well as CCKBC (n=6) were found to be immunonegative for Cr (**Figure 25**).

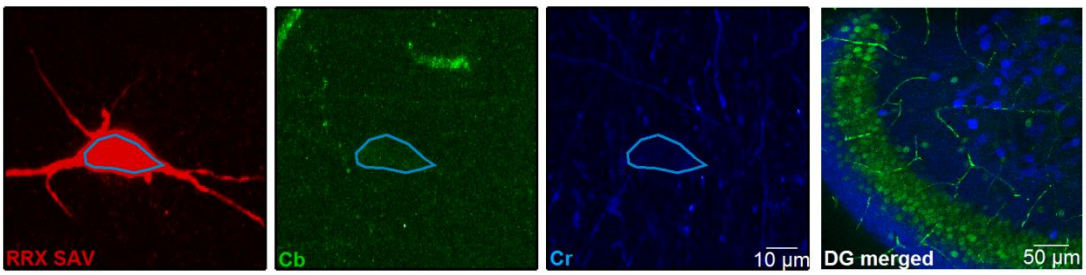

Figure 25 : Staining of D-T cells against calretinin (Cr)
Example image of a D-T cell immunonegative for Cr.
Far right: Picture of the dentate gyrus were the granule cells are Cb^+ and the hilus interneurons are Cr^+ as evidence of the success of the antibody labeling.

Consequently, we conclude that the D-T cells population is a heterogeneous population of Cb^+ cells and that their mobile buffering fraction is likely from the Cb protein and not from the Cr protein. However, no imunno-positivities for other calcium binding proteins were further investigated.

4.3.4 Extrusion rate and rundown of the extrusion rate over time

In addition to extrapolating the buffering capacity, we can deduce the extrusion rate and the calcium entry from the above described relationship (**Equation 4** and **Equation 5**). The extrusion rate arises from the slope of the linear fit in the decay time constant vs the kappa_dye **(Figure 21**). The extrusion rates (γ) were as follows: 925 s^{-1}, 1497 s^{-1} and 1117 s^{-1} for CCKBC, PVBC and D-T cells respectively. Extrusion can depend on the diameter of the dendrite, as large diameter dendrites have a small surface-to-volume ratio (SVR). Thus, we calculated the SVR based on the measured diameter of the dendrites at the point where we imaged (see **3.12**), but we saw no difference among interneurons in proximal dendrites diameters; and in the SVR; 5.5± 0.5μm^{-1}, 5.5± 0.9μm^{-1}, 5.4± 0.4μm^{-1} for CCKBC, PVBC and D-T cells respectively.

Therefore, we conclude that PVBC have a faster extrusion rate than CCKBC and D-T cells.

As mentioned in the introduction (see **1.3.2**), altering the buffering capacity (by washing out a mobile buffer) is expected to affect the $[Ca]_i$ according to the single compartment model, and since the extrusion pumps are sensitive to the $[Ca^{2+}]_i$ and the $[ATP]_i$ and calmodulin (see **1.3.3**), a long recording may lead to a rundown of [ATP].

Consequently, to confirm that by washing out the mobile endogenous buffering fraction over the recording period, we do not alter the availability of $[Ca^{2+}]_i$ and/or that the depletion of [ATP] is similar over neurons, we carried out a new series of buffering capacity measurements. However, instead of having only 2 time point measurements we measure bAP-CaT every 5 minutes starting from the opening of the cell until 40 minutes (**Figure 26A**). We then binned our time point measurements to get 3 different ranges: 5-10min, 15-20min, 25-40min (**Figure 26B**). Indeed, no difference in τ from 25 minutes to 40 minutes was seen. When plotting the different γ obtained from the linear fit of the distinct time point measurements, we did not see any difference in the extrusion rate over time between CCKBC and D-T cells (**Figure 26C**). This result indicates that washing out a calcium binding protein does not influence the efficiency of the extrusion pumps. Nevertheless, a time dependent-rundown of the extrusion is similarly seen in both CCKBC and D-T cells, and thus is

independent of the interneuron subtypes but may be a consequence of our long recording period.

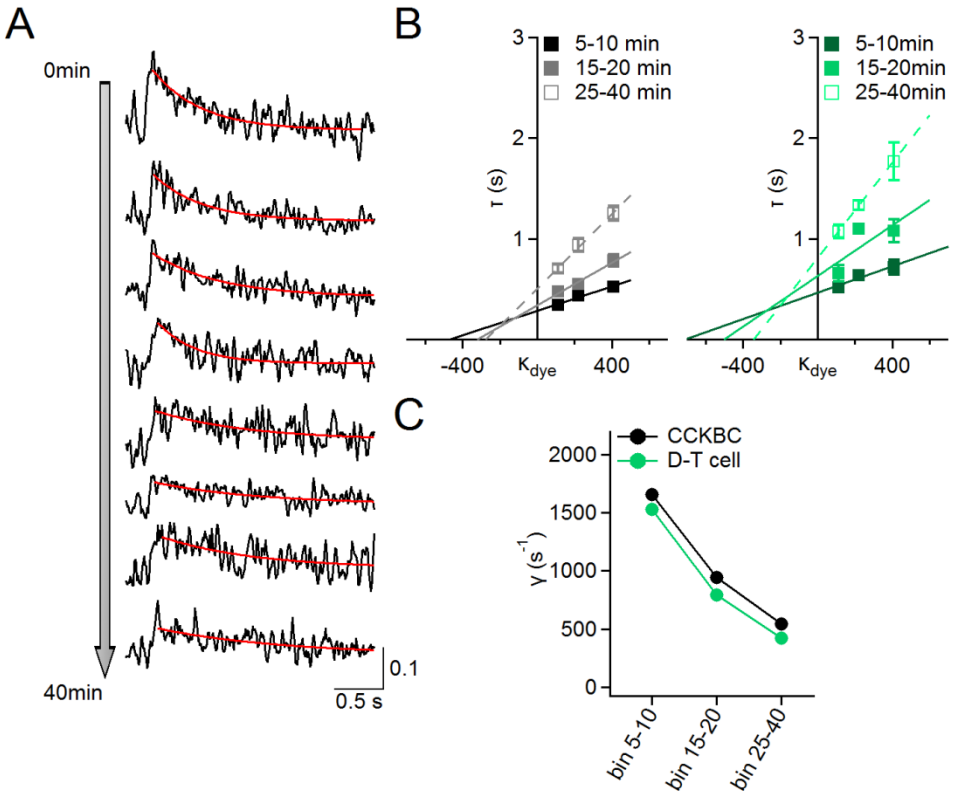

Figure 26 : Extrusion run-down over time is similar between CCKBC and D-T cells
A) Example trace of a CCKBC's bAP-CaT recording over 40 minutes in the same proximal dendrite. Note the decrease in ΔF/F and the increase in τ.
B) kappa plot of CCKBC (black, n=26) and D-T cells (green, n=15) at different time points: 5-10, 15-20 and 25-40 minutes.
C) Plot of the clearance rate obtained from the slope in the kappa plot in B and plotted against the recording time. Note the similar run down of the clearance in both CCKBC and D-T cells.

4.3.5 Assessment of the calcium entry produced by 3 somatic AP

The amplitude of calcium entry in the absence of perturbations caused by the whole-cell recording can be derived from the y-axis intercept of the inverse amplitude vs kappa-dye plot from the early time point measure (**Figure 21**). From this measure we can calculate the relative $[Ca^{2+}]$ increase during a 3AP induced calcium transient. Thus we measured the dynamic range of OGB6F (RF=1.85) and Fluo4 (RF= 16.6) **Equation 1**. Assuming an equilibrium between the free calcium and the dye bound calcium OGB6F (K_d= 3.1µM) and

Fluo4 (K_d= 335nM), we solved the classical calibration equation from Grynkievicz 1985 (Grynkiewicz, Poenie et al. 1985): **Equation 10**.

From 3AP stimulation induced calcium transient, we found that CCKBC had an increase over $[Ca^{2+}]_{resting}$ of $[Ca^{2+}]$ = 79.95 nM, PVBC of $[Ca^{2+}]$ = 62.54 nM and D-T cells of $[Ca^{2+}]$ = 74.17 nM.

4.3.6 Dendritic calcium apparent diffusion coefficient and its action range

To better understand the calcium diffusion along interneurons' dendrites, we next examined the calcium apparent diffusion coefficient (D_{app}). D_{app} describes the diffusion of calcium in both its free and buffer-bound states. Thus the D_{app} equation (**Equation 6**) takes into account the D_{app} of mobile calcium binding proteins as well as the D_{app} of free calcium. However, the calculation of D_{app} for the CCKBC could be simplified as we did not measure a mobile buffer fraction. In addition, our measure of fixed buffer in CCKBC predicts a slow diffusion of calcium in comparison to calcium diffusion in the absence of any buffers (D_{Ca}^{2+} = 223µm2/s Allbritton, Meyer et al. 1992). D_{app} for CCKBC was found to be 1.14 ± 0.29µm^2/s. The diffusion coefficient of PV in the soma is 43µm^2/s, but in dendrites is 12 µm^2/s (Schmidt, Brown et al. 2003). The value of the diffusion coefficient of PV within dendrites was used in **Equation 6** to assess PVBC D_{app}. Because of the fast diffusion of PV, PVBC have a dendritic D_{app}= 10.37± 2.3µm^2/s. In addition to the mobile coefficient of PV, **Equation 6** considers the D_{Ca}^{2+} value, but as PV mobility, the mobility of free calcium may as well be reduced in dendrites. Indeed the previously mentioned D_{Ca}^{2+} was determined from a cytoplasmic extract of *Xenopus* oocytes which may appear different depending on the cell compartment.

Finally, although we determined that our population of D-T cells likely had a heterogeneous mobile buffering profile; we used the diffusion coefficient of Cb D28k to estimate D_{app} in those cells. The mobile coefficient of Cb D28k was previously evaluated by Schmidt et al (Schmidt, Schwaller et al. 2005) and was measured at 20µm^2/s. Thus, D-T cells' D_{app} is 10.87± 1.5µm^2/s.

The spatial diffusion of calcium is not only sensitive to the endogenous buffer but also to calcium extrusion (Goldberg, Tamas et al. 2003). Indeed, extrusion and buffering work in tandem to limit the spatial action of calcium. However the D_{app} measure only takes into account the endogenous buffering capacity of the cell. Thus, D_{app} by itself is not sufficient to understand the spatial extent of dendritic calcium signals. Consequently, we have determined the spatial action range of calcium entering a cell's dendrite to further characterize how far a

free calcium ion could travel to bind a hypothetical calcium sensor. To do so, **Equation 9** was solved and the calcium action range was found to be 0.77µm, 1.5µm and 2.87µm for CCKBC, PVBC and D-T cells respectively.

From this value, we can conclude that CCKBC tightly restrict calcium entry to less than 1µm, and so calcium is more broadly activating calcium dependent processes in PVBC and DT dendrites than in CCKBC dendrites (**Figure 27**).

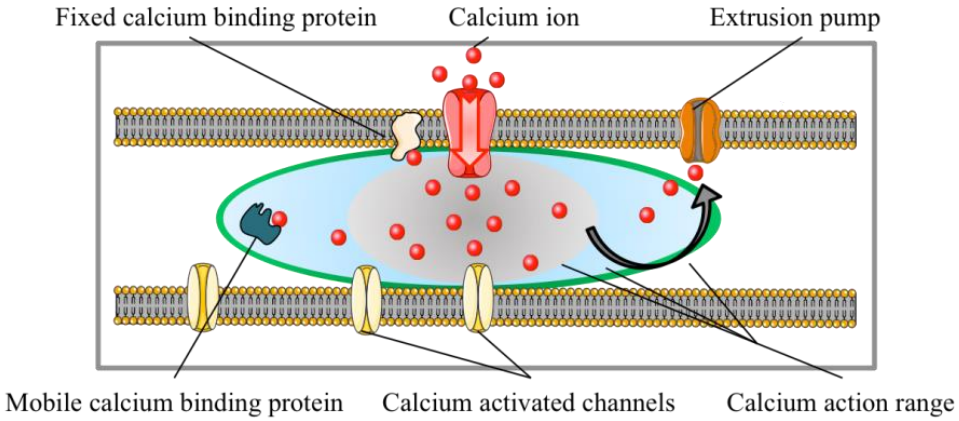

Figure 27 : Summary of the calcium entry regulation in CCKBC, PVBC, and D-T cells
Upon opening of calcium source (VGCC), free calcium is rapidly bound by fixed (anchored to the membrane) and/or mobile (free in the cytoplasm) buffers. Note that the colored clouds in the dendrite interior indicate the spatial range of calcium for CCKBC (grey), PVBC (blue) and D-T cells (green)

4.4 Resting calcium concentration of CCKBC, PVBC, and D-T cells

The amount of free calcium at rest determines the occupancy of any calcium binding proteins, and thus the available buffering capacity when an action potential or other signal causes calcium entry. Thus, the difference in buffering capacity seen in the interneurons subclasses might be explained by a difference in resting calcium concentration ($[Ca^{2+}]_{rest}$). To test this hypothesis, Dr Matthews used fluorescence lifetime imaging (FLIM) to measure $[Ca^{2+}]_{rest}$ in the 3 interneurons subtypes studied (see **3.9**). By measuring the lifetime of OGB1 in the soma and proximal dendrites, the $[Ca^{2+}]_{rest}$ is determined. Cells were recorded under AP5 (20µm) and CNQX (5µM) to avoid any synaptic inputs contributing to calcium entry and thus bias the recording of $[Ca^{2+}]_{rest}$. Frame images of the soma were acquired during whole cell recording at the cells' resting membrane potential (V_m=-62.8 ± 1.3mV, -59.22 ± 1.8mV and -63.8 ± 2.3mV for CCKBC, PVBC and D-T cells respectively). The OGB1 lifetime decay curve was measured from a ROI at the soma (**Figure 28A** and **3.9**). This lifetime was then

fitted with a biexponential decay (see **3.9** and **Figure 28B**). $[Ca^{2+}]_{rest}$ of PV basket cells was measured at 140 ± 28.9 nM, while CCK basket cells and DT cells were measured at 106 ± 7.3 nM and 111 ± 15.8 nM respectively (**Figure 28C**). There is no significant difference in $[Ca^{2+}]_{rest}$ between the interneuron subtypes (1-way ANOVA and Tukey test, P-value>0.05), so the reported difference in buffering capacity is not due to differing levels of buffer occupancy at rest in these cells.

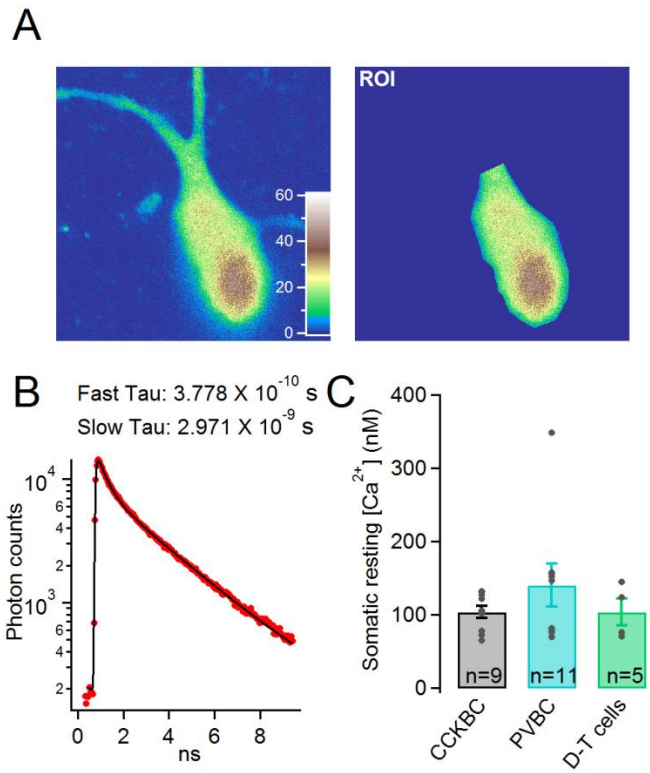

Figure 28 : Similar calcium resting concentration in CCKBC, PVBC and D-T cells

A) FLIM image of an interneuron's soma, with the example of a ROI targeting the soma. Color scale represents the photon count/pixel.

B) Lifetime curve of the ROI containing a fast and a slow decay time constant. This curve is used to extrapolate the actual somatic resting calcium concentration ($[Ca2^+]_r$) from the neurons studied.

C) Quantification of $[Ca2^+]_r$ of CCKBC, PVBC and D-T cells.

4.5 Dendritic synaptic activation leads to calcium transient

4.5.1 iGluSnFR injection

In order to understand how calcium signaling accumulates upon dendritic input, we designed a series of experiments using virus injection in mice. As mentioned in the Materials and Methods (**3.11.1**), iGluSnFR is an interesting tool giving us a read out of glutamate receptor activation by the variation of ΔF/F of a glutamate receptor sensor positioned in the dendritic membrane of neurons. We thus injected this virus to a PV Cre reporter line to specifically induce iGluSnFR in PV^+ interneurons (see **3.11.3**).

Unfortunately, although the virus was strongly expressed in PV^+ interneurons, those cells were unhealthy when patched to perform the experiment. A quick check of the iGluSnFR

response was done in one of the interneurons patched to see whether indeed the viral construct was expressed and functional. By placing a stimulating electrode near the dendrite of the patched neurons in stratum radiatum, we successfully imaged iGluSnFR response (**Figure 29**).

The ultimate goal of this experiment was to simultaneously record glutamate (iGluSnFR, green) and calcium (calcium dye: Xrhod5f, red) signals upon Shaffer Collaterals stimulation.

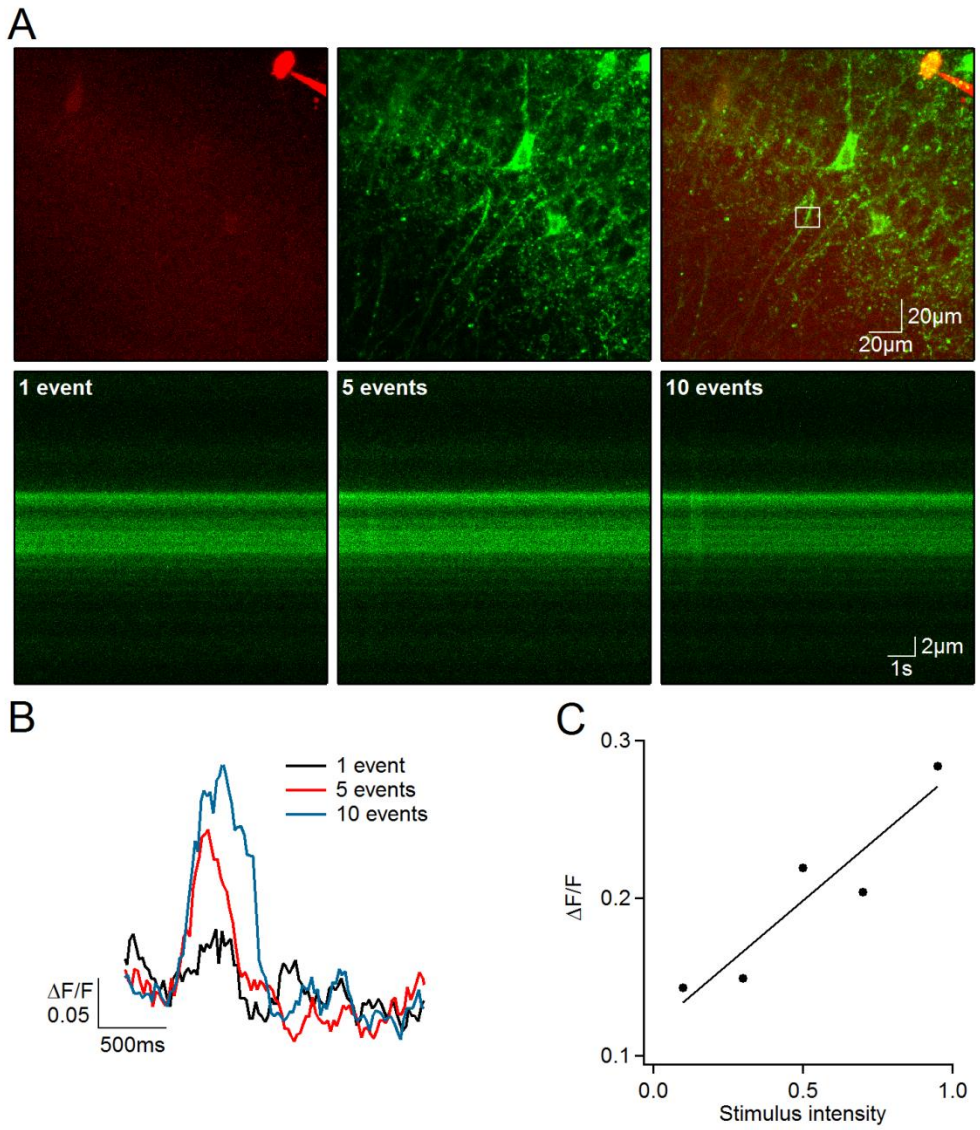

Figure 29 : Example of iGluSnFR response induced by stimulating the Shaffer Collaterals

A) Overview of the cell patched (red), also expressing the iGlusnFR virus (green). The cell was not healthy (V_m= -30mV) and died quickly after the whole cell configuration. However, different trains of presynaptic stimulations were evoked leading to iGluSnFR responses (line scans, 1, 5 and 10 events.)

B) ΔF/F of the iGluSnFR response upon 1, 5 and 10 events.

C) Linear increase of ΔF/F induced by 10 stimuli vs the increase in stimulus intensity.

These experiments were stopped after 3 batches of virus injection in mice, due to a low viability of interneurons transfected with iGluSnFR virus as well as poor breeding of the PVCre mouse line.

4.5.2 Synaptic stimulation induced calcium transient

Instead of using iGluSnFR expression in interneurons to understand how those interneurons integrate their dendritic input, we thought to minimally stimulate the CA3 Shaffer Collaterals to elicit an EPSP arriving in the dendritic shaft in interneurons and measure the resulting dendritic calcium transient. By this experiment, our goal was to first of all see whether a synaptic input leads to a calcium entry, and additionally, investigated the spatial distribution of calcium entry.

As a second goal, we wanted to do a pairing of stimulated EPSP with bAP, and study how it affects the calcium signal since we found different backpropagation properties of our interneurons of interest (see following results **4.6**).

To get a bigger field of view, interneurons were patched using a 40X objective (HCX, apochromat, water immersive, 0.8NA) Different stimulus intensities were applied to determine the minimal stimulation giving a physiological EPSP amplitude response monitored via the patch pipette (**Figure 30**). Once the minimal stimulation was determined, we rapidly scanned the dendrites to locate the site of the synaptic input. In some cases, we could find a section of dendrites with calcium responses temporally linked to the synaptic stimulation.

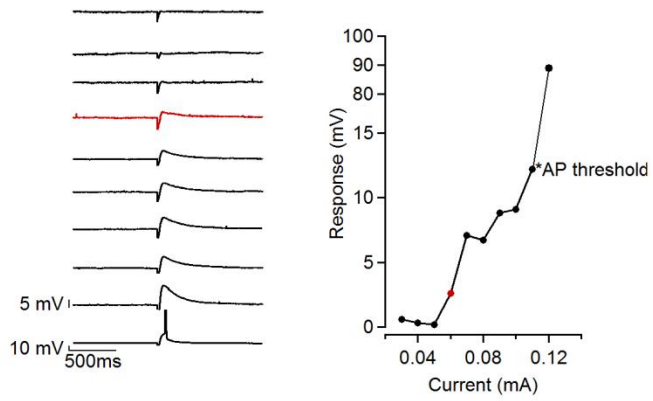

Figure 30 : Setting the minimal stimulation intensity in CCKBC
Left: Example responses at increasing stimulus intensities from a CCKBC. Bottom trace shows an AP at a different scale.
Right: Increasing the stimulating intensity leads to an increase in the EPSP amplitude until reaching the AP threshold of the cell. The red point represents the minimal EPSP response of the cell ($EPSP_{amp}$= 2.6mV)

This experiment could be successfully performed on one cell. Calcium entry was elicited upon Shaffer collateral stimulation and we additionally could induce the complete pairing protocol in one CCKBC (**Figure 31**).

From this single cell experiment, no conclusion can be drawn yet on the dendritic calcium signaling buildup of interneurons. However, this result is promising to acquire a first overview on the experiment design and its outcome. Indeed, these experiments are complicated to set up. First, interneurons have to be patched in a lower magnification to conserve a big field of view. Second of all, after being held for at least 20minutes in order to see most of the dendrite arbor, and checking that the stimulating intensity gives a minimal EPSP response, calcium entry had to be "chased" in every dendritic location until obtaining successful and reliable response. Finally, it appears that the dendrite location where the calcium entry occurs upon minimal stimulation was not stable for long periods. Thus inducing all the paired protocols were challenging.

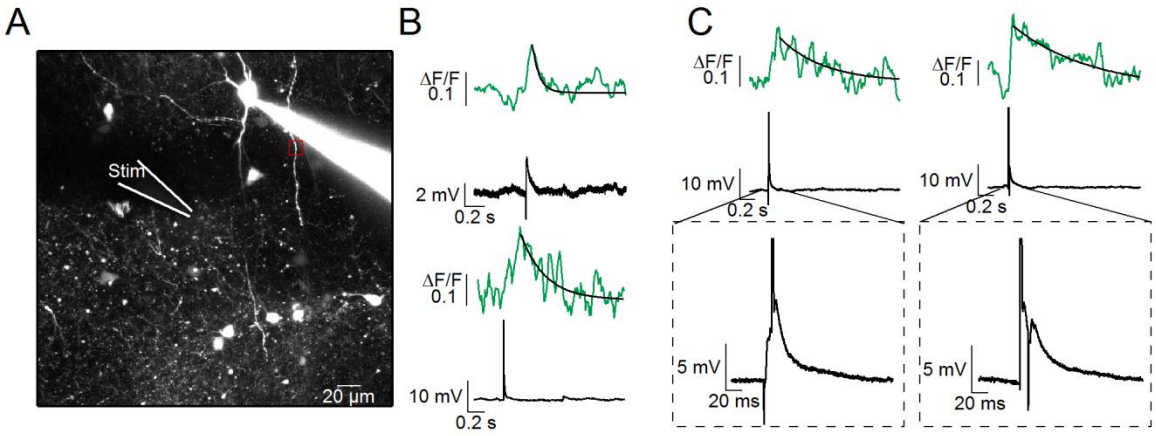

Figure 31 : Calcium signaling differs from synaptic stimulation to bAP in CCKBC

A) Overview of a CCKBC patched in stratum radiatum and the stim electrode placed nearby. Red square: Dendritic calcium signal upon Shaffer Collateral stimulation. Cell was patched with TMR (100µM) and OGB1 (100µM)

B) Top: Calcium transient in response to a physiological synaptic stimulus $EPSP_{amp}$ = 3.2mV. Note the fast τ = 70ms, $\Delta F/F$ = 0.14. Bottom: bAP-CaT, note the slower τ = 293ms, for a small increase in $\Delta F/F$ = 0.22.

C) Calcium transient induced by pairing a stim EPSP with a bAP (left) or vice versa (right) with a 10ms interval. Pairing first a stimulated EPSP with a bAP induced $\Delta F/F$ = 0.19 and τ = 587ms. Reversing the pairing (first bAP then stim EPSP) increased the $\Delta F/F$ = 0.30 and slowed the τ = 973ms.

Nevertheless, in this single cell example, we can see that the order of pairing an EPSP to a bAP is important to induce coincidence detection of bAP and synaptic input and thus a supralinearity of calcium signal. In this cell pairing bAP-EPSP led to a nearly calcium

supralinearity in comparison to the calcium transient induced by bAP or synaptic stimulation alone, and the calcium transient amplitude is nearly the sum of both calcium transient amplitude induced by bAP and the stimulated EPSP. In addition, pairing EPSP-bAP did not induce a supralinear calcium transient but rather the average calcium transient amplitude between the bAP-CaT and the stimulated EPSP induce calcium transient.

4.6 bAP-CaT toward CCKBC, PVBC and D-T cells' dendritic tree: contribution of the endogenous buffer

When an action potential travels back toward the dendritic shaft, it is accompanied by a depolarization of the neuron's membrane. This depolarization causes an opening of voltage gated channels and thus leads to a calcium entry (Catterall 2000; Simms and Zamponi 2014). This feature is important for coincidence detection, synaptic excitability and is involved in spike timing dependent plasticity (Kaiser, Zilberter et al. 2001; Topolnik, Chamberland et al. 2009; Evans and Blackwell 2015). Therefore, we measured the back propagation of action potential induced calcium transient (bAP-CaT) in our interneurons of interest by imaging line scans in dendrites up to 250 µm away from the soma using OGB6F (100µM) and Fluo4 (100µM) while the cells received a somatic depolarization-induced 3 action potentials (**Figure 32**). The ΔF/F measured in each segment of dendrites was normalized to the most proximal measure in the same dendrite (<20µm).

CCKBC and PVBC have a detectable but decreasing bAP-CaT up to 130µm away from the soma while D-T cells showed almost no change in ΔF/F amplitude up to 225µm (**Figure 32C**).

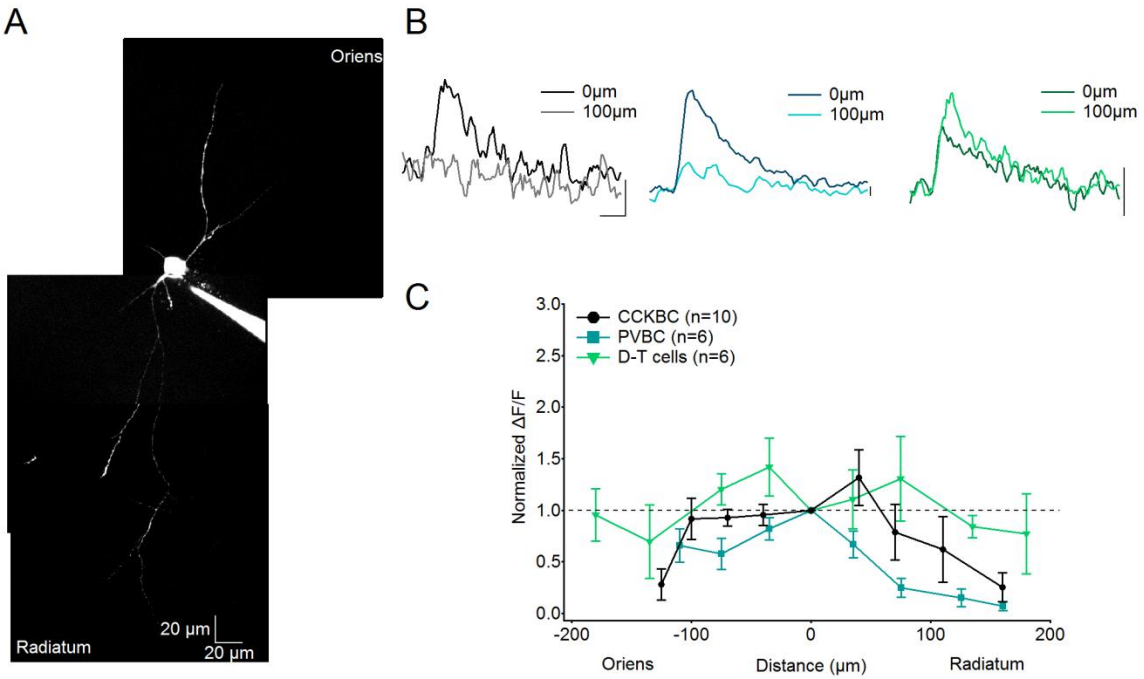

Figure 32 : bAP-CaT in CCKBC, PVBC and D-T cells
A) Overview of a neuron showing dendrites running toward both oriens and radiatum strata.
B) Single trace example of the bAP-CaT in CCKBC, PVBC, and D-T cells at 0µm (proximal site) and 100µm (medial site). Axes: x:250ms, y: 0.1 ΔF/F
C) Quantification of bAP-CaT in the 3 interneurons subtypes. Note that CCKBC and PVBC have large decrease in bAP-CaT amplitude at 100µm, while D-T cells have a stable bAP-CaT. ΔF/F is normalized to the most proximal value of the same dendrite (<20µm).

Two hypotheses can be drawn which might explain the difference in bAP-CaT seen in CCKBC, PVBC and D-T cells: (1) although the SVR is similar between cell types in proximal dendrite, there may be a difference of diameter along the dendritic tree of CCKBC, PVBC and D-T cells. However, plotting the dendrite diameter over the distance from the soma reveals a similar variation in dendrite's diameters over the distance in the 3 interneurons subtypes (**Figure 33**). Nevertheless, we cannot exclude a difference in the distribution of voltage gated calcium channels or distinct distribution of extrusion pumps along the dendritic tree of CCKBC, PVBC, and D-T cells (**1.3.1.1.2**). The second hypothesis is: (2) the unique local endogenous buffering capacity of the 3 interneurons subtypes shape their bAP-CaT.

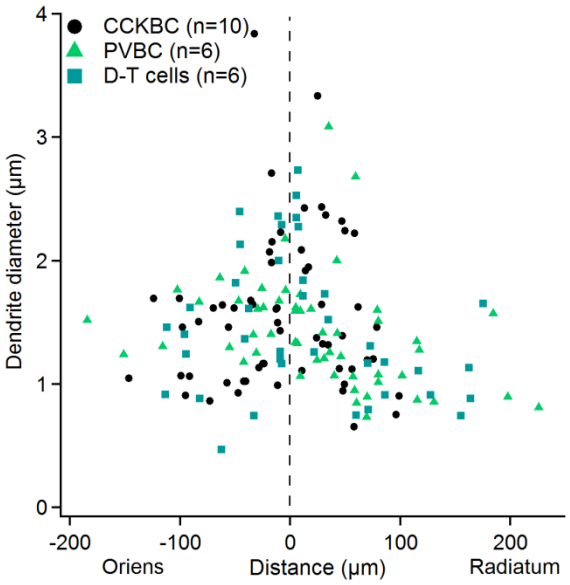

Figure 33 : Similar decrease in dendrite diameter with the distance (from soma) in CCKBC, PVBC and D-T cells

The dendrite diameters are plotted against the distance from the soma. Note the same trend of CCKBC, PVBC, and D-T cells in the decrease of their dendrite's diameters over the distance.

To assess this 2nd hypothesis, we measured bAP-CaT once more, but minimally disturbing the mobile endogenous buffering capacity of PVBC and D-T cells. We thus used the bolus of dye technique. Briefly, interneurons were patched for 5 minutes in order to avoid washing out calcium binding proteins. Meanwhile, a stimulating pipette was approached adjacent to the soma, to somatically stimulate the targeted neurons. To avoid any en passant fiber stimulation, AP5 (20µM) and CNQX (5µM) were constantly perfused in the bath. Indeed by the application of this glutamatergic blocker cocktail, we can assume that only the somatic stimulation induced the cell to fire APs and that it was not depolarized by any other source.

The ΔF/F data obtained with the bolus of dye technique were plotted vs distance as for 100µM dye condition. The non-binned data are in accord with the values obtained in the patch clamp recording mode of CCKBC, PVBC and D-T cells (**Figure 34B**), indicating no alteration of the bAP-CaT once calcium binding proteins have been washed out. Thus we can conclude that bAP-CaT is not influenced by the mobile endogenous buffering capacity of each interneuron subtype studied.

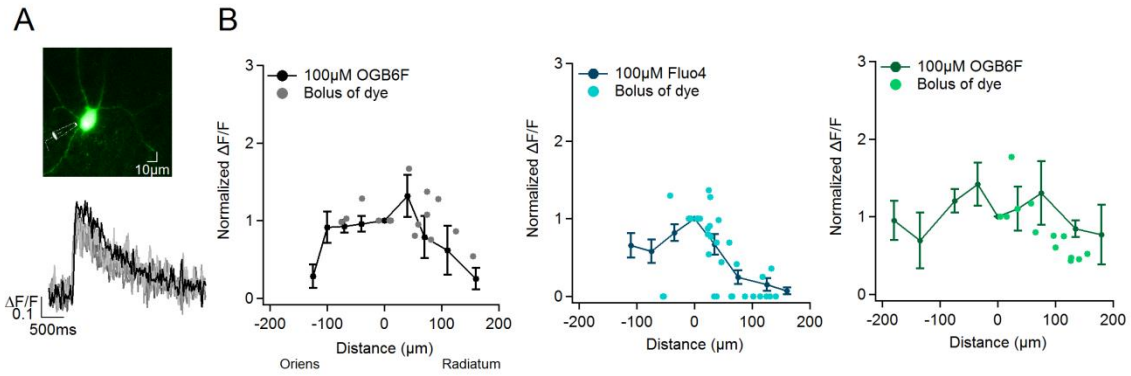

Figure 34 : Minimally disturbing mobile endogenous buffering fraction does not disturb the bAP-CaT of CCKBC, PVBC and D-T cells

A) Image of a neuron filled with the bolus of dye technique (OGB1 500µM) and trace of bAP-CaT over a recording period of 10 minutes following the bolus loading of OGB1. Note the stability of the calcium transients' ΔF/F and τ recorded in the proximal dendrite every 2 minutes during a 10 minutes period (5 traces first trace black, then progressively lighter gray).

B) Comparison between the bolus of dye technique and the patch clamp technique on the bAP-CaT in CCKBC (black), PVBC (blue) and D-T cells (green). The unbinned ΔF/F of the bolus of dye technique is in agreement with the binned ΔF/F data obtained with the patch clamp technique from CCKBC, PVBC and D-T cells.

The next question arising was: are bAP-CaT modulated by the fixed endogenous buffering capacity of the interneurons subtypes?

To answer this question, we carried out a new set of bAP-CaT in the 3 interneurons subtypes but out-competing the endogenous buffer capacity (**Figure 35**).

To do so, neurons were patched with a concentration of high affinity calcium dye (1mM OGB1 or 1.3mM Fluo4, κ_{dye}=2259 and 2264 respectively). As seen in the **Figure 35B** out-competing the endogenous buffer does not influence the bAP-CaT of both PVBC and D-T cells. However, it is another picture for the CCKBC. Indeed out-competing the endogenous buffer reveals a gradient of fixed endogenous buffer along the dendrites of CCKBC (**Figure 35B**). The fixed endogenous buffering capacity is stronger in distal dendrites than in proximal dendrites, indeed the calcium entry is now detectable and even amplified at up to 200µm compared to the proximal calcium transient amplitude (**Figure 35B**).

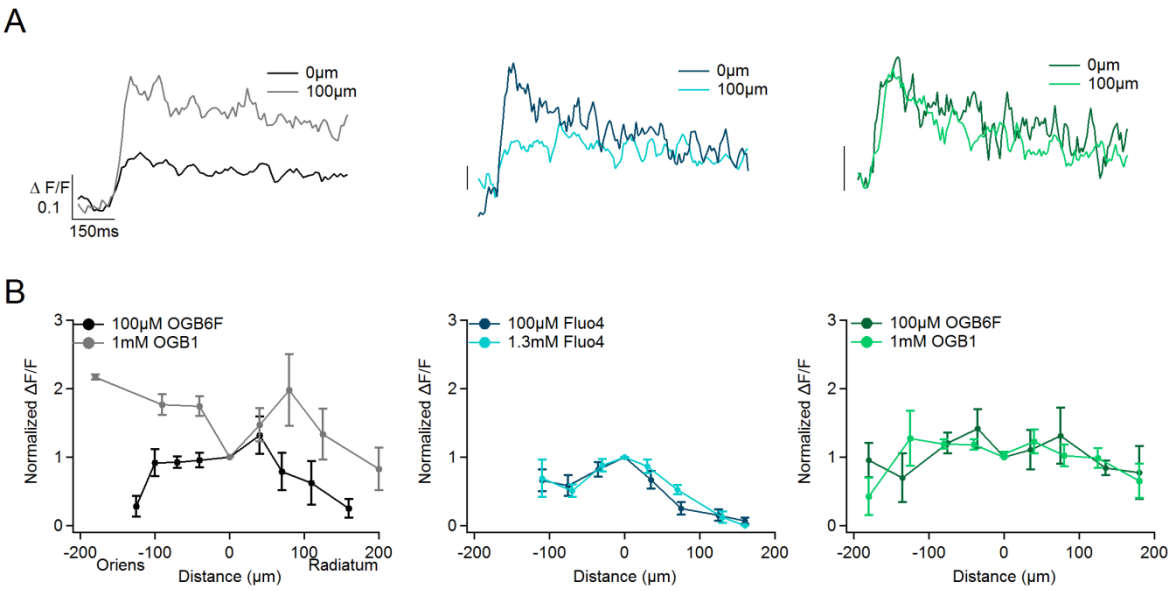

Figure 35 : Out-competing endogenous buffering capacity uncover distal calcium entry in CCKBC

A) Single trace example of a proximal and distal bAP-CaT recorded with high calcium dye in CCKBC (black), PVBC (blue) and D-T cells (green). Note the amplification of ΔF/F in CCKBC in distal position.

B) Plot of normalized ΔF/F against the distance. Comparison of the binned data obtained with low calcium dye concentration and high calcium dye concentration. PVBC and D-T cells show similar bAP-CaT pattern however, CCKBC's bAP-CaT is amplified and more detectable in distal part when its fixed endogenous buffer is out-competed by the calcium dye.

Consequently, it seems that CCKBC restrict their calcium entry even more in the distal portion, both in radiatum and oriens sites, than in proximal dendrites.

4.6.1 Assessing the gradient of endogenous buffer in dendrites of CCKBC using glutamate uncaging technique

To confirm that synaptic input leads to calcium entry, but also that a gradient of endogenous buffer is present in CCKBC's dendrites (**Figure 35**), we uncaged glutamate at proximal and distal dendritic positions and longitudinally imaged calcium entry while monitoring EPSP response with the patch pipette. This longitudinal scan is important to be able later on to calculate the actual diffusion of calcium along the dendritic portion imaged.

The aim of this experiment was to collect data on the diffusion of calcium along proximal and distal dendrites. Since immobile endogenous buffers restrict the diffusion of calcium (see **1.3.2**), if there is a gradient of endogenous buffer in CCKBC as the bAP-CaT data seems to indicate, we should perceive a difference in the apparent diffusion in proximal and distal dendrites of these CCKBC.

CCKBC are primarily aspiny, glutamate uncaging spots (markpoint) were randomly drawn on dendritic segments until a calcium transient induced by the uncaging EPSP (uEPSP) was detectable. In 10 out of 30 positions (n=6 CCKBC), the uEPSP was accompanied by a calcium transient. In the remaining cases, the uEPSP did not illicit a calcium response. uEPSP amplitudes were similar along the dendritic arbor of CCKBC (**Figure 36B)**.

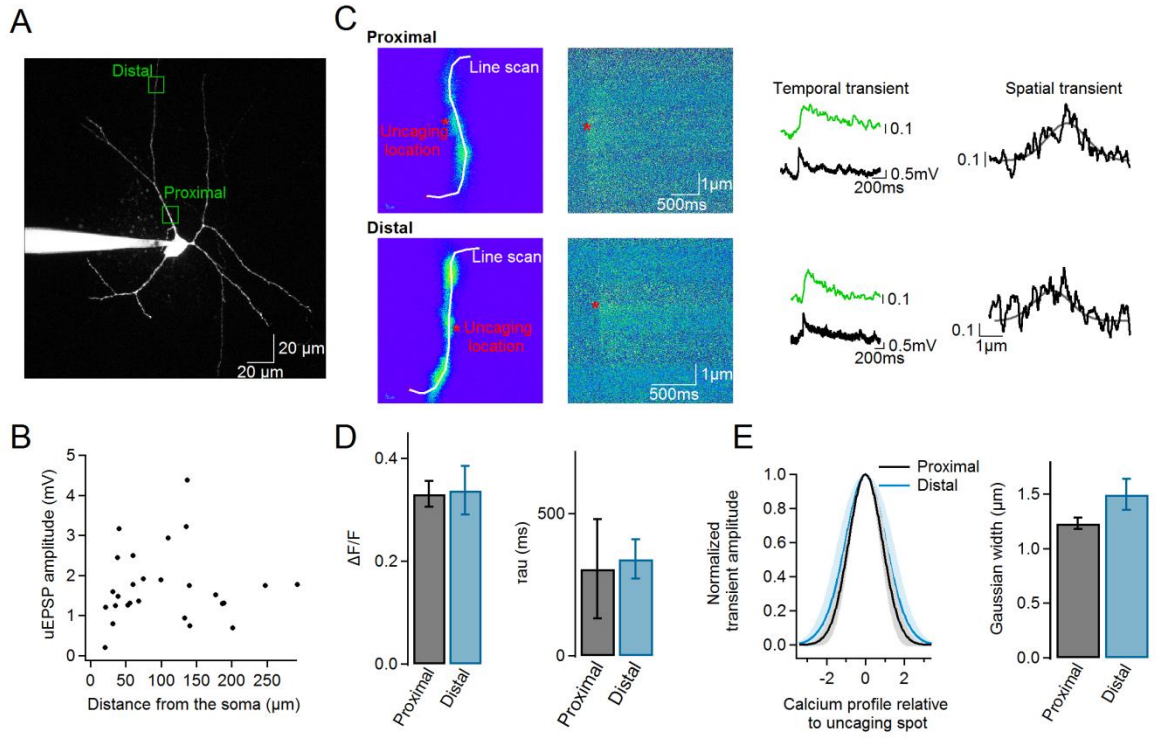

Figure 36 : uEPSP at CCKBC's dendrites induces calcium transient with similar extent in proximal and distal dendrites portion.

A) Overview of a CCKBC patched under the 2P microscope.

B) Plot representing the amplitude of uEPSP vs the distance from the soma. No trend is observable indicating an even distribution of glutamate receptors.

C) Example of uEPSP induced calcium transient in proximal and distal dendritic portion of a CCKBC. Note that 2 calcium transient profiles are taken from each line scan image. A horizontal profile allowing us to calculate the ΔF/F and the τ of the uEPSP-induced calcium transient at the uncaging location. The vertical profile is an average of the first 100ms after the uncaging stimulus, permitting us to measure the width of the calcium transient relative to the uncaging location.

D) Calcium transient amplitude and decay time constant were measured and appear similar in proximal and distal regions ($\Delta F/F_{prox}$= 0.33 ± 0.03, $\Delta F/F_{dist}$= 0.34 ± 0.04, τ_{prox}=306 ± 175ms, τ_{dist}=340 ± 69ms).

E) Additionally, the calcium signal spatial distribution is comparable. The half-width of the fitted Gaussian is: 1.23 ± 0.05µm and 1.40 ± 0.14µm for proximal and distal dendrite portion respectively. Shading represents the SEM. n=3 proximal, n=4 distal.

Calcium transient amplitude is similar between proximal and distal dendrites as well as the decay time constant (**Figure 36D)**. Additionally, the initial spatial distribution of the calcium response is similar between proximal and distal dendrite (**Figure 36E)**.

We then attempted to extract the apparent diffusion coefficient of free calcium from the longitudinal scan taken (**see 3.8.4**).

Unfortunately, the data set was too noisy to clearly obtain relevant values of the apparent diffusion coefficient (D_{app}=2-8µm^2 /s, D_{app}=8-23 µm^2 /s for proximal and distal respectively), and to draw firm conclusions about the possible gradient of endogenous buffer in CCKBC.

4.7 Calcium signaling properties during network activity

4.7.1 Induction of network activity in submerged slices

In order to characterize the behavior of CCKBC, PVBC and D-T cells during hippocampal network activity and thus study their calcium signaling properties, we pharmacologically induced network activity in hippocampal slices using carbachol (Cch).

To allow simultaneous calcium imaging without optical constraints, we needed to elicit network activity in submerged slices. We therefore followed the method from Hajós *et al.* (Hajos, Ellender et al. 2009). To induce reliable network activity seen as extracellular recordings of the rhythmic activity of the stratum pyramidal, different features have to be well controlled; the perfusion rate of the slice was set higher than in the other experiments, and thus get a better oxygenation of the slice (2.6-3 mL/min) (Hajos, Ellender et al. 2009). Furthermore, to better preserve the network inside the hippocampus we increased the slice thickness to 400µm compare to 300µm in the usual experiments (Wu, Luk et al. 2005). In addition, we verified the influence of the temperature on the network activity and found that only the event frequency was increased when elevating the temperature (**Figure 37C**) which was also reported by Kowalczyk *et al* (Kowalczyk, Golebiewski et al. 2001). Finally, TTX (1µM) was applied in the bath in a subset of experiments in order to control that the activities seen are real events and not artifacts. As seen in the **Figure 37B** and **C**, TTX abolished network activity induced by bath application of Cch. 20µM Cch concentration was taken from Hajós study, but at this concentration, our preliminary experiments showed the interneurons' resting membrane potential was too depolarized (V_m= -40 to -44mV). We thus decreased Cch to 10µM and found no alteration of the event frequency recorded in the field of CA1 pyramidal layer (**Figure 37C**). Additionally, the interneurons resting membrane potential was

slightly less depolarized to V_m= -49.5 ± 1.7mV (**Figure 39**). We therefore used Cch at 10µM for our subsequent experiments.

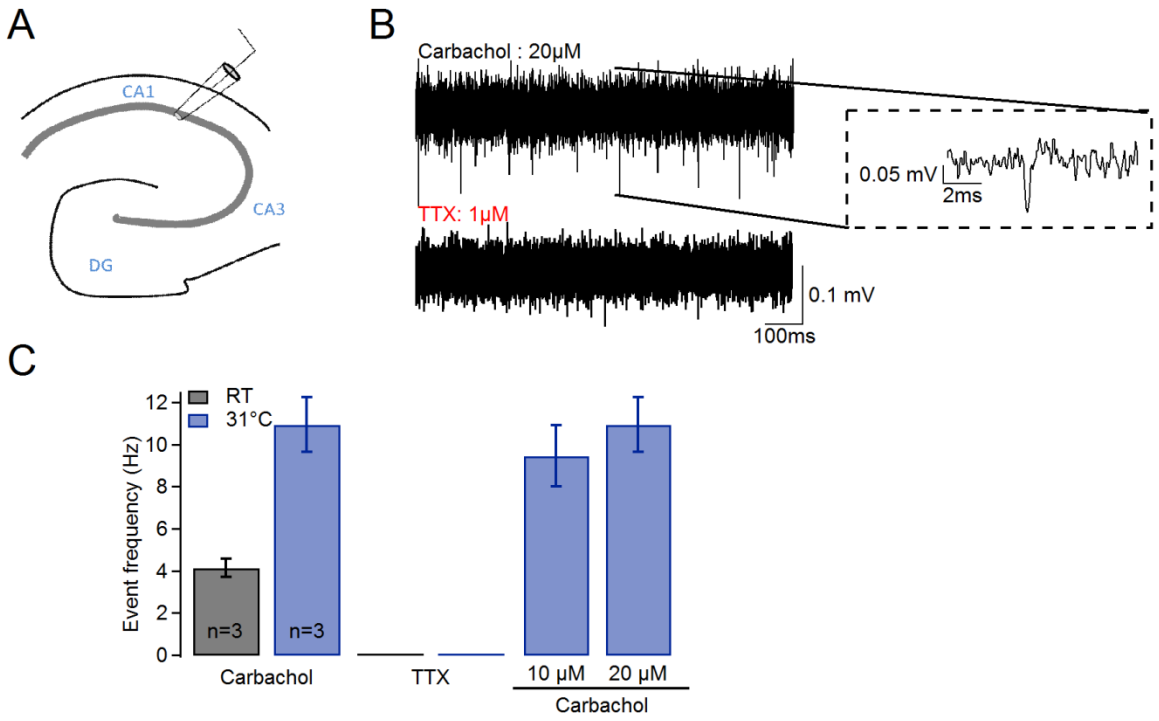

Figure 37 : Pharmacologically eliciting network activity in submerged chamber
A) Schematic view of the field electrode placed on the CA1 pyramidal layer.
B) Field potential recording of the CA1 region during Carbachol (20µM) application and after bath application of TTX (1µM). Note the abolishment of network activity with TTX.
C) Quantification of the event frequencies at room temperature (RT) and at 31°C. Note the increase in event frequency with increasing temperature, but not with decreasing the carbachol concentration

Another way to elicit network activity in slices is to electrically stimulate CA3 pyramidal axons and record the field potential of CA1 pyramidal layer (**Figure 38A**). Compared to inducing network activity pharmacologically in slices, it was much harder to induce activity in slices using electrical stimulation. Nevertheless, we elaborated a protocol with an incremental stimulation of CA3 pyramidal cells' axons (see **3.6**) and induced network activity recorded in CA1 pyramidal cell layer (**Figure 38A**). However the activity frequency was not consistent over time (**Figure 38B slice 1**) and among slices (**Figure 38B** bottom graphs). Additionally, ectopic high frequency activity was seen over the recording time (**Figure 38B** top trace example).

Consequently we decided to focus our efforts on the pharmacologically induced network activity that was more reliable and reproducible among slices and animals, and investigate further interneuron's calcium signaling during network activity.

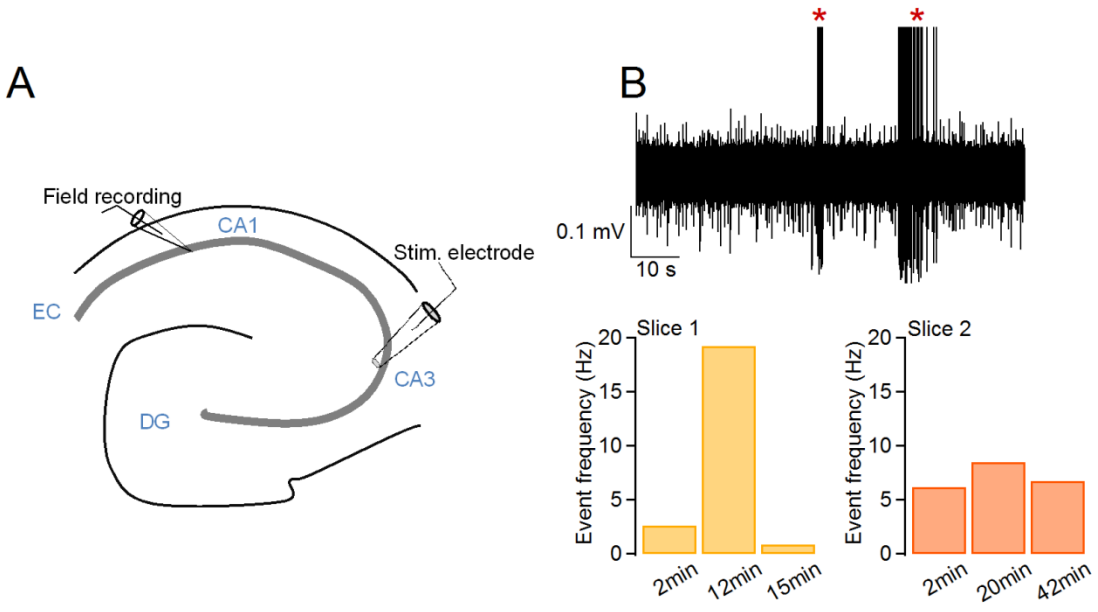

Figure 38 : Electrically eliciting network activity in submerged chamber
A) Schematic view of the field electrode placed on the CA1 pyramidal layer and the stimulating electrode in CA3 region.
B) Field potential recording of the CA1 region after electrical stimulation induced network activity. Note the periodic high activity frequency activity observed (*)
C) Quantification of the event frequencies over time in two different slices. Note the increase in event frequency in slice 1 and the unreliable effect between slices.

4.7.2 CCKBC behavior in an active network

4.7.2.1 Electrophysiology features

Interneuron firing was analyzed during carbachol induced network activity. We used the GADGFP line to first characterize the interneurons' electrophysiology features and thus only selected the CCKBC and D-T cells. Due to the fact that interneuron identity was only determined post-recording, the majority of recorded cells (10/12) were CCKBC. Consequently, only the data from the CCKBC will be further discussed in this section.

Upon Cch application, CCKBC fired spontaneous AP, had a depolarized resting membrane potential and an increased EPSPs frequency (**Figure 39**). Interestingly, these features seen in

CCKBC were previously shown by Nagode *et al* where they reported spontaneous firing of CCKBC during Cch application. (Nagode, Tang et al. 2011; Nagode, Tang et al. 2014).

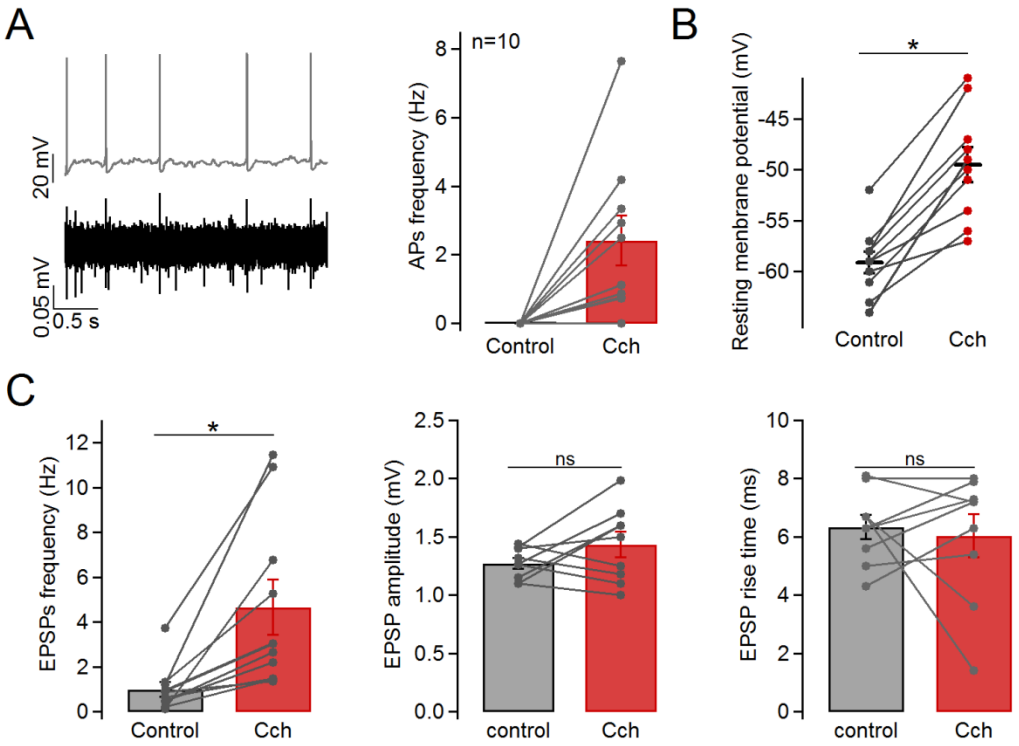

Figure 39 : CCKBC's electrophysiological characteristics during network activity induced by Cch

A) Trace of a CCKBC spontaneously firing in phase with some of the local field potential events. Right, quantification of the firing frequency of CCKBC after 10µM Cch bath application ($f_{control}$= 0 and f_{Cch}= 2.41 ± 0.72 Hz).

B) CCKBC have a more depolarized resting membrane potential when Cch in applied in the bath, on average $V_{m\ control}$= -59.1 ± 1.06mV and $V_{m\ Cch}$= -49.5 ± 1.70 mV (paired t test, P-value < 0.05)

C) An increase in EPSP frequency is seen upon Cch application ($f_{control}$= 0.99 ± 0.33 Hz, f_{Cch}= 4.66 ± 1.22Hz, paired t test, P-value < 0.05) with no change in the amplitude and rise time of the EPSPs before and after Cch application ($EPSPAmp_{control}$= 1.27 ± 0.044 mV, $EPSPAmp_{Cch}$= 1.44 ± 0.11 mV, $EPSPrise_{control}$= 6.33 ± 0.41 ms, $EPSPrise_{Cch}$= 6.037 ± 0.74 ms, paired t test, P-value > 0.05)

As a step toward understanding the cause of the spontaneous firing of CCKBC with application of Cch, we examined whether this feature was due to an intrinsic change in excitability of CCKBC or to the increase in the synaptic drive from the EPSPs frequency augmentation. However, when we blocked the glutamatergic drive by adding CNQX (5µM) and AP5 (20µM) in the bath, CCKBC still spontaneously fired APs (**Figure 40A**).

This result indicates that the spontaneous firing of CCKBC upon Cch application is most likely due to an intrinsic change in their excitability (depolarized V_m, activation of muscarinic

and nicotinic receptors) instead of an increase in the surrounding glutamatergic drive from the spontaneous activity of CA1 pyramidal cells.

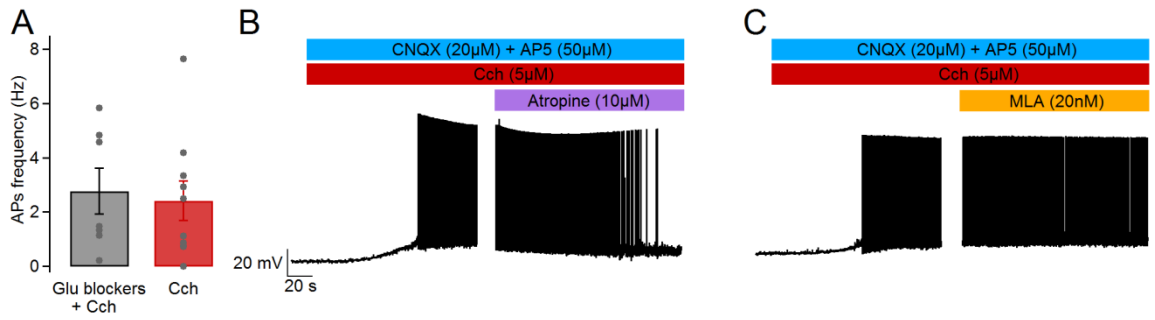

Figure 40 : Spontaneous firing of CCKBC upon Cch application is not abolished by blocking the glutamatergic drive, or by MLA but is blocked by atropine
A) Quantification of the APs frequency with and without glutamatergic blocker (CNQX: 20µM and AP5: 50µM). Note the similar APs frequency although the glutamatergic drive is blocked (f_{Cch}= 2.41 ± 0.72Hz, $f_{Cch+Glu\ blockers}$= 2.78 ± 0.84Hz)
B) Example trace of a CCKBC firing APS and its abolishment with atropine (10µM). Note that the [Cch] was 5µM.
C) Applying MLA, a specific blocker of α7 nicotinic receptor, did not stop the spontaneous firing of CCKBC upon Cch application.

Since the glutamatergic drive blockage does not affect the firing of CCKBC, we verified that we could block it using cholinergic blockers.

Two different blockers were used: the specific nicotinic α7 receptor blocker MLA and the competitive antagonist of muscarinic cholinergic receptors atropine. When MLA was applied in the presence of 5µM Cch, the firing of CCKBC was not altered (n=2) (**Figure 40C)**, however atropine did abolish the spontaneous firing of CCKBC upon Cch application (n=2) (**Figure 40C**).

From these experiments we conclude that the spontaneous firing seen in CCKBC after application of Cch is mediated not by nicotinic receptors but by muscarinic receptor activation, likely from M1 and M3 receptor expressed in CCKBC, and that this M1 and M3r activation triggers a modification in their intrinsic excitability (Armstrong and Soltesz 2012).

We next investigated any alteration in intrinsic excitability from our current clamp (CC) recorded CCKBC upon Cch application. As seen in the **Figure 41** an increase in the after-depolarization potential (ADP) and a decrease in after-hyperpolarization potential (AHP) is observed when Cch is bath applied. ADP and AHP are linked in a way that suppression of the AHP would lead to a longer depolarization and thus a greater ADP (see **1.3.4.2**). One promising component of the I_{AHP} is the SK current produced by potassium dependent calcium

channels (see **1.3.4.2**), known to alter the firing properties of hippocampal pyramidal neurons (Pedarzani, McCutcheon et al. 2005).

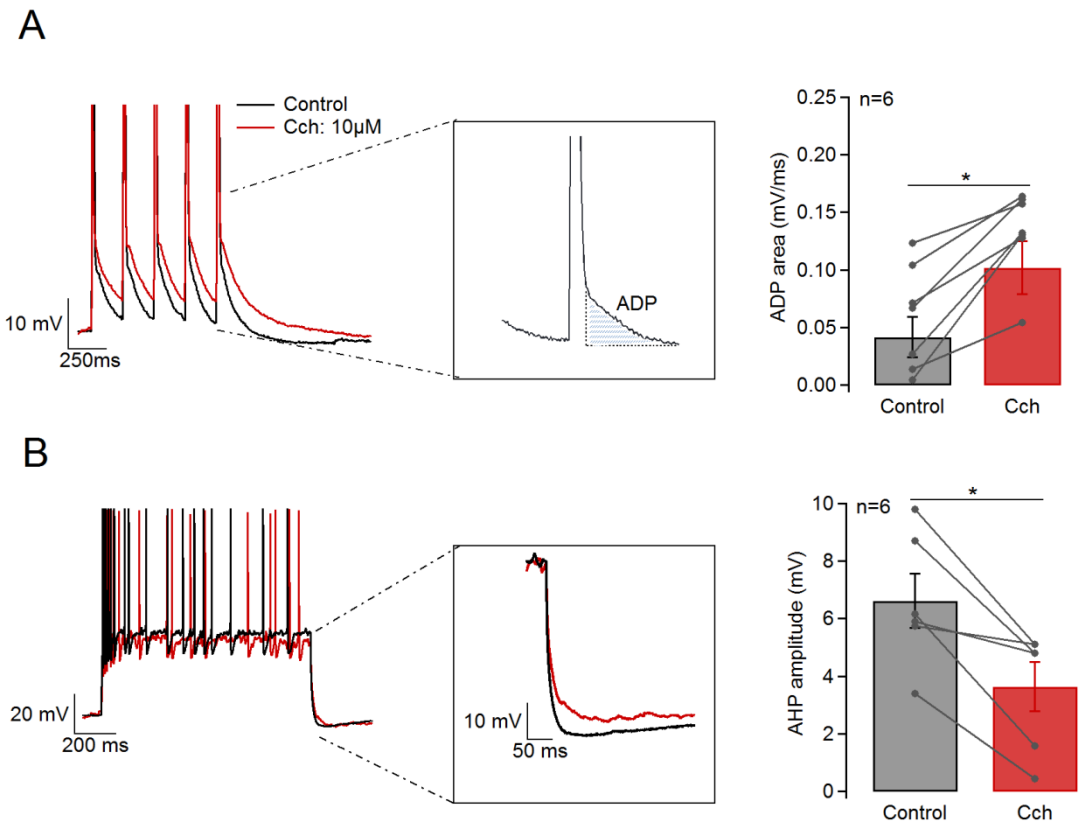

Figure 41 : Variation of ADP and AHP in CCKBC upon Cch application
A) ADP represents the depolarized area seen in the APs late phase. ADP was calculated before (control) and after Cch application. Note the increase in ADP when Cch is bath applied (0.04 ± 0.017, 0.1 ± 0.023 for control and Cch conditions respectively, paired t test, P-value< 0.05).
B) AHP is measured at the peak hyperpolarization following a depolarizing step inducing the same number of AP in control and Cch condition. Note the decrease in AHP in Cch condition (6.62 ± 0.94mV, 3.63 ± 085 mV for control and Cch conditions respectively, paired t test, P-value< 0.05).

Therefore, to confirm the previous change in intrinsic excitability detected in CC, we did some measurement of SK current in CCKBC in voltage clamp (VC) mode.

Interneurons were stimulated using a square step of 200ms and 80mV amplitude. At this voltage stimulation, CCKBC should produce action current; however sodium and potassium current were blocked by bath applying TTX (1µM) and TEA (1mM).

The SK and BK mediated current correspond to the rebound current seen at the termination of the depolarizing step (**Figure 42**). The SK current itself is represented by the component of this rebound current since BK channels are blocked by TEA. Consequently, the maximum

amplitude seen in the first 50ms was measured and considered as the CCKBC SK current (see left trace in **Figure 42**). A control measure of the SK current was first acquired, and then Cch was applied 10 minutes before a new acquisition of the current induced by the previous protocol. Finally, apamin, a specific blocker of SK current was applied 10 minutes prior a new acquisition.

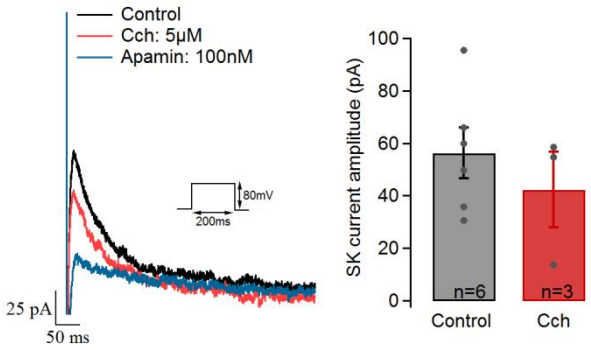

Figure 42 : CCKBC possess SK current which is sensitive to Cch
Left: SK current trace taken following a depolarizing step of 200ms.
Right: quantification of the SK current amplitude in control (TTX 1µM, TEA: 1mM), and in Cch (5µM) after subtraction of the remaining current amplitude measured in apamin (100nM). Note the decrease in SK current amplitude when Cch is applied.

The quantification (see right plot in **Figure 42**) represents the remaining current amplitude after subtraction of the residual current in apamin condition.

From this quantification, we conclude that CCKBC contain a SK current: 56.2 ± 9.6pA, but much smaller than the one measured in pyramidal cells: 374.9 ± 28.3pA (Pedarzani, McCutcheon et al. 2005). In addition, the SK current seems to slightly decrease to: 42.3 ± 14.4 pA with Cch. However, these data are preliminary and further measurement of SK current should be carried on to further explore this possible link between muscarinic activation and calcium dependent potassium channel modulation.

4.7.2.2 Calcium signaling features

Apart from the change in electrophysiological features, CCKBC experienced a variation in calcium signaling upon Cch induced network activity.

By qualitatively examining the bAP-CaT shape before and after Cch application, we discovered that Cch has an impact on the amplitude and the decay time constant of calcium transients elicited by AP (**Figure 43**).

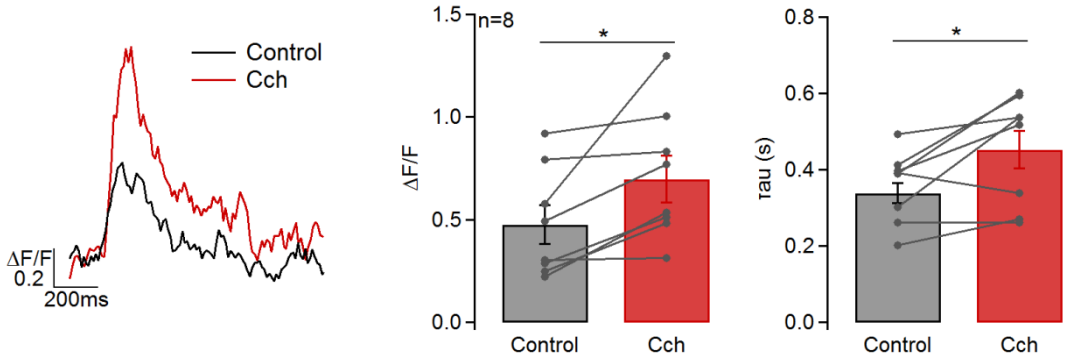

Figure 43 : Cch induces an increase in ΔF/F and τ in CCKBC
Left: Calcium transient induced by 5 bAP in control and Cch conditions.
Right: Quantification of the ΔF/F and τ in control and Cch application. Note the increase in both ΔF/F; control= 0.48 ± 0.09, Cch= 0.70 ± 0.11 (paired t test, P-value< 0.05) and τ; control= 339 ± 26ms and Cch= 452 ± 50ms (paired t test, P-value< 0.05).

A change in ΔF/F might reveal an increase in calcium entry; however the increase in τ may reflect a run-down of the extrusion pumps explained previously (**Figure 26**). Indeed the cell was patched 10 minutes before the Cch bath application and was held 10 more minutes with Cch before the bAP-CaT protocol. So it is possible that the increase in τ is actually the consequence of the run-down in extrusion pumps also seen in the extrusion over time experiment (see section **4.3.4**). Nevertheless, the increase in ΔF/F is not in accordance with the previous run-down observations, because we would expect a decrease in ΔF/F. Consequently, the results suggest an increase in the source of calcium upon Cch application.
In addition to this observation, an increase in baseline brightness was also detected in CCKBC upon Cch application. To verify that this increase was not only due to the spontaneous firing of CCKBC, we applied TTX (1µM) and then applied CCh (**Figure 44**).

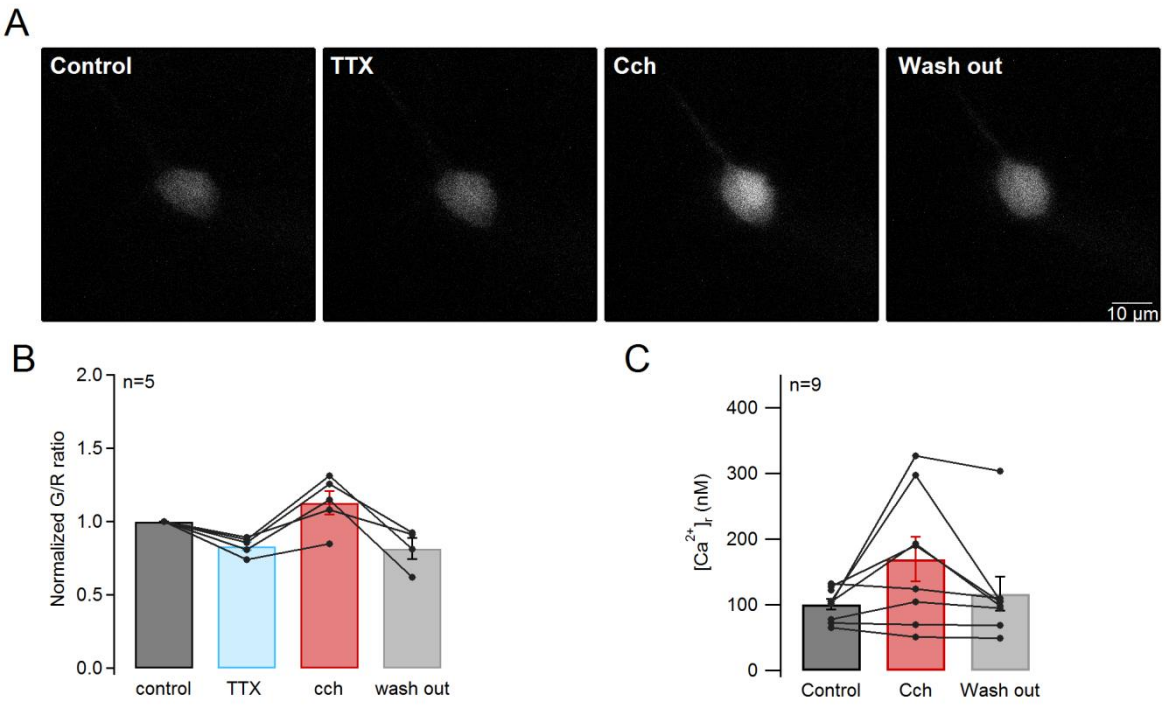

Figure 44 : Cch induces an increase in baseline brightness in CCKBC soma
A) Frame image of a CCKBC soma in control, TTX and Cch application and wash out. Each drug was bath applied 10 minutes before taking the frames. Images were acquired with the same excitation and PMT settings have the same color scale applied to illustrate the increase in baseline brightness in Cch.
B) Quantification of the green/red ratio (G/R) in the soma of CCKBC normalized to the control condition. Note the increase in G/R ratio when Cch is bath applied.
C) Quantification of the $[Ca^{2+}]r$ using the FLIM technique ($[Ca^{2+}]r$= 101.05 ± 7.7 nM, 169.4 ± 33.64 nM, 116.84 ± 25.9 nM for control, Cch and wash out condition respectively.

We observed an increase in the G/R ratio calculated from a ROI drawn on the CCKBC' soma when Cch was applied (**Figure 44B**) although TTX was blocking the firing pattern of CCKBC, a change in the brightness indicates a change in the resting calcium concentration. Indeed the calcium dye brightness is dependent on its bound state to calcium. Thus an increase in resting calcium concentration is seen as an increase in brightness. However, this dye brightness is dependent on the type of calcium dye used and the imaging conditions in confocal calcium imaging (PMT settings and laser settings). Thus, to accurately quantify the resting calcium concentration variation in CCKBC while applying Cch, Dr Elizabeth Matthews used the FLIM technique (**Figure 44C**). She showed a trend of $[Ca^{2+}]_r$ increase with Cch application but no statistically significant difference (1-way ANOVA, pvalue>0.05). From this experiment, we conclude that Cch application does increase the calcium source either from VGCC, cholinergic receptors permeable to calcium, an inhibition of SK current or from a release of intracellular calcium stores with a slight but non-significant increase of the

$[Ca^{2+}]_r$ ([Ca2+]r = 101.05 ± 7.7 nM, 169.4 ± 33.64 nM, 116.84 ± 25.9 nM for control, Cch and wash out condition respectively).

Finally, at the level of single CCKBC dendrites, distinct calcium responses were seen upon M1 and M3 activation.

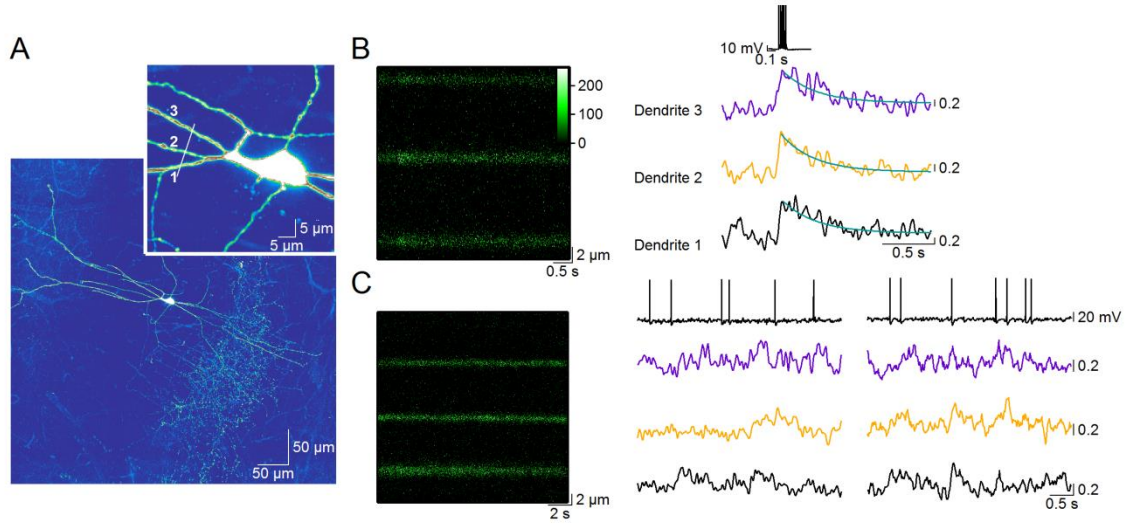

Figure 45 : CCKBC exhibit different dendritic calcium transients upon Cch application
A) Overview of the CCKBC recorded. The numbers 1,2 and 3 reflect the different dendrites recorded
B) Somatic current injection and evoked calcium transients in the 3 dendrites of interest. Note the similar amplitude ($\Delta F/F_{dend1}$= 1.20, $\Delta F/F_{dend2}$= 1.18, $\Delta F/F_{dend3}$= 1.17) and decay time constant (τ_{dend1}= 324ms, τ_{dend2}= 314ms, τ_{dend3}= 312ms) of all 3 dendrites.
C) Bath application of Cch (10µM) induced spontaneous activity in the CCKBC (electrophysiology trace on top) and some calcium transients were visible in dendrite 3 and 2 but not in one. Additionally, calcium transients were not elicited in the same dendritic branch.

As seen in **Figure 45**, three dendrites could be simultaneously recorded during Cch induced network activity. Different calcium transients in those three dendrites were visualized. For instance, some calcium transients were phase locked with bAP, but not all bAP induced a calcium transient. Indeed, the calcium transient in the dendrite 1 in the bottom left panel of **Figure 45C** (black trace), with no corresponding transient in either dendrite 3 or 2 (Green and blue trace respectively). Additionally, calcium transients were recorded without any substantial time locked electrical signals. In conclusion, it seems that dendrites may have their own unique calcium signaling and thus might behave as a single unit of input integration within the cell upon network activity.

4.8 Study of somato-dendritic calcium signaling of Purkinje cells

As a side project, we have combined patch clamp recording with confocal calcium imaging in cerebellar Purkinje cells and studied their calcium signaling.

Mice with constitutive knock out of RIM4γ protein developed hind limb impairment together with a body weight loss. Since RIM4γ is found in very high levels in the cerebellum (Alvarez-Baron, Michel et al. 2013) and the cerebellum coordinates motor controls, a specific RIM4γ KO under the PCP2 promoter has been generated in the laboratory. The PCP2 promoter is solely expressed in Purkinje cells, which are the single output neurons from the cerebellum (Witter, Rudolph et al. 2016). Therefore, in contrast to the constitutive knock out where all region of the brain are lacking RIM4γ, only the Purkinje cells do not contain RIM4γ proteins. These PCP2RIM4γ mice appear to have the same motor phenotype as mice with constitutive knock out of RIM4γ protein, which endorses the implication of Purkinje cells in the motor impairment seen.

RIM4γ's role is so far not properly understood but has been reported to act on dendritic development (Alvarez-Baron, Michel et al. 2013). In contrast to the presynaptic RIM1 proteins (Mittelstaedt, Alvarez-Baron et al. 2010), RIM4γ isoform is not only located in the presynaptic zone but is also diffused in the axon and dendrites of cortical neurons (Alvarez-Baron, Michel et al. 2013). Thus the role of RIM4γ proteins may be more diversified than its RIM1 homolog which tether calcium channels through the active zone via its C_2B domain. As with RIM1, RIM4γ proteins contain a C_2B domain. Therefore, to further study the role of RIM4γ in Purkinje cells, we measured calcium transients evoked by climbing fiber stimulation in the dendrites of Purkinje cells to apprehend the possible dysfunctionality of calcium signaling in Purkinje cells which lack RIM4γ.

A PC cell was patched in whole cell mode and complex spikes were elicited using a stimulation electrode placed next to the cell soma. A complex spike is formed of sodium APs and 3 to 4 calcium spikes generated in the dendrite of Purkinje cells (**Figure 46C**).

Prior to imaging, the Purkinje cell was filled for 10 minutes to let the dye fully equilibrate and to permit visualization of its dendritic arbor. As seen in the **Figure 46A**, the dendritic tree of Purkinje cells was separated into proximal, medial and distal tertiary branches relative to the soma. Purkinje cells display different firing pattern from tonic to bursting (Llinas and Sugimori 1980), which was also noticed in our recordings (**Figure 46B**).

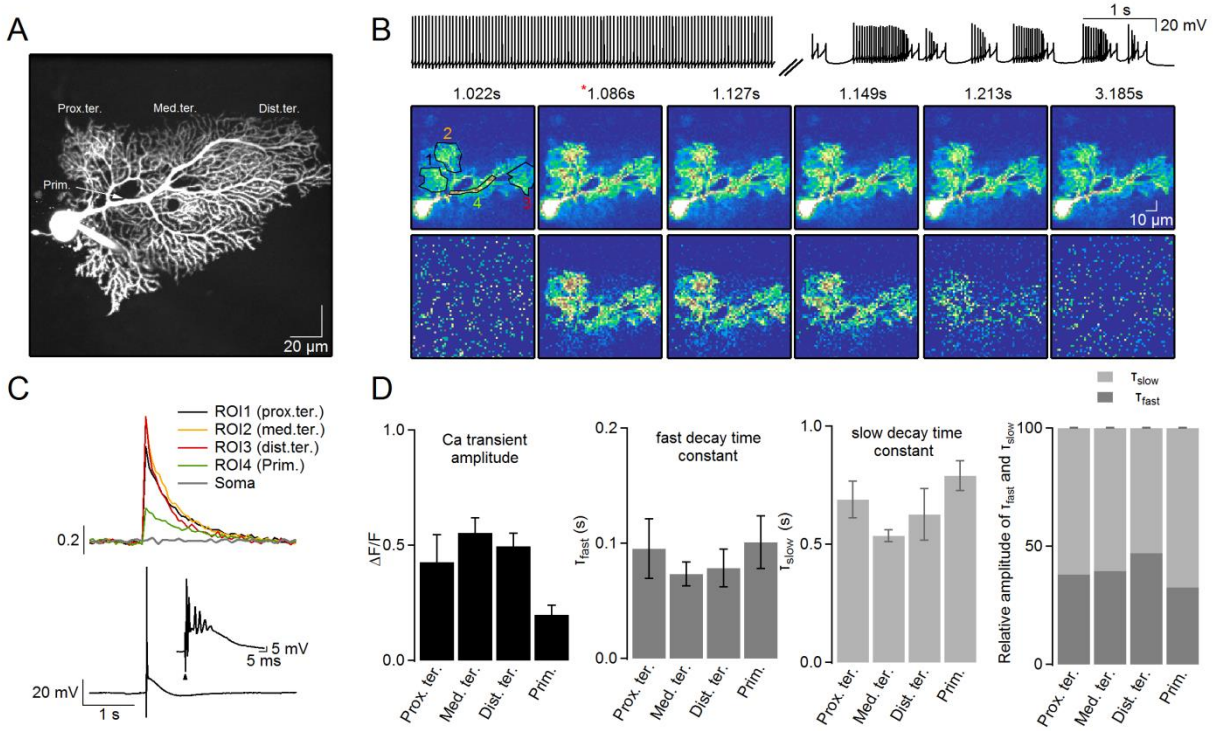

Figure 46 : Climbing fiber stimulation induced calcium transient in the dendritic shaft of Purkinje cells

A) Overview of a recorded Purkinje cell. A stimulating electrode is positioned next to the soma of the patch Purkinje cell to elicit a complex spike. Tertiary branches are separated into proximal, medial and distal relative to the soma.

B) Top: Spontaneous firing of PC. This cell was first tonically active and then displayed a bursting firing pattern. Bottom: T-series example of the PC dendritic tree before, during and after climbing fiber stimulation. Note the increase in fluorescence (Normalized T-series to the baseline, second row of images) when a complex spike is elicited. (*) represents the time of the climbing fiber stimulation.

C) Example trace of a complex spike elicited by climbing fiber stimulation (artefact of stimulation is shown by the black triangle) and the concomitant calcium transient recorded in soma tertiary and primary branches of the dendritic arbor of Purkinje cell.

D) Evaluation of ΔF/F, τ_{fast}, τ_{slow} and the relative contribution of τ_{fast}, τ_{slow} to the total decay time constant of the calcium transient from Purkinje cells (n=10). Note the similar calcium transient parameters in proximal, medial and distal tertiary branches. However, the calcium transient amplitude in primary branches is smaller than in tertiary branches (ΔF/F= 0.2 ± 0.04; 0.43 ± 0.11; 0.553 ± 0.06; 0.50 ± 0.05, for primary, proximal, medial and distal tertiary branches respectively). In addition, the decay time constant seems similar among the different part of the dendritic tree of Purkinje cells: τ_{fast}=100 ± 22ms; 95 ± 26ms; 73 ± 10ms; 78 ± 16ms; and τ_{slow}= 790 ± 62ms; 688 ± 77ms; 536± 26ms; 626 ± 109ms; for primary, proximal, medial and distal tertiary branches respectively. Finally, the relative amplitude of τ_{fast}, τ_{slow} seems similar: τ_{fast}/τ_{slow}= 32.5/67.4 ± 6.1%; 38/62 ± 5.4%; 39.4/60.5 ± 4.2%; 47/53 ± 4.5% for primary, proximal, medial and distal tertiary branches respectively.

Time series of frame images were taken during climbing fiber stimulation in order to evaluate the concomitant calcium transient within the dendrites of Purkinje cells. It appears that the calcium transient fully invaded the dendritic tree of Purkinje cells, however, the calcium

transient amplitude from the primary branches looked smaller. This finding may be explained by a difference in VGCC distribution since it is established that VGCC are more prominent in tertiary dendrites of Purkinje cells (Ross and Werman 1987). In addition calcium transient τ was measured by fitting a biexponential. This nonlinear calcium transient kinetic is explained by the two types of mobile buffer (PV and Cb) in Purkinje cells: PV accelerates calcium transient τ in the first 300ms without acting on the calcium transient amplitude while Cb affects both the calcium amplitude and τ (Schmidt, Stiefel et al. 2003).

No difference so far have been found in the double exponential fit of the decay time constant among proximal, medial, distal tertiary branches and primary branches (**Figure 46 C** and **D**). This is a bit surprising since Ross study showed different time course of calcium transient between proximal and distal tertiary branches (Ross and Werman 1987), and was explained by a possible difference in endogenous buffer concentration along the dendritic arbor of Purkinje cells. However only 10 cells have been recorded and so a greater number of replicates is needed.

Thus far, only WT cells have been recorded but the ultimate goal of this experiment is to compare the calcium signaling of WT to RIM4KO Purkinje cells and further conclude about the possible role of RIM4γ in shaping Purkinje cell calcium signaling.

5 Discussion

5.1 Biophysical determination of CCKBC, PVBC and D-T cells' calcium signaling

Calcium entry, buffering capacity, calcium diffusion environment, and calcium extrusion rate were determined in PVBC, CCKBC and D-T cells using confocal calcium imaging and were found to be unique for each interneuron subtype. Qualitative observations made on the calcium transient shape of CCKBC, PVBC and D-T cells (**Figure 19**) had pointed to distinct calcium entries, extrusion rates and endogenous buffering capacities which match reasonably well with the later quantification of those biophysical parameters underlying the calcium transient amplitude and decay time constant.

Calcium entry in CCKBC, PVBC and D-T cells have four fold smaller calcium entries than excitatory neurons (Helmchen, Imoto et al. 1996) which might be explained by a difference in their calcium channels distribution (see **1.3.1**). In addition, PVBC have the smallest calcium entry in comparison to CCKBC and D-T cells, which corroborates well the state of the literature (Aponte, Bischofberger et al. 2008; Evstratova, Chamberland et al. 2011).

The measurement of the buffering capacity was realized using the added buffering approach and particular attention was taken to record cells' calcium transient at an early and late time point. By recording the bAP-CaT at different time points, we have been able to distinguish between the fixed and the mobile endogenous buffering fraction of CCKBC, PVBC, and D-T cells. This distinction of mobile and immobile buffer was not applied in most of the determinations of endogenous buffering capacity in cells (Kaiser, Zilberter et al. 2001; Aponte, Bischofberger et al. 2008; Liao and Lien 2009; Evstratova, Chamberland et al. 2011; Lorincz, Kisfali et al. 2016), despite the fact that fixed buffer retards the calcium diffusion and mobile buffer accelerates it. However, in our endogenous buffering capacity measurement in CCKBC, PVBC and D-T cells, we have clearly identified a difference of buffering capacity, both mobile and immobile within interneuron subtypes.

PVBC and D-T cells contain a high, mobile endogenous buffering fraction that permits an apparent diffusion coefficient of calcium up to $10\mu m^2/s$. In contrast, our measurement of endogenous buffering capacity in CCKBC reveals no mobile buffer fraction, which confirms the immuno-histological studies performed on CCKBC (Pettit and Augustine 2000; Somogyi,

Baude et al. 2004), and in which no immuno-positivity was found for PV, Cr and Cb. This result further confirms the selection of PV^- BC from the Tg(Gad2-EGFP)DJ31Gsat mouse line used in this thesis.

CCKBC, by only containing a fixed endogenous buffering capacity have a tight spatial compartmentalization of their dendritic calcium (λ= 0.77µm) in the vicinity of the calcium source, which implies that, CCKBC have only very local activation of calcium-dependent processes.

Since fixed buffers are not easily saturated, spatial and temporal input summation may occur, but the free calcium will only be bound by an immobile fraction, leading to a slow diffusion of calcium. This may give the possibility to a second "release of free calcium" as calcium is gradually released by the immobile buffer after the termination of calcium entry from either VGCC or glutamate receptors. This successive calcium release might reflect a "memory trace" of the previous dendrite activation. By such features, the summation of inputs received by CCKBC will be more accurate in a spatial manner than in a temporal integration which support their electrophysiology characteristics and their modulatory role in the hippocampal network (Armstrong and Soltesz 2012).

The buffering capacity of the D-T cells consists of almost 2-fold larger total endogenous buffering capacity when comparing the both BC. Furthermore, this endogenous buffering capacity is formed of a mobile fraction comparable to PVBC mobile fraction and a fixed fraction equivalent to the one measured in CCKBC. By having such a large endogenous buffer amount, we may expect a strong influence on the calcium transient amplitude. However, our data suggest a similar calcium entry in D-T cells and CCKBC, and so the calcium entry seems not sized to correspond to the cell's buffering capacity. The similar calcium entry found between CCKBC and D-T cells was not reported by Evstratova's study where they measured CCKBC and SC-AC entry, which may be due to a difference in the targeted SC-AC subpopulation (Evstratova, Chamberland et al. 2011).

As our immunostaining revealed, D-T cells are a mixed population of Cb^+ and Cb^- cells. This mixed population is reflected by the high variability of the buffering capacity plot, and so, the actual endogenous buffering capacity of D-T cells may be under- or over-estimated.

Our calculation of the apparent diffusion coefficient takes into account the mobility of Cb but as it was shown by Schmidt *et al*, Cb appears immobile in dendrites and spines of Purkinje cells (Schmidt, Schwaller et al. 2005). Therefore, D-T cells could potentially have a larger fixed endogenous buffering capacity than a mobile one, leading to a limited spatial spread of their calcium signal and restricted activation of calcium dependent processes.

In addition to their mobile endogenous buffering fraction, PVBC exhibit a 5-fold smaller immobile fraction than CCKBC. Such small fixed endogenous buffering capacity was also reported OLM cells (Liao and Lien 2009; Matthews, Schoch et al. 2013) and in terminal boutons of the cerebellar mossy fiber after dialyzing the mobile endogenous buffer (Delvendahl, Jablonski et al. 2015).

Since PV is the main mobile buffer in PVBC and is a slow buffer (**Table 1**), the amplitude of the calcium events should not be influenced by the endogenous buffer, but the apparent diffusion of calcium will be greatly increased, thanks to the high affinity and mobility of PV. As was shown by Eggermann's study, PV can act as an anti-facilitating molecule, by its potency to block spatial synaptic summation and supralinearity of calcium signaling (Eggermann and Jonas 2012). However, a local barrage of input should locally saturate the PV, which is a high affinity buffer, and would lead to a greater concentration of free calcium that would then be available to open more voltage gated channels as well as calcium dependent channels, and ultimately could induce a form of plasticity (Burnashev and Rozov 2005).

To confirm that PV was indeed washed out in our recorded PVBC, a series of PVBC recordings at different time points were performed, followed by an immunostaining against PV. A large SEM (**Figure 23**) of PV intensity ratios for each time point was noticeable. An explanation of this variation could be that PVBC may have different starting concentrations of PV in their somata. Therefore, because the starting PV's concentration differs, the end point of PV wash out achieved during our selected time points is variable. Indeed Donato's study showed that PV level is regulated by learning in CA3 PVBC (Donato, Rompani et al. 2013), which could also be the case in CA1 PVBC. In addition, PV proteins have been observed to be regulated as a function of experience and/or training (Donato, Rompani et al. 2013; Donato, Chowdhury et al. 2015): Thus the PV level may be regulated by both internal and external factors that we cannot control for. A recent study from Honeycutt *et al* (Honeycutt, Keary Iii et al. 2016) have shown that PV levels decrease in the hippocampus of young adult (6 months) to adult rat (12 months) compared to adolescent rat (1 month). However, this finding was specific to the CA1 and DG but not CA3 and should not account for the variability seen in the PV wash out data since the mice were all in similar range of age (from p28-45).

The slope of the τ versus the dye kappa permits us to extract information about the extrusion rate of CCKBC, PVBC and D-T cells. This extrusion appears similar in CCKBC and D-T

cells but faster in PVBC. The subsequent extrusion rates extrapolated are in the range of the extrusion rates determined in proximal dendrite of pyramidal cell (Sabatini, Oertner et al. 2002).

The small calcium entry combined with a fast extrusion rate and a large mobile buffer emphasize once more the tight spatio-temporal control of calcium signals that PVBC exert in their dendrites and which allow these signals to follow high frequency input integration. In addition, the extrusion rate of $1400s^{-1}$ is fast enough to overcome the equilibrium of PV (on-rate= $3\text{-}10\mu M^{-1}/s$, off-rate= $0.9\text{-}1.3s^{-1}$), and so, a portion of free calcium should be extruded even before having been bound by PV (Lee, Schwaller et al. 2000). Interestingly, Sabatini's study reported a small difference in the clearance rate of large proximal apical dendrite and smaller distal dendrites, which is expected due to a difference in dendrite diameters and so a larger surface-to-volume ratio (SVR) in distal dendrites (Sabatini, Oertner et al. 2002). The difference in extrusion rate found between our interneuron subtypes is not likely to be from either a difference in proximal dendrite diameter or due to a difference in SVR since we measured no difference in SVR in CCKBC, D-T cells and PVBC.

The previously mentioned extrusion rate from CCKBC, PVBC and D-T cells were obtained from the slope of the early measure of the tau vs $kappa_{dye}$ plot. By carefully looking at the extrusion rate between the early and late measurement of the bAP-CaT in CCKBC, PVBC and D-T cells, we could see a slight decrease of the extrusion rate in CCKBC, PVBC and D-T cells between the early and late measure indicated by the different slopes of the line fitted to the early and late data. This decrease in extrusion rate was more apparent in PVBC and D-T cells where a calcium binding protein was washed out over the course of the recording in comparison to CCKBC which has only a fixed endogenous buffer fraction.

The extrusion pumps are dependent on $[Ca^{2+}]_i$, $[ATP]_i$ and in the case of PMCA upon the binding of calmodulin (Brini and Carafoli 2011). The change in $[Ca^{2+}]_i$ could possibly be the cause of the rundown of the extrusion pumps, as a long duration recording altered intracellular functions or caused intracellular calcium concentration to gradually rise. However, the free calcium concentration change could not have exceeded the nM range because a large brightness increase of the calcium dye would be seen, and would have alerted us to the unhealthiness of the cell and the cell would have been discarded. Our criterion for including cells in the data set was a stable membrane potential over the recording period and less than 30% change in the input resistance. Additionally, a slight increase in the $[Ca^{2+}]_i$ cannot saturate the PMCA pumps (K_d: 1-10μM) but might saturate calmodulin (K_d<50nM) and so

decrease the binding interaction with PMCA. Thus, there is a slight possibility that a change in $[Ca^{2+}]_i$ might cause the extrusion pump rundown. Another potential explanation of the extrusion pumps rundown is $[ATP]_i$. 4mM of ATP is present in our intracellular solution and the ATP concentration in a normal cell range from 0.6-1.5mM (Ainscow, Mirshamsi et al. 2002). Thus this $[ATP]_i$ should be sufficient for cell metabolism. Nevertheless, ATP hydrolyses rapidly, thus a long cell recording may cause less ATP availability and so may lead to an inactivation of the PMCA. Thus, the slower decay time constant measured over the recording time in both CCKBC and D-T cells might be due to the inactivation of PMCA.

To overcome the possibility that a wash out of calcium binding protein could cause the rundown of the extrusion pumps, we decided to investigate further the different decrease in extrusion rate between CCKBC and D-T cells by adding more time points in our measurement of proximal bAP-CaT. We noticed a time-dependent rundown of extrusion in both CCKBC and D-T cells from the different slopes of the line fitted to the time points recording. Nevertheless, this time-dependent rundown of extrusion was similar in the two subpopulations, regardless of any calcium binding washed out. This finding brings us to conclude that the rundown is more likely metabolic than dependent on free calcium concentration alteration or loss of endogenous buffering.

A similar depression of the extrusion pumps was also reported by Scheuss *et al* during their recording (Scheuss, Yasuda et al. 2006). Scheuss *et al* have reported that depression of the extrusion pumps was masked when a high affinity dye was used (Scheuss, Yasuda et al. 2006). The first buffering capacity measurements were done in CCKBC and D-T cells using OGB6F, which is a low affinity dye, but the rundown experiments were performed with OGB1 (high affinity calcium dye).Thus, we cannot exclude the possibility in our recordings that we missed a potential difference in CCKBC and D-T cells rundown by using a high affinity dye and that a possible difference in extrusion pump rundown might have been masked in the CCKBC and D-T cells recordings.

The rundown of the extrusion pumps should not affect the bAP-CaT amplitude, which is mediated by calcium channels. However, we also saw a decrease in calcium transient amplitude accompanied by a long decay time constant. One possible explanation could be that in parallel to a rundown of the extrusion pumps, other alterations of intracellular calcium signaling happened.

One possible technical explanation could be that the calcium dye did not reach equilibrium at the time of the recording. This explanation is true for the first 10-15 minutes of the recording

((Helmchen, Imoto et al. 1996)), since the calcium dye fully equilibrates within 10 minutes in proximal dendrites. However, the later time recordings should not be affected, but the calcium transient amplitude still decreased with the long duration recordings.

The depolarization of the membrane leading to a bAP is mediated by sodium and potassium channels, and some potassium channels (SK and BK channels see **1.3.4.2**) are calcium dependent. With an increase in calcium accumulation over the recording, those channels could be more activated leading to more hyperpolarization of the membrane, and so to less activation of VGCC which would ultimately decrease the calcium transient amplitude. Analyzing the action potential shape of the early and late measurement revealed no change in the AP amplitude (CCKBC: 108.13 ± 2.8 mV and 108.026 ± 3.1mV for early and late respectively, paired t test, P-value>0.05) and in AHP (CCKBC: -0.80± 0.4 mV and -1.3 ± 0.4mV for early and late respectively paired t test, P-value>0.05), but a change in the ADP was observed (CCKBC: early= 10.3 ± 1.4mV and late= 6.6± 1.9mV, paired t test, P-value<0.05) which is mediated by cationic channels. Similarly, inactivation of VGCC can occur with an increase in $[Ca^{2+}]_i$ (Budde, Meuth et al. 2002) and particularly the L-type VGCC, and so would further decrease the calcium transient amplitude, since 70% of the calcium entry is mediated by L-type channels in CCKBC and D-T cells.

5.2 bAP-CaT in interneurons and gradient of endogenous buffer in CCKBC

Backpropagation of action potentials is generated by the activation of sodium channels in the dendritic tree; potassium channels are also important since their activation will shut down the depolarization of the dendritic membrane (Stuart, Spruston et al. 1997). Upon the depolarization of the dendrite membrane, VGCC are activated with a concomitant calcium entry (bAP-CaT). The role of the bAP is to inform the dendritic arbor of the output state of the cell, and this might serve as a link between presynaptic excitation and postsynaptic response important for certain forms of plasticity (STDP).

Our measurements of bAP-CaT indicate that the perisomatic targeting interneurons have a poor propagation of bAP-CaT, whereas it is stable for D-T cells. This poor backpropagation in interneurons was verified in the literature (Stuart and Hausser 1994) and more specifically in CCKBC (Evstratova, Chamberland et al. 2011) and in PVBC (Aponte, Bischofberger et al. 2008; Camire and Topolnik 2014). However, the stable backpropagation seen in D-T cells was not reported by Evstratova *et al* where they described a poor bAP-CaT in SC-AS

(Evstratova, Chamberland et al. 2011). The subpopulation reported in their study may be a subset or a slightly different population than our D-T cell population recorded here, as they did not use a fluorescently labeled mouse line. Thus STDP induction via coincidence detection of bAP and synaptic input might be facilitated in D-T cells where this coincidence detection is more likely to occur but will be less suitable for the perisomatic inhibitors.
Another possible explanation of the difference seen in bAP-CaT in CCKBC, PVBC and D-T cells could be from a difference in dendritic branching and diameter (Stuart, Spruston et al. 1997). Cable properties and diameters of dendrites are different in Cb^+ interneurons compared to Cb^- interneurons (Emri, Antal et al. 2001). Since CCKBC and PVBC are immuno-negative for Cb and D-T is immuno-positive for it, the difference in bAP-CaT could be affected by this difference in dendrite cable properties. Nevertheless, the dendrite diameters of CCKBC, PVBC and D-T cells at the position we recorded are all in the same range from proximal to distal position, and thus we do not expect dendrite morphology to account for the propagation of the bAP-CaT.

As we have reported a difference in the amount and mobility of endogenous buffering capacity in CCKBC, PVBC and D-T cells, we investigated its effect on the bAP-CaT. The wash out of mobile calcium binding proteins did not influence the bAP-CaT, which was surprising, since having no more mobile endogenous fraction in PVBC and D-T cells should affect the diffusion of free calcium, leading to more free calcium accumulation and so the possible activation of calcium dependent potassium channels leading to less backpropagation.

We also verified the effect of the fixed buffer on the bAP-CaT. Out-competing the endogenous buffer with a high concentration of high affinity calcium dye did not affect the bAP-CaT of PVBC and D-T cells, which confirms that the previous bAP-CaT determined with normal calcium dye concentration (100µM) is not a matter of non-equilibration or diffusion of the dye within the dendritic tree. In CCKBC, out competing the endogenous buffer revealed bAP-CaT in distal dendrites. This difference in buffer could be due to the heterogeneity of the fixed buffer in proximal versus distal dendrites/ either a greater forward rate constant or a larger concentration. A similar difference in buffering capacity was hypothesized by Ross in Purkinje cells were he examined different calcium transient decay time constant between proximal and distal tertiary branches of Purkinje cells (Ross and Werman 1987). However, this difference may also be coming from a differential extrusion pumps distribution. A difference in sodium channel, potassium channel or VGCC distribution should not contribute to this finding since the same protocol of 3 somatic APs was induced in

normal calcium dye concentration (100µM) and high calcium dye concentration (1mM). Thus our hypothesis was that a gradient of endogenous fixed buffer is present in CCKBC dendrites and so since fixed buffer tightly restricts calcium diffusion, the apparent calcium diffusion coefficient must be larger in proximal dendrites than distal ones. Knowing that radiatum interneuron's proximal dendrites are enriched with $GABA_a$ receptors and distal dendrites areas are more targeted by glutamatergic input (Pettit and Augustine 2000), we can envisage that this feature, together with the dendritic gradient of endogenous buffers work in concert to ensure a strong compartmentalized input integration at distal positions where the likelihood of calcium entry is high (via glutamatergic excitation) and a less regulated calcium signal in proximal sites where only small calcium entry will occur since it is enriched with $GABA_a$ receptors. We can further expand this concept to view endogenous buffer as being a filter that tunes intracellular calcium in distal dendrites to convey specific connectivity pattern. Therefore, it seems that the gradient of endogenous buffer in CCKBC matches the input connectivity distribution along their dendritic arbor.

To confirm the gradient of dendritic endogenous in CCKBC, uncaging experiments on proximal and distal dendrites were performed. We sought to illicit a calcium entry from a single postsynaptic cite via glutamate uncaging. Calcium entry could have been via calcium-permeable AMPAR or VGCC opened by local depolarization. The mathematical model of diffusion which was applied to this data set required that the calcium entry mimic a point source, which in theory has very large amplitude a localized spread. The analysis require a large enough calcium transient in which the increase in local calcium could be traced over a long enough time to deduce the apparent diffusion coefficient of calcium. However, calcium entry induced by a synaptic event was small ($\Delta F/F \sim 0.3$) and so the signal to noise ratio was not good enough to be able to accurately extrapolate the apparent coefficient diffusion of calcium. We thus tried to increase the stimulation intensity, which increased the calcium signaling but unfortunately recruited more VGCC and so led to a too broad spread of calcium entry. The D_{app} values obtained were not reproducible within a same scan due to unreliable fit. A first explanation may be a too low signal to noise ratio, that lead to a too noisy trace and a low detection of the calcium transient diffusion and thus an incorrect estimate of the apparent calcium diffusion coefficient.

A second more physiologically related hypothesis may be heterogeneity of the apparent calcium diffusion coefficient along the dendritic tree of CCKBC. Dendrites are densely packed compartment and tortuous, such feature may underlie more complex phenomenon that calcium diffusion theory accounts for; for instance a difference in viscosity within the same

dendritic portion, or more subcellular organelles (mitochondria, endoplasmic reticulum). Additionally, a difference in the proximity of the calcium source to extrusion pumps may shorten the diffusion of calcium substantially.

5.3 Synaptic input induced calcium in CCKBC

By stimulating the Shaffer Collaterals, we could induce dendritic calcium entry upon a synaptic event. In one example, a bAP-CaT and a synaptic input could be simultaneously recorded in the same dendritic portion. It appears that, bAP-CaT produce slightly larger amplitude of calcium entry, and slower decay time constant than the synaptic input induced calcium transient. The depolarization induced by a bAP is less localized than the EPSP, thus more VGCC in a larger dendritic volume should be recruited, which is reflected in a larger calcium entry which takes supposedly longer to be bound and extruded reflecting the longer decay time constant.

In this same cell we could induce a pairing protocol of bAP and stimulated EPSP alternating the order of the pairing stimuli. Pairing first a bAP with an EPSP should give a supralinearity of the calcium signaling, because NMDAR needs both glutamate and depolarization to free itself from the magnesium block (Rozsa, Zelles et al. 2004; Higley and Sabatini 2008). Thus it is not surprising that in this cell, the pairing of first the bAP and then the synaptic EPSP induce supralinearity of the calcium signal and a sublinear calcium signal when the order was reversed (**Figure 31**). This finding is in opposition with Nevian and Sakmann's results in stellate cells (Nevian and Sakmann 2004), where the supralinearity of calcium signal was reported with pairing EPSP-bAP, although mediated by NMDAR activation.

It has not been so far shown that NMDAR play a major role in plasticity in CCKBC, and so we cannot exclude another mechanism for STDP in CCKBC, for instance by means of L-type channels (Weisskopf, Bauer et al. 1999) or T-type calcium channels (Simms and Zamponi 2014) both expressed in CCKBC (Evstratova, Chamberland et al. 2011).

5.4 CCKBC behavior during network activity

Theta rhythm is mediated by the cholinergic septum drive to the hippocampus (Cobb and Davies 2005). By simulating network activity with a cholinergic agonist (carbachol, Cch) we aimed to understand the calcium signaling involvement in interneurons during network activity. CCKBC and PVBC exhibit different behavior when activated by CCh (Nagode, Tang

et al. 2011; Bell, Bell et al. 2015) due to their different expression of muscarinic receptors (see **1.4**)

Our experiment revealed a depolarization of the resting membrane potential and a spontaneous firing of CCKBC upon cholinergic drive activation, also confirmed by Bell's study in which they optogenetically activated cholinergic septum afferents and reported a depolarization leading to action potentials in VIP positive BC (Bell, Bell et al. 2015). The membrane depolarization was also reported in OLM cells (Lawrence, Statland et al. 2006) and muscarinic activation tuned OLM cells' action potential frequency to theta phase (Lawrence, Grinspan et al. 2006).

In OLM cells, muscarinic receptor activation (M1 and M3) regulates a calcium-activated potassium conductance (I_{AHP}), and a calcium-dependent cationic conductance (I_{CAT}) responsible for the appearance of an I_{ADP} (Lawrence, Grinspan et al. 2006). Similar results were obtained in our CCKBC measurement, where the muscarinic blocker atropine abolished the spontaneous firing induced by a cholinergic agonist. Thus, because CCKBC contain muscarinic receptors (M1 and M3) (Armstrong and Soltesz 2012), a modulation of I_{AHP} or I_{ADP} by muscarinic receptor could be the mechanism involved in their spontaneous firing. AHP was indeed decreased after Cch application and the ADP component was increased which is in line with the regulation of OLM cells by M1r and M3r.

A component of the AHP is mediated by SK channels, a calcium dependent potassium channel. SK channels were shown to have an indirect relationship with muscarinic receptor and metabotropic glutamatergic receptor activation within CA1 pyramidal cells. Indeed muscarinic and glutamatergic receptors inactivate SK channels, which in normal condition indirectly inhibit NMDAR by reinforcing the magnesium block through membrane hyperpolarization. Thus upon M1r activation, the SK channel negative feedback on NMDAR is removed allowing more calcium entry into spines and/or dendrites (Buchanan, Petrovic et al. 2010; Giessel and Sabatini 2010; Tigaret, Olivo et al. 2016). Consequently we can speculate that CCKBC fire action potential upon Cch induced network activity via an activation of M1 and M3 receptors that inhibit SK current. This leads to increase in CCKBC excitability linked to a depolarized resting membrane potential, resulting in APs firing. As a confirmation of this hypothesis, the SK current present in CCKBC was slightly decreased upon Cch application, but these data are preliminary, further recordings should be carried out.

Recruitment of additional calcium sources upon Cch induced network activity could be a good hypothesis to explain the large increase in the amplitude of the bAP-CaT. Indeed

CCKBC contain nicotinic receptor (α7) that are permeable to calcium and this α7 nicotinic receptor was shown to mediate calcium signaling in neurons (Shen and Yakel 2009). In addition, the I_{CAT} regulated by muscarinic receptor activation could also be a potential source of increased calcium entry.

CCKBC have also a slight increase in their resting calcium concentration during Cch which is not persistent when Cch was washed out and did not depend on their spontaneous firing. Nevertheless, accurate measurement of the actual resting calcium concentration in CCKBC before and after Cch application did not reveal a statistically significant increase. However, by looking carefully at the data, it seems that half of CCKBC had an increase in resting calcium concentration, whereas the other half did not. The lack of statistical significance may therefore be due to heterogeneity in the effect of Cch on CCKBC. α7 nicotinic receptors are also involved in the recruitment of calcium release from the internal store (Shen and Yakel 2009) and may potentially increase the resting calcium concentration seen in some CCKBC.

Finally, in some CCKBC, we could record spontaneous ongoing dendritic calcium signaling during network activity, and in one particular cell, 3 dendrites were imaged at the same time. Surprisingly, these three dendrites showed independent calcium transients which did not strictly match the AP measured in the soma of this CCKBC. In this particular example, the glutamatergic drives was not blocked and so we cannot say whether the calcium transients recorded were from a back propagating AP or via a synaptic event, or a combination of synaptic and somatic activity. What is still interesting is that the different dendrites of a single cell could act as a unitary unit of integration which could depend on the distribution of VGCC and extrusion pumps but also on the proportion of endogenous buffer.

6 Perspectives

Undeniably, this thesis research raises an abundance of perspectives and open questions.

As a confirmation that endogenous buffering capacity shapes the summation of calcium signaling, the synaptic stimulation paired with bAP-CaT experiments should be expanded. Indeed, only the proof of principle has been established and no definitive conclusion can be derived from it. Whether this buildup of calcium signaling within dendrites is different among CCKBC, PVBC and D-T cells will also yield information on their possible intrinsic plasticity.

Another important point toward understanding the difference in calcium signaling in CCKBC, PVBC and D-T cells would be to map their VGCC and glutamate receptors. As pointed out in the introduction, the literature covering this topic is quite sparse especially in interneurons. This VGCC and glutamate receptors mapping could be performed by immunostaining, and should give some insight about the source of the dendritic calcium entry in our interneurons of interest. Indeed, in this thesis work, no attention has been taken to determine the source of the calcium entry, although it has been shown by Topolnik, that CCKBC and D-T cells have different calcium entry sources (Topolnik 2012) and that the major calcium entry source in PVBC is from calcium permeable AMPAR (Camire and Topolnik 2012; Camire and Topolnik 2014).

Finally, a last question would be to understand how the interneurons behavior during oscillations is correlated with their calcium signaling. However, those experiments are challenging due to simultaneous ongoing mechanisms: muscarinic activation leading to changes in intrinsic activity, increase in calcium entry, and possible recruitment of the internal store. As we have seen in **4.7.2.2**, CCKBC undergo numerous of intrinsic changes during network activity, and it was difficult for us to extract information about their calcium signaling features in the course of network activity. Nevertheless, the questions of whether different dendrites of the same interneuron are integrating synaptic and somatic activity differently, especially if this different integration depends somehow on network activity or cholinergic drive remains unresolved and is of great interest.

References

Acsady, L., D. Arabadzisz, et al. (1996). "Correlated morphological and neurochemical features identify different subsets of vasoactive intestinal polypeptide-immunoreactive interneurons in rat hippocampus." Neuroscience **73**(2): 299-315.

Acsady, L., T. J. Gorcs, et al. (1996). "Different populations of vasoactive intestinal polypeptide-immunoreactive interneurons are specialized to control pyramidal cells or interneurons in the hippocampus." Neuroscience **73**(2): 317-334.

Ainscow, E. K., S. Mirshamsi, et al. (2002). "Dynamic imaging of free cytosolic ATP concentration during fuel sensing by rat hypothalamic neurones: evidence for ATP-independent control of ATP-sensitive K(+) channels." J Physiol **544**(Pt 2): 429-445.

Airaksinen, M. S., J. Eilers, et al. (1997). "Ataxia and altered dendritic calcium signaling in mice carrying a targeted null mutation of the calbindin D28k gene." Proc Natl Acad Sci U S A **94**(4): 1488-1493.

Akerman, K. E., R. Shariatmadari, et al. (2004). "Ca2+-dependent potentiation of muscarinic receptor-mediated Ca2+ elevation." Cell Calcium **36**(5): 397-408.

Alger, B. E., D. A. Nagode, et al. (2014). "Muscarinic cholinergic receptors modulate inhibitory synaptic rhythms in hippocampus and neocortex." Front Synaptic Neurosci **6**: 18.

Allbritton, N. L., T. Meyer, et al. (1992). "Range of messenger action of calcium ion and inositol 1,4,5-trisphosphate." Science **258**(5089): 1812-1815.

Alvarez-Baron, E., K. Michel, et al. (2013). "RIM3gamma and RIM4gamma are key regulators of neuronal arborization." J Neurosci **33**(2): 824-839.

Amaral, D. G. (1993). "Emerging principles of intrinsic hippocampal organization." Curr Opin Neurobiol **3**(2): 225-229.

Amaral, D. G. and M. P. Witter (1989). "The three-dimensional organization of the hippocampal formation: a review of anatomical data." Neuroscience **31**(3): 571-591.

Andersen, P. (2007). The Hippocampus Book, Oxford University Press, USA.

Aponte, Y., J. Bischofberger, et al. (2008). "Efficient Ca2+ buffering in fast-spiking basket cells of rat hippocampus." J Physiol **586**(8): 2061-2075.

Arendt, O., B. Schwaller, et al. (2013). "Restricted diffusion of calretinin in cerebellar granule cell dendrites implies Ca(2)(+)-dependent interactions via its EF-hand 5 domain." J Physiol **591**(16): 3887-3899.

Armstrong, C. and I. Soltesz (2012). "Basket cell dichotomy in microcircuit function." J Physiol **590**(Pt 4): 683-694.

Assaf, S. Y. and J. J. Miller (1978). "The role of a raphe serotonin system in the control of septal unit activity and hippocampal desynchronization." Neuroscience **3**(6): 539-550.

Augustine, G. J., F. Santamaria, et al. (2003). "Local calcium signaling in neurons." Neuron **40**(2): 331-346.

Axmacher, N., F. Mormann, et al. (2006). "Memory formation by neuronal synchronization." Brain Res Rev **52**(1): 170-182.

Bartos, M., H. Alle, et al. (2011). "Role of microcircuit structure and input integration in hippocampal interneuron recruitment and plasticity." Neuropharmacology **60**(5): 730-739.

Baude, A., C. Bleasdale, et al. (2007). "Immunoreactivity for the GABAA receptor alpha1 subunit, somatostatin and Connexin36 distinguishes axoaxonic, basket, and bistratified interneurons of the rat hippocampus." Cereb Cortex **17**(9): 2094-2107.

Baylor, S. M. and S. Hollingworth (1998). "Model of sarcomeric Ca2+ movements, including ATP Ca2+ binding and diffusion, during activation of frog skeletal muscle." J Gen Physiol **112**(3): 297-316.

Becker, W. (2012). The Bh TCSPC Handbook: Time-correlated Single Photon Counting Modules SPC-130, SPC-134, SPC-130 EM, SPC-134 EM, SPC-140, SPC-144, SPC-150, SPC-154, SPC-630, SPC-730, SPC-830 ; Simple-Tau Systems, SPCM Software, SPCImage Data Analysis, Becker et Hickl.

Bell, L. A., K. A. Bell, et al. (2015). "Activation of muscarinic receptors by ACh release in hippocampal CA1 depolarizes VIP but has varying effects on parvalbumin-expressing basket cells." J Physiol **593**(1): 197-215.

Berridge, M. J., P. Lipp, et al. (2000). "The versatility and universality of calcium signalling." Nat Rev Mol Cell Biol **1**(1): 11-21.

Bezaire, M. J. and I. Soltesz (2013). "Quantitative assessment of CA1 local circuits: knowledge base for interneuron-pyramidal cell connectivity." Hippocampus **23**(9): 751-785.

Blaustein, M. P. and W. J. Lederer (1999). "Sodium/calcium exchange: its physiological implications." Physiol Rev **79**(3): 763-854.

Bliss, T. V. and T. Lomo (1973). "Long-lasting potentiation of synaptic transmission in the dentate area of the anaesthetized rabbit following stimulation of the perforant path." J Physiol **232**(2): 331-356.

Bloodgood, B. L. and B. L. Sabatini (2007). "Ca(2+) signaling in dendritic spines." Curr Opin Neurobiol **17**(3): 345-351.

Bosman, L. W. and A. Konnerth (2009). "Activity-dependent plasticity of developing climbing fiber-Purkinje cell synapses." Neuroscience **162**(3): 612-623.

Brini, M., D. Bano, et al. (2000). "Effects of PMCA and SERCA pump overexpression on the kinetics of cell Ca(2+) signalling." EMBO J **19**(18): 4926-4935.

Brini, M. and E. Carafoli (2011). "The plasma membrane Ca(2)+ ATPase and the plasma membrane sodium calcium exchanger cooperate in the regulation of cell calcium." Cold Spring Harb Perspect Biol **3**(2).

Buchanan, K. A., M. M. Petrovic, et al. (2010). "Facilitation of long-term potentiation by muscarinic M(1) receptors is mediated by inhibition of SK channels." Neuron **68**(5): 948-963.

Budde, T., S. Meuth, et al. (2002). "Calcium-dependent inactivation of neuronal calcium channels." Nat Rev Neurosci **3**(11): 873-883.

Buhl, E. H., K. Halasy, et al. (1994). "Diverse sources of hippocampal unitary inhibitory postsynaptic potentials and the number of synaptic release sites." Nature **368**(6474): 823-828.

Burnashev, N. and A. Rozov (2005). "Presynaptic Ca2+ dynamics, Ca2+ buffers and synaptic efficacy." Cell Calcium **37**(5): 489-495.

Buzsaki, G. (1986). "Hippocampal sharp waves: their origin and significance." Brain Res **398**(2): 242-252.

Buzsaki, G. (2002). "Theta oscillations in the hippocampus." Neuron **33**(3): 325-340.

Buzsaki, G. and X. J. Wang (2012). "Mechanisms of gamma oscillations." Annu Rev Neurosci **35**: 203-225.

Camire, O. and L. Topolnik (2012). "Functional compartmentalisation and regulation of postsynaptic Ca2+ transients in inhibitory interneurons." Cell Calcium **52**(5): 339-346.

Camire, O. and L. Topolnik (2014). "Dendritic calcium nonlinearities switch the direction of synaptic plasticity in fast-spiking interneurons." J Neurosci **34**(11): 3864-3877.

Campanac, E., C. Gasselin, et al. (2013). "Enhanced intrinsic excitability in basket cells maintains excitatory-inhibitory balance in hippocampal circuits." Neuron **77**(4): 712-722.

Caporale, N. and Y. Dan (2008). "Spike timing-dependent plasticity: a Hebbian learning rule." Annu Rev Neurosci **31**: 25-46.

Carafoli, E. (1992). "The Ca2+ pump of the plasma membrane." J Biol Chem **267**(4): 2115-2118.

Carafoli, E., L. Santella, et al. (2001). "Generation, control, and processing of cellular calcium signals." Crit Rev Biochem Mol Biol **36**(2): 107-260.

Caride, A. J., A. G. Filoteo, et al. (2001). "Delayed activation of the plasma membrane calcium pump by a sudden increase in Ca2+: fast pumps reside in fast cells." Cell Calcium **30**(1): 49-57.

Catterall, W. A. (2000). "Structure and regulation of voltage-gated Ca2+ channels." Annu Rev Cell Dev Biol **16**: 521-555.

Cea-del Rio, C. A., J. J. Lawrence, et al. (2011). "Cholinergic modulation amplifies the intrinsic oscillatory properties of CA1 hippocampal cholecystokinin-positive interneurons." J Physiol **589**(Pt 3): 609-627.
Cea-del Rio, C. A., C. J. McBain, et al. (2012). "An update on cholinergic regulation of cholecystokinin-expressing basket cells." J Physiol **590**(Pt 4): 695-702.
Chen, S., F. Benninger, et al. (2014). "Role of small conductance Ca(2)(+)-activated K(+) channels in controlling CA1 pyramidal cell excitability." J Neurosci **34**(24): 8219-8230.
Chiovini, B., G. F. Turi, et al. (2014). "Dendritic spikes induce ripples in parvalbumin interneurons during hippocampal sharp waves." Neuron **82**(4): 908-924.
Clapham, D. E. (2007). "Calcium signaling." Cell **131**(6): 1047-1058.
Cobb, S. R., E. H. Buhl, et al. (1995). "Synchronization of neuronal activity in hippocampus by individual GABAergic interneurons." Nature **378**(6552): 75-78.
Cobb, S. R. and C. H. Davies (2005). "Cholinergic modulation of hippocampal cells and circuits." J Physiol **562**(Pt 1): 81-88.
Colgin, L. L. (2016). "Rhythms of the hippocampal network." Nat Rev Neurosci **17**(4): 239-249.
Cope, D. W., G. Maccaferri, et al. (2002). "Cholecystokinin-immunopositive basket and Schaffer collateral-associated interneurones target different domains of pyramidal cells in the CA1 area of the rat hippocampus." Neuroscience **109**(1): 63-80.
Csicsvari, J., B. Jamieson, et al. (2003). "Mechanisms of gamma oscillations in the hippocampus of the behaving rat." Neuron **37**(2): 311-322.
Cummings, J. A., R. M. Mulkey, et al. (1996). "Ca2+ signaling requirements for long-term depression in the hippocampus." Neuron **16**(4): 825-833.
Daw, M. I., L. Tricoire, et al. (2009). "Asynchronous transmitter release from cholecystokinin-containing inhibitory interneurons is widespread and target-cell independent." J Neurosci **29**(36): 11112-11122.
Delvendahl, I., L. Jablonski, et al. (2015). "Reduced endogenous Ca2+ buffering speeds active zone Ca2+ signaling." Proc Natl Acad Sci U S A **112**(23): E3075-3084.
Donato, F., A. Chowdhury, et al. (2015). "Early- and late-born parvalbumin basket cell subpopulations exhibiting distinct regulation and roles in learning." Neuron **85**(4): 770-786.
Donato, F., S. B. Rompani, et al. (2013). "Parvalbumin-expressing basket-cell network plasticity induced by experience regulates adult learning." Nature **504**(7479): 272-276.
Dumenieu, M., N. Fourcaud-Trocme, et al. (2015). "Afterhyperpolarization (AHP) regulates the frequency and timing of action potentials in the mitral cells of the olfactory bulb: role of olfactory experience." Physiol Rep **3**(5).
Dutar, P., M. H. Bassant, et al. (1995). "The septohippocampal pathway: structure and function of a central cholinergic system." Physiol Rev **75**(2): 393-427.
Eggermann, E. and P. Jonas (2012). "How the 'slow' Ca2+ buffer parvalbumin affects transmitter release in nanodomain-coupling regimes." Nature Neuroscience **15**(1): 20-22.
Emri, Z., K. Antal, et al. (2001). "Electrotonic profile and passive propagation of synaptic potentials in three subpopulations of hippocampal CA1 interneurons." Neuroscience **104**(4): 1013-1026.
Evans, R. C. and K. T. Blackwell (2015). "Calcium: amplitude, duration, or location?" Biol Bull **228**(1): 75-83.
Evstratova, A., S. Chamberland, et al. (2011). "Cell type-specific and activity-dependent dynamics of action potential-evoked Ca2+ signals in dendrites of hippocampal inhibitory interneurons." J Physiol **589**(Pt 8): 1957-1977.
Faber, E. S., A. J. Delaney, et al. (2005). "SK channels regulate excitatory synaptic transmission and plasticity in the lateral amygdala." Nat Neurosci **8**(5): 635-641.
Fakler, B. and J. P. Adelman (2008). "Control of K(Ca) channels by calcium nano/microdomains." Neuron **59**(6): 873-881.
Fierro, L. and I. Llano (1996). "High endogenous calcium buffering in Purkinje cells from rat cerebellar slices." J Physiol **496 (Pt 3)**: 617-625.

Forro, T., O. Valenti, et al. (2015). "Temporal organization of GABAergic interneurons in the intermediate CA1 hippocampus during network oscillations." Cereb Cortex **25**(5): 1228-1240.
Freund, T. F. (2003). "Interneuron Diversity series: Rhythm and mood in perisomatic inhibition." Trends Neurosci **26**(9): 489-495.
Freund, T. F. and G. Buzsaki (1996). "Interneurons of the hippocampus." Hippocampus **6**(4): 347-470.
Freund, T. F., A. I. Gulyas, et al. (1990). "Serotonergic control of the hippocampus via local inhibitory interneurons." Proc Natl Acad Sci U S A **87**(21): 8501-8505.
Freund, T. F. and I. Katona (2007). "Perisomatic inhibition." Neuron **56**(1): 33-42.
Fukuda, T. and T. Kosaka (2000). "Gap junctions linking the dendritic network of GABAergic interneurons in the hippocampus." J Neurosci **20**(4): 1519-1528.
Fukuda, T. and T. Kosaka (2003). "Ultrastructural study of gap junctions between dendrites of parvalbumin-containing GABAergic neurons in various neocortical areas of the adult rat." Neuroscience **120**(1): 5-20.
Geiger, J. R., J. Lubke, et al. (1997). "Submillisecond AMPA receptor-mediated signaling at a principal neuron-interneuron synapse." Neuron **18**(6): 1009-1023.
Geiger, J. R., T. Melcher, et al. (1995). "Relative abundance of subunit mRNAs determines gating and Ca2+ permeability of AMPA receptors in principal neurons and interneurons in rat CNS." Neuron **15**(1): 193-204.
Giessel, A. J. and B. L. Sabatini (2010). "M1 muscarinic receptors boost synaptic potentials and calcium influx in dendritic spines by inhibiting postsynaptic SK channels." Neuron **68**(5): 936-947.
Glickfeld, L. L. and M. Scanziani (2006). "Distinct timing in the activity of cannabinoid-sensitive and cannabinoid-insensitive basket cells." Nat Neurosci **9**(6): 807-815.
Goldberg, J. H., G. Tamas, et al. (2003). "Calcium microdomains in aspiny dendrites." Neuron **40**(4): 807-821.
Goldberg, J. H., G. Tamas, et al. (2003). "Ca2+ imaging of mouse neocortical interneurone dendrites: Ia-type K+ channels control action potential backpropagation." J Physiol **551**(Pt 1): 49-65.
Goldberg, J. H. and R. Yuste (2005). "Space matters: local and global dendritic Ca2+ compartmentalization in cortical interneurons." Trends Neurosci **28**(3): 158-167.
Goldberg, J. H., R. Yuste, et al. (2003). "Ca2+ imaging of mouse neocortical interneurone dendrites: contribution of Ca2+-permeable AMPA and NMDA receptors to subthreshold Ca2+dynamics." J Physiol **551**(Pt 1): 67-78.
Grynkiewicz, G., M. Poenie, et al. (1985). "A new generation of Ca2+ indicators with greatly improved fluorescence properties." J Biol Chem **260**(6): 3440-3450.
Gulyas, A. I., N. Hajos, et al. (1996). "Interneurons containing calretinin are specialized to control other interneurons in the rat hippocampus." J Neurosci **16**(10): 3397-3411.
Gulyas, A. I., M. Megias, et al. (1999). "Total number and ratio of excitatory and inhibitory synapses converging onto single interneurons of different types in the CA1 area of the rat hippocampus." J Neurosci **19**(22): 10082-10097.
Hajos, N., T. J. Ellender, et al. (2009). "Maintaining network activity in submerged hippocampal slices: importance of oxygen supply." Eur J Neurosci **29**(2): 319-327.
Hajos, N., J. Palhalmi, et al. (2004). "Spike timing of distinct types of GABAergic interneuron during hippocampal gamma oscillations in vitro." J Neurosci **24**(41): 9127-9137.
Heizmann, C. W. and K. Braun (1992). "Changes in Ca(2+)-binding proteins in human neurodegenerative disorders." Trends Neurosci **15**(7): 259-264.
Helmchen, F. and W. Denk (2005). "Deep tissue two-photon microscopy." Nat Methods **2**(12): 932-940.
Helmchen, F., K. Imoto, et al. (1996). "Ca2+ buffering and action potential-evoked Ca2+ signaling in dendrites of pyramidal neurons." Biophys J **70**(2): 1069-1081.
Helmchen, F. and D. W. Tank (2011). A single-compartment model of calcium dynamics in nerve terminals and dendrites. Imaging in Neuroscience: A Laboratory Manual. F. K. Helmchen, A. Cold Spring Harbor, NY, USA, Cold Spring Harbor Laboratory Press**:** 355-368.

Herrera, G. M. and M. T. Nelson (2002). "Differential regulation of SK and BK channels by Ca(2+) signals from Ca(2+) channels and ryanodine receptors in guinea-pig urinary bladder myocytes." J Physiol **541**(Pt 2): 483-492.

Higley, M. J. and B. L. Sabatini (2008). "Calcium signaling in dendrites and spines: practical and functional considerations." Neuron **59**(6): 902-913.

Honeycutt, J. A., K. M. Keary Iii, et al. (2016). "Developmental Age Differentially Mediates the Calcium-Binding Protein Parvalbumin in the Rat: Evidence for a Selective Decrease in Hippocampal Parvalbumin Cell Counts." Dev Neurosci **38**(2): 105-114.

Hu, H., J. Gan, et al. (2014). "Interneurons. Fast-spiking, parvalbumin(+) GABAergic interneurons: from cellular design to microcircuit function." Science **345**(6196): 1255263.

Hu, H., M. Martina, et al. (2010). "Dendritic mechanisms underlying rapid synaptic activation of fast-spiking hippocampal interneurons." Science **327**(5961): 52-58.

Ishizuka, N., W. M. Cowan, et al. (1995). "A quantitative analysis of the dendritic organization of pyramidal cells in the rat hippocampus." J Comp Neurol **362**(1): 17-45.

Jonas, P., J. Bischofberger, et al. (2004). "Interneuron Diversity series: Fast in, fast out--temporal and spatial signal processing in hippocampal interneurons." Trends Neurosci **27**(1): 30-40.

Kaiser, K. M., Y. Zilberter, et al. (2001). "Back-propagating action potentials mediate calcium signalling in dendrites of bitufted interneurons in layer 2/3 of rat somatosensory cortex." J Physiol **535**(Pt 1): 17-31.

Kawaguchi, Y. and K. Hama (1987). "Fast-spiking non-pyramidal cells in the hippocampal CA3 region, dentate gyrus and subiculum of rats." Brain Res **425**(2): 351-355.

Kawaguchi, Y., H. Katsumaru, et al. (1987). "Fast spiking cells in rat hippocampus (CA1 region) contain the calcium-binding protein parvalbumin." Brain Res **416**(2): 369-374.

Kepecs, A. and G. Fishell (2014). "Interneuron cell types are fit to function." Nature **505**(7483): 318-326.

Khachaturian, Z. S. (1994). "Calcium hypothesis of Alzheimer's disease and brain aging." Ann N Y Acad Sci **747**: 1-11.

Klausberger, T. (2009). "GABAergic interneurons targeting dendrites of pyramidal cells in the CA1 area of the hippocampus." Eur J Neurosci **30**(6): 947-957.

Klausberger, T., P. J. Magill, et al. (2003). "Brain-state- and cell-type-specific firing of hippocampal interneurons in vivo." Nature **421**(6925): 844-848.

Klausberger, T., L. F. Marton, et al. (2004). "Spike timing of dendrite-targeting bistratified cells during hippocampal network oscillations in vivo." Nat Neurosci **7**(1): 41-47.

Klausberger, T., L. F. Marton, et al. (2005). "Complementary roles of cholecystokinin- and parvalbumin-expressing GABAergic neurons in hippocampal network oscillations." J Neurosci **25**(42): 9782-9793.

Klausberger, T. and P. Somogyi (2008). "Neuronal diversity and temporal dynamics: the unity of hippocampal circuit operations." Science **321**(5885): 53-57.

Koh, D. S., J. R. Geiger, et al. (1995). "Ca(2+)-permeable AMPA and NMDA receptor channels in basket cells of rat hippocampal dentate gyrus." J Physiol **485 (Pt 2)**: 383-402.

Kosaka, T., J. Y. Wu, et al. (1988). "GABAergic neurons containing somatostatin-like immunoreactivity in the rat hippocampus and dentate gyrus." Exp Brain Res **71**(2): 388-398.

Kowalczyk, T., H. Golebiewski, et al. (2001). "Window effect of temperature on carbachol-induced theta-like activity recorded in hippocampal formation in vitro." Brain Res **901**(1-2): 184-194.

Kullmann, D. M. and K. P. Lamsa (2011). "LTP and LTD in cortical GABAergic interneurons: emerging rules and roles." Neuropharmacology **60**(5): 712-719.

Lamsa, K., E. E. Irvine, et al. (2007). "NMDA receptor-dependent long-term potentiation in mouse hippocampal interneurons shows a unique dependence on Ca(2+)/calmodulin-dependent kinases." J Physiol **584**(Pt 3): 885-894.

Lamsa, K. P., J. H. Heeroma, et al. (2007). "Anti-Hebbian long-term potentiation in the hippocampal feedback inhibitory circuit." Science **315**(5816): 1262-1266.

Lapointe, V., F. Morin, et al. (2004). "Synapse-specific mGluR1-dependent long-term potentiation in interneurones regulates mouse hippocampal inhibition." J Physiol **555**(Pt 1): 125-135.
Laude, A. J. and A. W. Simpson (2009). "Compartmentalized signalling: Ca2+ compartments, microdomains and the many facets of Ca2+ signalling." FEBS J **276**(7): 1800-1816.
Lawrence, J. J., Z. M. Grinspan, et al. (2006). "Muscarinic receptor activation tunes mouse stratum oriens interneurones to amplify spike reliability." J Physiol **571**(Pt 3): 555-562.
Lawrence, J. J., J. M. Statland, et al. (2006). "Cell type-specific dependence of muscarinic signalling in mouse hippocampal stratum oriens interneurones." J Physiol **570**(Pt 3): 595-610.
Lee, S. H., I. Marchionni, et al. (2014). "Parvalbumin-positive basket cells differentiate among hippocampal pyramidal cells." Neuron **82**(5): 1129-1144.
Lee, S. H., C. Rosenmund, et al. (2000). "Differences in Ca2+ buffering properties between excitatory and inhibitory hippocampal neurons from the rat." J Physiol **525 Pt 2**: 405-418.
Lee, S. H., B. Schwaller, et al. (2000). "Kinetics of Ca2+ binding to parvalbumin in bovine chromaffin cells: implications for [Ca2+] transients of neuronal dendrites." J Physiol **525 Pt 2**: 419-432.
Lei, S. and C. J. McBain (2002). "Distinct NMDA receptors provide differential modes of transmission at mossy fiber-interneuron synapses." Neuron **33**(6): 921-933.
Liao, C. W. and C. C. Lien (2009). "Estimating intracellular Ca2+ concentrations and buffering in a dendritic inhibitory hippocampal interneuron." Neuroscience **164**(4): 1701-1711.
Llinas, R. and M. Sugimori (1980). "Electrophysiological properties of in vitro Purkinje cell somata in mammalian cerebellar slices." J Physiol **305**: 171-195.
Lopez-Bendito, G., K. Sturgess, et al. (2004). "Preferential origin and layer destination of GAD65-GFP cortical interneurons." Cereb Cortex **14**(10): 1122-1133.
Lorincz, T., M. Kisfali, et al. (2016). "Phenotype-dependent Ca(2+) dynamics in single boutons of various anatomically identified GABAergic interneurons in the rat hippocampus." Eur J Neurosci **43**(4): 536-547.
Losonczy, A., L. Zhang, et al. (2002). "Cell type dependence and variability in the short-term plasticity of EPSCs in identified mouse hippocampal interneurones." J Physiol **542**(Pt 1): 193-210.
Lumpkin, E. A. and A. J. Hudspeth (1998). "Regulation of free Ca2+ concentration in hair-cell stereocilia." J Neurosci **18**(16): 6300-6318.
Mann, E. O., J. M. Suckling, et al. (2005). "Perisomatic feedback inhibition underlies cholinergically induced fast network oscillations in the rat hippocampus in vitro." Neuron **45**(1): 105-117.
Maravall, M., Z. F. Mainen, et al. (2000). "Estimating intracellular calcium concentrations and buffering without wavelength ratioing." Biophys J **78**(5): 2655-2667.
Markram, H., A. Roth, et al. (1998). "Competitive calcium binding: implications for dendritic calcium signaling." J Comput Neurosci **5**(3): 331-348.
Marsicano, G. and B. Lutz (1999). "Expression of the cannabinoid receptor CB1 in distinct neuronal subpopulations in the adult mouse forebrain." Eur J Neurosci **11**(12): 4213-4225.
Marvin, J. S., B. G. Borghuis, et al. (2013). "An optimized fluorescent probe for visualizing glutamate neurotransmission." Nat Methods **10**(2): 162-170.
Matthews, E. A. and D. Dietrich (2015). "Buffer mobility and the regulation of neuronal calcium domains." Front Cell Neurosci **9**: 48.
Matthews, E. A., S. Schoch, et al. (2013). "Tuning local calcium availability: cell-type-specific immobile calcium buffer capacity in hippocampal neurons." J Neurosci **33**(36): 14431-14445.
Mattson, M. P. and S. L. Chan (2003). "Calcium orchestrates apoptosis." Nat Cell Biol **5**(12): 1041-1043.
Matyas, F., T. F. Freund, et al. (2004). "Convergence of excitatory and inhibitory inputs onto CCK-containing basket cells in the CA1 area of the rat hippocampus." Eur J Neurosci **19**(5): 1243-1256.
McQuiston, A. R. and D. V. Madison (1999). "Muscarinic receptor activity has multiple effects on the resting membrane potentials of CA1 hippocampal interneurons." J Neurosci **19**(14): 5693-5702.

McQuiston, A. R. and D. V. Madison (1999). "Nicotinic receptor activation excites distinct subtypes of interneurons in the rat hippocampus." J Neurosci **19**(8): 2887-2896.
Miles, R., K. Toth, et al. (1996). "Differences between somatic and dendritic inhibition in the hippocampus." Neuron **16**(4): 815-823.
Mittelstaedt, T., E. Alvarez-Baron, et al. (2010). "RIM proteins and their role in synapse function." Biol Chem **391**(6): 599-606.
Muller, A., M. Kukley, et al. (2005). "Endogenous Ca2+ buffer concentration and Ca2+ microdomains in hippocampal neurons." J Neurosci **25**(3): 558-565.
Nagode, D. A., A. H. Tang, et al. (2011). "Optogenetic release of ACh induces rhythmic bursts of perisomatic IPSCs in hippocampus." PLoS One **6**(11): e27691.
Nagode, D. A., A. H. Tang, et al. (2014). "Optogenetic identification of an intrinsic cholinergically driven inhibitory oscillator sensitive to cannabinoids and opioids in hippocampal CA1." J Physiol **592**(1): 103-123.
Neher, E. and G. J. Augustine (1992). "Calcium gradients and buffers in bovine chromaffin cells." J Physiol **450**: 273-301.
Neu, A., C. Foldy, et al. (2007). "Postsynaptic origin of CB1-dependent tonic inhibition of GABA release at cholecystokinin-positive basket cell to pyramidal cell synapses in the CA1 region of the rat hippocampus." J Physiol **578**(Pt 1): 233-247.
Nevian, T. and B. Sakmann (2004). "Single spine Ca2+ signals evoked by coincident EPSPs and backpropagating action potentials in spiny stellate cells of layer 4 in the juvenile rat somatosensory barrel cortex." J Neurosci **24**(7): 1689-1699.
Nissen, W., A. Szabo, et al. (2010). "Cell type-specific long-term plasticity at glutamatergic synapses onto hippocampal interneurons expressing either parvalbumin or CB1 cannabinoid receptor." J Neurosci **30**(4): 1337-1347.
Nó, R. L. d. (1934). "Studies on the structure of the cerebral cortex. II, Continuation of the study of the ammonic system." Journal für Psychologie und Neurologie.
Norenberg, A., H. Hu, et al. (2010). "Distinct nonuniform cable properties optimize rapid and efficient activation of fast-spiking GABAergic interneurons." Proc Natl Acad Sci U S A **107**(2): 894-899.
Nowycky, M. C. and M. J. Pinter (1993). "Time courses of calcium and calcium-bound buffers following calcium influx in a model cell." Biophys J **64**(1): 77-91.
Oh, M. M., F. A. Oliveira, et al. (2013). "Altered calcium metabolism in aging CA1 hippocampal pyramidal neurons." J Neurosci **33**(18): 7905-7911.
Park, J. Y., S. Remy, et al. (2010). "A post-burst after depolarization is mediated by group i metabotropic glutamate receptor-dependent upregulation of Ca(v)2.3 R-type calcium channels in CA1 pyramidal neurons." PLoS Biol **8**(11): e1000534.
Park, J. Y. and N. Spruston (2012). "Synergistic actions of metabotropic acetylcholine and glutamate receptors on the excitability of hippocampal CA1 pyramidal neurons." J Neurosci **32**(18): 6081-6091.
Paxinos, G. and C. Watson (1998). The Rat Brain in Stereotaxic Coordinates, Academic Press.
Pedarzani, P., J. E. McCutcheon, et al. (2005). "Specific enhancement of SK channel activity selectively potentiates the afterhyperpolarizing current I(AHP) and modulates the firing properties of hippocampal pyramidal neurons." J Biol Chem **280**(50): 41404-41411.
Perez, Y., F. Morin, et al. (2001). "A hebbian form of long-term potentiation dependent on mGluR1a in hippocampal inhibitory interneurons." Proc Natl Acad Sci U S A **98**(16): 9401-9406.
Pettit, D. L. and G. J. Augustine (2000). "Distribution of functional glutamate and GABA receptors on hippocampal pyramidal cells and interneurons." J Neurophysiol **84**(1): 28-38.
Pitler, T. A. and B. E. Alger (1992). "Postsynaptic spike firing reduces synaptic GABAA responses in hippocampal pyramidal cells." J Neurosci **12**(10): 4122-4132.
Pitler, T. A. and B. E. Alger (1994). "Depolarization-induced suppression of GABAergic inhibition in rat hippocampal pyramidal cells: G protein involvement in a presynaptic mechanism." Neuron **13**(6): 1447-1455.

Pouille, F. and M. Scanziani (2001). "Enforcement of temporal fidelity in pyramidal cells by somatic feed-forward inhibition." Science **293**(5532): 1159-1163.
Pouille, F. and M. Scanziani (2004). "Routing of spike series by dynamic circuits in the hippocampus." Nature **429**(6993): 717-723.
Ribak, C. E., L. Seress, et al. (1993). "Electron microscopic immunocytochemical study of the distribution of parvalbumin-containing neurons and axon terminals in the primate dentate gyrus and Ammon's horn." J Comp Neurol **327**(2): 298-321.
Ross, W. N. and R. Werman (1987). "Mapping calcium transients in the dendrites of Purkinje cells from the guinea-pig cerebellum in vitro." J Physiol **389**: 319-336.
Rozsa, B., G. Katona, et al. (2008). "Dendritic nicotinic receptors modulate backpropagating action potentials and long-term plasticity of interneurons." Eur J Neurosci **27**(2): 364-377.
Rozsa, B., T. Zelles, et al. (2004). "Distance-dependent scaling of calcium transients evoked by backpropagating spikes and synaptic activity in dendrites of hippocampal interneurons." J Neurosci **24**(3): 661-670.
Rynkowski, M. A., G. H. Kim, et al. (2008). "A mouse model of intracerebral hemorrhage using autologous blood infusion." Nat Protoc **3**(1): 122-128.
Sabatini, B. L., M. Maravall, et al. (2001). "Ca(2+) signaling in dendritic spines." Curr Opin Neurobiol **11**(3): 349-356.
Sabatini, B. L., T. G. Oertner, et al. (2002). "The life cycle of Ca(2+) ions in dendritic spines." Neuron **33**(3): 439-452.
Sah, P. and E. S. Faber (2002). "Channels underlying neuronal calcium-activated potassium currents." Prog Neurobiol **66**(5): 345-353.
Sala, F. and A. Hernandez-Cruz (1990). "Calcium diffusion modeling in a spherical neuron. Relevance of buffering properties." Biophys J **57**(2): 313-324.
Scheuss, V., R. Yasuda, et al. (2006). "Nonlinear [Ca2+] signaling in dendrites and spines caused by activity-dependent depression of Ca2+ extrusion." J Neurosci **26**(31): 8183-8194.
Schmidt, H., O. Arendt, et al. (2007). "Parvalbumin is freely mobile in axons, somata and nuclei of cerebellar Purkinje neurones." J Neurochem **100**(3): 727-735.
Schmidt, H., E. B. Brown, et al. (2003). "Diffusional mobility of parvalbumin in spiny dendrites of cerebellar Purkinje neurons quantified by fluorescence recovery after photobleaching." Biophys J **84**(4): 2599-2608.
Schmidt, H., B. Schwaller, et al. (2005). "Calbindin D28k targets myo-inositol monophosphatase in spines and dendrites of cerebellar Purkinje neurons." Proc Natl Acad Sci U S A **102**(16): 5850-5855.
Schmidt, H., K. M. Stiefel, et al. (2003). "Mutational analysis of dendritic Ca2+ kinetics in rodent Purkinje cells: role of parvalbumin and calbindin D28k." J Physiol **551**(Pt 1): 13-32.
Schwaller, B. (2009). "The continuing disappearance of "pure" Ca2+ buffers." Cell Mol Life Sci **66**(2): 275-300.
Schwaller, B. (2010). "Cytosolic Ca2+ buffers." Cold Spring Harb Perspect Biol **2**(11): a004051.
Schwaller, B., I. Durussel, et al. (1997). "Comparison of the Ca2+-binding properties of human recombinant calretinin-22k and calretinin." J Biol Chem **272**(47): 29663-29671.
Schwaller, B., I. V. Tetko, et al. (2004). "Parvalbumin deficiency affects network properties resulting in increased susceptibility to epileptic seizures." Mol Cell Neurosci **25**(4): 650-663.
Schwartzkroin, P. A. and D. D. Kunkel (1985). "Morphology of identified interneurons in the CA1 regions of guinea pig hippocampus." J Comp Neurol **232**(2): 205-218.
Scoville, W. B. and B. Milner (1957). "Loss of recent memory after bilateral hippocampal lesions." J Neurol Neurosurg Psychiatry **20**(1): 11-21.
Sedova, M. and L. A. Blatter (1999). "Dynamic regulation of [Ca2+]i by plasma membrane Ca(2+)-ATPase and Na+/Ca2+ exchange during capacitative Ca2+ entry in bovine vascular endothelial cells." Cell Calcium **25**(5): 333-343.

Seress, L., A. I. Gulyas, et al. (1993). "Distribution, morphological features, and synaptic connections of parvalbumin- and calbindin D28k-immunoreactive neurons in the human hippocampal formation." J Comp Neurol **337**(2): 208-230.
Shen, J. X. and J. L. Yakel (2009). "Nicotinic acetylcholine receptor-mediated calcium signaling in the nervous system." Acta Pharmacol Sin **30**(6): 673-680.
Sik, A., M. Penttonen, et al. (1995). "Hippocampal CA1 interneurons: an in vivo intracellular labeling study." J Neurosci **15**(10): 6651-6665.
Simms, B. A. and G. W. Zamponi (2014). "Neuronal voltage-gated calcium channels: structure, function, and dysfunction." Neuron **82**(1): 24-45.
Sjostrom, P. J., E. A. Rancz, et al. (2008). "Dendritic excitability and synaptic plasticity." Physiol Rev **88**(2): 769-840.
Sloviter, R. S. and G. Nilaver (1987). "Immunocytochemical localization of GABA-, cholecystokinin-, vasoactive intestinal polypeptide-, and somatostatin-like immunoreactivity in the area dentata and hippocampus of the rat." J Comp Neurol **256**(1): 42-60.
Somogyi, J., A. Baude, et al. (2004). "GABAergic basket cells expressing cholecystokinin contain vesicular glutamate transporter type 3 (VGLUT3) in their synaptic terminals in hippocampus and isocortex of the rat." Eur J Neurosci **19**(3): 552-569.
Somogyi, P., A. J. Hodgson, et al. (1984). "Different populations of GABAergic neurons in the visual cortex and hippocampus of cat contain somatostatin- or cholecystokinin-immunoreactive material." J Neurosci **4**(10): 2590-2603.
Strehler, E. E. and M. Treiman (2004). "Calcium pumps of plasma membrane and cell interior." Curr Mol Med **4**(3): 323-335.
Stuart, G. and M. Hausser (1994). "Initiation and spread of sodium action potentials in cerebellar Purkinje cells." Neuron **13**(3): 703-712.
Stuart, G., N. Spruston, et al. (1997). "Action potential initiation and backpropagation in neurons of the mammalian CNS." Trends Neurosci **20**(3): 125-131.
Stuart, G. J. and N. Spruston (2015). "Dendritic integration: 60 years of progress." Nat Neurosci **18**(12): 1713-1721.
Svoboda, K. and R. Yasuda (2006). "Principles of two-photon excitation microscopy and its applications to neuroscience." Neuron **50**(6): 823-839.
Tigaret, C. M., V. Olivo, et al. (2016). "Coordinated activation of distinct Ca(2+) sources and metabotropic glutamate receptors encodes Hebbian synaptic plasticity." Nat Commun **7**: 10289.
Tillotson, D. and A. L. Gorman (1980). "Non-uniform Ca2+ buffer distribution in a nerve cell body." Nature **286**(5775): 816-817.
Tillotson, D. L. and A. L. Gorman (1983). "Localization of neuronal Ca2+ buffering near plasma membrane studied with different divalent cations." Cell Mol Neurobiol **3**(4): 297-310.
Timmermann, D. B., R. E. Westenbroek, et al. (2002). "Distribution of high-voltage-activated calcium channels in cultured gamma-aminobutyric acidergic neurons from mouse cerebral cortex." J Neurosci Res **67**(1): 48-61.
Tonini, R., T. Ferraro, et al. (2013). "Small-conductance Ca2+-activated K+ channels modulate action potential-induced Ca2+ transients in hippocampal neurons." J Neurophysiol **109**(6): 1514-1524.
Topolnik, L. (2012). "Dendritic calcium mechanisms and long-term potentiation in cortical inhibitory interneurons." Eur J Neurosci **35**(4): 496-506.
Topolnik, L., S. Chamberland, et al. (2009). "Activity-dependent compartmentalized regulation of dendritic Ca2+ signaling in hippocampal interneurons." J Neurosci **29**(14): 4658-4663.
Tran-Van-Minh, A., T. Abrahamsson, et al. (2016). "Differential Dendritic Integration of Synaptic Potentials and Calcium in Cerebellar Interneurons." Neuron **91**(4): 837-850.
Traub, R. D., N. Kopell, et al. (2001). "Gap junctions between interneuron dendrites can enhance synchrony of gamma oscillations in distributed networks." J Neurosci **21**(23): 9478-9486.

Tricoire, L., K. A. Pelkey, et al. (2011). "A blueprint for the spatiotemporal origins of mouse hippocampal interneuron diversity." J Neurosci **31**(30): 10948-10970.
Tukker, J. J., P. Fuentealba, et al. (2007). "Cell type-specific tuning of hippocampal interneuron firing during gamma oscillations in vivo." J Neurosci **27**(31): 8184-8189.
Vanderwolf, C. H. (1989). "A general role for serotonin in the control of behavior: studies with intracerebral 5,7-dihydroxytryptamine." Brain Res **504**(2): 192-198.
Vinet, J. and A. Sik (2006). "Expression pattern of voltage-dependent calcium channel subunits in hippocampal inhibitory neurons in mice." Neuroscience **143**(1): 189-212.
Wagner, J. and J. Keizer (1994). "Effects of rapid buffers on Ca2+ diffusion and Ca2+ oscillations." Biophys J **67**(1): 447-456.
Wanaverbecq, N., S. J. Marsh, et al. (2003). "The plasma membrane calcium-ATPase as a major mechanism for intracellular calcium regulation in neurones from the rat superior cervical ganglion." J Physiol **550**(Pt 1): 83-101.
Weisskopf, M. G., E. P. Bauer, et al. (1999). "L-type voltage-gated calcium channels mediate NMDA-independent associative long-term potentiation at thalamic input synapses to the amygdala." J Neurosci **19**(23): 10512-10519.
Wierenga, C. J., F. E. Mullner, et al. (2010). "Molecular and electrophysiological characterization of GFP-expressing CA1 interneurons in GAD65-GFP mice." PLoS One **5**(12): e15915.
Wilms, C. D., H. Schmidt, et al. (2006). "Quantitative two-photon Ca2+ imaging via fluorescence lifetime analysis." Cell Calcium **40**(1): 73-79.
Wilson, R. I., G. Kunos, et al. (2001). "Presynaptic specificity of endocannabinoid signaling in the hippocampus." Neuron **31**(3): 453-462.
Witter, L., S. Rudolph, et al. (2016). "Purkinje Cell Collaterals Enable Output Signals from the Cerebellar Cortex to Feed Back to Purkinje Cells and Interneurons." Neuron **91**(2): 312-319.
Witter, M. P., A. W. Griffioen, et al. (1988). "Entorhinal projections to the hippocampal CA1 region in the rat: an underestimated pathway." Neurosci Lett **85**(2): 193-198.
Wu, C., W. P. Luk, et al. (2005). "Size does matter: generation of intrinsic network rhythms in thick mouse hippocampal slices." J Neurophysiol **93**(4): 2302-2317.
Xu, T., M. Naraghi, et al. (1997). "Kinetic studies of Ca2+ binding and Ca2+ clearance in the cytosol of adrenal chromaffin cells." Biophys J **73**(1): 532-545.
Zhou, Z. and E. Neher (1993). "Mobile and immobile calcium buffers in bovine adrenal chromaffin cells." J Physiol **469**: 245-273.
Zilberter, Y. (2000). "Dendritic release of glutamate suppresses synaptic inhibition of pyramidal neurons in rat neocortex." J Physiol **528**(Pt 3): 489-496.

Appendix

Virus injection in mouse: dosage and study endpoints

Mouse anesthetic dosage:

Mix to inject: 10%ketamin (100mg/kg), and 2% Xylazin (16mg/kg)

Mouse (g)	Mix (mL)
19	0.095
20	0.1
21	0.105
22	0.110
25	0.125

The pain killer Buprenovet (0.05mg/kg) was injected prior the surgery and twice per day for 4 days post-surgery.
The antibiotic Gabrilen (5mg/kg) was injected prior the surgery and twice per day for 4 days post-surgery.

Study endpoints:

The following severity criteria lead to the premature termination of the experiment (Section 31 (1), No. 1, d)

In the course of every experiment it is mandatory to ensure the least possible pain or stress burden for the experimental animal. The state of the animal was assessed on a daily basis and rated according to the following criteria. It has to be considered that the summation of symptoms of one or several categories may lead to reach the next higher index of severity.

Symptom	**Category**	**Plan of action**
No symptoms	0	-
Rough hair coat	A	Monitor animal (once daily)
Lack of appetite	A	Monitor animal (once daily), soak food pellets
Animal is isolating itself	A	Monitor animal (once daily), soak food pellets
Signs of pain (hunched posture)	B	Analgesic, intravenous infusion
Locomotoric abnormalities	B	Analgesic

Dehydration	B	Intravenous infusion
Loss of weight (>20%)	B	Intravenous infusion, special diet
Labored breathing/Wheezing	C	Consult vet
Apathy	C	Consult vet
Self-mutilation	C	Consult vet
Moribundity	D	Sacrifice animal

Index of severity	**Instructions of action**
A = mild	Inform the principal investigator The symptom/s has/have to be monitored closely and frequently.
B = moderate	The animal has to be checked at least once per day. The named veterinary surgeon or the principal investigator has to be involved as soon as two or more symptoms belonging to category B become prevalent.
C = severe	The named veterinary surgeon has to examine the animal. An intervention is needed!
D = animals needs to be painlessly sacrificed	The animal has to be sacrificed immediately.

Abbreviations

ACSF	Artificial cerebro-spinal fluid
AP	Action potential
AP5	DL-2-Amino-5-phosphonopentanoic acid (NMDAR antagonist)
bAP	Back propagating action potential
bAP-CaT	Backpropagating action potential-induced calcium transient
BC	Basket cells
$[Ca^{2+}]r$	Resting calcium concentration
Cb	Calbindin
CC	Current clamp
CCKBC	Cholecystokinin expressing basket cells
CCK	Cholecystokinin
CNQX	6-cyano-7-nitroquinoxaline-2,3-dione (AMPAR/Kainate antagonist)
Cr	Calretinin
D_{app}	Apparent diffusion coefficient
D-T cells	Dendritic targeting cells
DG	Dentate gyrus
DSI	Depolarization induced suppression of inhibition
EPSP	Excitatory post synaptic potential
EC	Entorhinal cortex
FB	Feedback
FF	Feedforward
FLIM	Fluorescence Life Time Imaging

γ	Clearance rate/extrusion rate
κ	Buffering capacity
K_d	Dissociation constant
LFP	Local field potential
MS-DBB	Medial septum diagonal band of Broca
OGB	Oregon green BAPTA
PFA	Paraformaldehyde
PMT	Photomultiplier tube
PVBC	Parvalbumin expressing basket cells
PV	Parvalbumin
ROI	Region Of Interest
SC-AC	Schaffer collateral associated cells
SEM	Standard error of the mean
SWR	Sharp wave ripples
τ	Decay time constant
TBS	Tris buffered saline
TRITON	Polyethylene glycol p-(1,1,3,3-tetrqmethylbutyl)-phenyl ether
TTX	Tetrodotoxin
VC	Voltage clamp
VGCC	Voltage gated calcium channels
VGLUT3	Vesicular glutamate transporter 3
VIP	Vasointestinal peptide

Acknowledgement

First, I would like to express all my gratitude to Dr. Elizabeth Matthews. Your kindness, your pedagogy and your knowledge guided me through the dark hole that is the PhD. Your enthusiasm and curiosity kept me motivated and conceded the frustrating and complicated experiments.

Thank you to Prof. Dr. Dirk Dietrich for the very helpful discussions and advices, and for your sense of details. Thank you to create a lab full of wonderful and supportive people.

I cordially thank my committee members, Prof. Dr. Walter Witke for being my second supervisor in this thesis, Dr. Morgane Le-Bon Jego and Prof Dr. Alf Lamprecht. I know time is precious and I thank all of you to free your busy schedule for providing me constructive criticisms on my thesis manuscript.

I would also like to thank the whole AG Dietrich with all present and past members for their support and live discussion:

A special mention to the girls: Sara, Pia and Vicky. Sara, for having me fell less alone in this small lab and understanding each other even with our broken English.
Pia; thank you for showing me to never give up even when all goes wrong with the project, and for always helping me in every context involving German.
Vicky; thank you for bringing a bit of France here, for your refreshing and amusing character, as well as for all the Mojito nights.
Warm thanks To the PhD office (Natascha, Vicky, Sara, Pia, Monika, Olli, Hyuntae and Arlind) for your support and chatting, I would have not managed to go over it without you.

Shane, thanks for all, I enjoyed sharing our office for the past 4 months. Thank you for your constructive advices, your brilliant mathematical mind set, and of course your kindness.

Camille; thank you for the coffee breaks and sharing with me your information about workshops and interesting seminars, as well as being a sympathetic ear.

Immense thanks to my family who supports the fact I am far away and missing a lot of events. Papa, Maman, merci de m'avoir enseigné que le travail fini toujours par payer. Merci d'avoir

toujours cru en moi. Mamy, merci de ton soutien et de me donner de la fierté dans ce que je réalise. Vanessa, merci d'être présente à chaque instant, et toi Jérémy reste fidèle à toi même.

Enfin je voudrais remercier mon amour Sébastien pour supporter mon caractère pas toujours facile, de rester attentionné ainsi que de m'avoir suivi dans cette folle aventure. Je n'aurais pu le faire sans toi. Merci d'être mon homme et de me pousser toujours plus loin. J'ai hâte de continuer notre histoire et de voir ce que la vie nous réserve.